Nitin thesis.docx

Bennett University

Document Details

Submission ID
trn:oid:::29034:134939416

Submission Date
Apr 12, 2026, 2:05 PM GMT+5:30

Download Date
Apr 12, 2026, 7:52 PM GMT+5:30

File Name
Nitin thesis.docx

File Size
10.9 MB

162 Pages

32,871 Words

185,521 Characters

9% Overall Similarity

The combined total of all matches, including overlapping sources, for each database.

Filtered from the Report

- Bibliography
- Quoted Text
- Cited Text
- Small Matches (less than 8 words)
- Submitted works

Exclusions

- 28 Excluded Sources
- 157 Excluded Matches

Match Groups

307 Not Cited or Quoted 9%
Matches with neither in-text citation nor quotation marks

0 Missing Quotations 0%
Matches that are still very similar to source material

0 Missing Citation 0%
Matches that have quotation marks, but no in-text citation

0 Cited and Quoted 0%
Matches with in-text citation present, but no quotation marks

Top Sources

6% Internet sources
8% Publications
0% Submitted works (Student Papers)

Integrity Flags

0 Integrity Flags for Review

No suspicious text manipulations found.

Our system's algorithms look deeply at a document for any inconsistencies that would set it apart from a normal submission. If we notice something strange, we flag it for you to review.

A Flag is not necessarily an indicator of a problem. However, we'd recommend you focus your attention there for further review.

Match Groups

307 Not Cited or Quoted 9%
Matches with neither in-text citation nor quotation marks

0 Missing Quotations 0%
Matches that are still very similar to source material

0 Missing Citation 0%
Matches that have quotation marks, but no in-text citation

0 Cited and Quoted 0%
Matches with in-text citation present, but no quotation marks

Top Sources

6% Internet sources
8% Publications
0% Submitted works (Student Papers)

Top Sources

The sources with the highest number of matches within the submission. Overlapping sources will not be displayed.

1	Internet	
www.researchgate.net		<1%
2	Publication	
Ashish Gupta, Greater Noida, Vikas Rastogi, Loveleen Kumar Bhagi. "Experimenta...		<1%
3	Internet	
www.mdpi.com		<1%
4	Internet	
c.coek.info		<1%
5	Internet	
link.springer.com		<1%
6	Publication	
Ashish Gupta. "Determination of residual stresses for helical compression spring ...		<1%
7	Internet	
www.springerprofessional.de		<1%
8	Internet	
ksme.or.kr		<1%
9	Publication	
S. Rani, A. K. Agrawal, V. Rastogi. "Vibration analysis for detecting failure mode a...		<1%
10	Internet	
autodocbox.com		<1%

11	Publication	"Advances in Engineering Design", Springer Science and Business Media LLC, 2023 <1%
12	Internet	repository.ju.edu.et <1%
13	Internet	core.ac.uk <1%
14	Internet	dspace.lib.cranfield.ac.uk <1%
15	Publication	Sushila Rani. "Parametric Evaluation and Dynamic Analysis of Turbine Blades–Da... <1%
16	Publication	Wu, H.. "Fracture toughness prediction of a valve body: Numerical analysis", Engi... <1%
17	Internet	eprints.soton.ac.uk <1%
18	Publication	Mohd Sarim Khan, C. Sasikumar. "A water droplet erosion-induced fatigue crack ... <1%
19	Internet	coek.info <1%
20	Publication	"Advances in Simulation, Product Design and Development", Springer Science an... <1%
21	Publication	Ravi Butola, Ravi Pratap Singh, Naman Choudhary, K. K. S. Mer, Jitendra Bhaskar, ... <1%
22	Publication	Zhiyun Wang, Jianxiong Gao, Yiping Yuan, Jianxing Zhou, Hui Zhang, Rui Pan, Junb... <1%
23	Internet	www.fracturae.com <1%
24	Publication	"Proceedings of the 5th China Aeronautical Science and Technology Conference", ... <1%

25 Publication
M. C. Antony Harison, M. Swamy, A. H. V. Pavan, G. Jayaraman. "Root Cause Analy... <1%

26 Publication
Ravi Butola, Ravi Pratap Singh, Naman Choudhary, K. K. S. Mer, Jitendra Bhaskar, ... <1%

27 Internet
ebiltegia.mondragon.edu:8080 <1%

28 Publication
Kwang-Ki Lee, Kwon-Hee Lee, Seung-Ho Han. "Use of an orthogonal array based o... <1%

29 Publication
Ravi Prakash Babu Kocharla, B. Raghu Kumar. "Modal Based Sensitivity Analysis o... <1%

30 Internet
ousar.lib.okayama-u.ac.jp <1%

31 Internet
www.slideshare.net <1%

32 Internet
www.studysmarter.co.uk <1%

33 Publication
"Proceedings of the 8th Pacific Rim International Congress on Advanced Material... <1%

34 Publication
Alberto Carpinteri, Pietro G. Gambarova, Giuseppe Ferro, Giovanni A. Plizzari. "Fr... <1%

35 Publication
Christopher Lane. "The Development of a 2D Ultrasonic Array Inspection for Singl... <1%

36 Publication
N. Bićanić, R. de Borst, H. Mang, G. Meschke. "Computational Modelling of Concre... <1%

37 Publication
Sergey A. Yufin. "Geoecology and Computers", CRC Press, 2018 <1%

38 Internet
ebin.pub <1%

39 Internet
www.veqter.co.uk <1%

40 Publication
"ICAF 2019 – Structural Integrity in the Age of Additive Manufacturing", Springer ... <1%

41 Publication
Colin Tong. "Introduction to Materials for Advanced Energy Systems", Springer Sc... <1%

42 Publication
J. Middleton, M. L. Jones, G. N. Pande. "Computer Methods in Biomechanics & Bio... <1%

43 Publication
Poursaeidi, Esmaeil, and Hosein Bakhtiari. "Fatigue crack growth simulation in a f... <1%

44 Publication
Xiaolei Wu, Yuntian Zhu. "Heterostructured Materials - Novel Materials with Unpr... <1%

45 Internet
archive.org <1%

46 Internet
docplayer.net <1%

47 Internet
iaeme.com <1%

48 Internet
pmc.ncbi.nlm.nih.gov <1%

49 Internet
www.frontiersin.org <1%

50 Internet
5dok.org <1%

51 Publication
Modern Cold Spray, 2015. <1%

52 Internet
dokumen.pub <1%

53 Internet
gyan.iitg.ernet.in <1%

54 Internet
repository.up.ac.za <1%

55 Internet
theses.hal.science <1%

56 Internet
www.jstage.jst.go.jp <1%

57 Publication
Mudassar Hussain Hashmi, Seyed Saeid Rahimian Koloor, Mohd Foad Abdul-Hami... <1%

58 Internet
engmatl.com <1%

59 Internet
standards.iteh.ai <1%

60 Internet
yetl.yabesh.ir <1%

61 Publication
Wei-Ze Wang, Fu-Zhen Xuan, Kui-Long Zhu, Shan-Tung Tu. "Failure analysis of the ... <1%

62 Internet
patents.google.com <1%

63 Publication
Pooja Rani, Atul K. Agrawal. "Fatigue Life Evaluation of a Low-Pressure Stage Stea... <1%

64 Internet
ir.canterbury.ac.nz <1%

65 Internet
theses.lib.polyu.edu.hk <1%

66 Publication
E. Poursaeidi, M. Salavatian. "Fatigue crack growth simulation in a generator fan ... <1%

67 Publication
Kyle S. Williams, Rijul R. Chauhan, Kenneth Cooper, Nathaniel Thomas, Karim Ah... <1%

68 Publication
L Bian. "Fatigue life prediction of the plates with an inclined surface crack", Inter... <1%

69 Publication
Loveleen Kumar Bhagi, Vikas Rastogi, Pardeep Gupta, Swastik Pradhan. "Dynami... <1%

70 Publication
Mark A. Bradford, Russell Q. Bridge, Stephen J. Foster. "Mechanics of Structures a... <1%

71 Publication
Park, Youngchul. "Hierarchical Finite Element Method for the Prognostic Analysis ... <1%

72 Publication
Ratilal, Raiyani Hitesh. "Experimental Investigation on Fracture Characteristic of ... <1%

73 Publication
Roman Drozdowski, Lutz Völker, Markus Häfele, Damian M Vogt. "Numerical and ... <1%

74 Publication
Taoufik Hachimi, Najat Zekriti, Rajaa Rhanim, Hassan Rhanim, Fatima Majid. "Cha... <1%

75 Internet
amslaurea.unibo.it <1%

76 Internet
escholarship.org <1%

77 Internet
www.research-collection.ethz.ch <1%

78 Publication
"Fatigue of Materials at Very High Numbers of Loading Cycles", Springer Science ... <1%

79 Publication
Amit Aherwar, Catalin I. Pruncu, Binnur Sagbas, Luciano Lamberti. "Advanced Tec... <1%

80 Publication
B. Staniša, V. Ivušić. "Erosion behaviour and mechanisms for steam turbine rotor ... <1%

81 Publication

Chang-Sheng Lin, Hung-Tse Chiang, Chuan-Hsing Hsu, Ming-Hsien Lin, Jui-Kai Liu, ... <1%

82 Publication

Hi-Keun Lee, Hyung-Sik Yang, So-Keul Chung. "Environmental and Safety Concern... <1%

83 Publication

Lecture Notes in Mechanical Engineering, 2014. <1%

84 Publication

Manvir S. Kushwaha. "Electronic, optical, and transport properties of semiconduc... <1%

85 Publication

McCloskey, Thomas. "Steam Turbines", Dekker Mechanical Engineering, 2003. <1%

86 Publication

Md Washim Akram, Md Hasanuzzaman, Md Naimur Rahman Antu, Tasnia Pasha. ... <1%

87 Publication

Seyed Ali Hosseini, Mohammad Ghodrati, Esmail Lakzian, Heuy Dong Kim. "Passiv... <1%

88 Publication

Sushila Rani, Atul K. Agrawal, Vikas Rastogi. "Failure analysis of a first stage IN73... <1%

89 Publication

Tom Proulx. "Engineering Applications of Residual Stress, Volume 8", River Publis... <1%

90 Publication

Wang, Le. "Quantifying Welding Residual Stresses and Their Evolutions Under Cyc... <1%

91 Publication

Wenjun Yang, Yinhao Wang, Jichen Li, Junfeng Hao, Jiran Gao. "Failure analysis of ... <1%

92 Publication

Yanyan Huang, Zizhen Yang, Jie Yang, Siyuan Zhang, Lingling Fan, Xuguang An, Li... <1%

93 Internet

dspace.plymouth.ac.uk <1%

94 Internet

link.library.deakin.edu.au <1%

95 Internet
vdoc.pub <1%

96 Internet
www.grafiati.com <1%

97 Internet
www.mrforum.com <1%

98 Publication
"Advances in Design, Simulation and Manufacturing III", Springer Science and Bu... <1%

99 Publication
"Advances in Materials Processing", Springer Science and Business Media LLC, 2020 <1%

100 Publication
Christopher Sagrillo, Leland Shimizu, Vinay K. Goyal. "Elastic-Plastic Fracture Mec... <1%

101 Publication
Ferreira, João Pedro Mota. "Pre-Strain Effects on Fatigue Crack Propagation Beha... <1%

102 Publication
Fusheng Wang, Zheng Wei, Pu Li, Lingjun Yu, Weichao Huang. "Initial Crack Propa... <1%

103 Publication
Gelfi, M.. "X-ray diffraction Debye Ring Analysis for STress measurement (DRAST): ... <1%

104 Publication
He Liu, Jianzhong Sun, Shiying Lei, Shungang Ning. "In-service aircraft engines tu... <1%

105 Publication
John Stringer. "Coatings in the electricity supply industry: past, present, and oppo... <1%

106 Publication
Lijie Qiao, Keyun Feng. "Failure analysis of the low-pressure blade lacing wire in s... <1%

107 Publication
Loveleen Kumar Bhagi, Vikas Rastogi, Pardeep Gupta. "Study of corrosive fatigue ... <1%

108 Publication
Mehta, Mehul Gunvantrai. "Development of Al-LM25-Fe3O4 MMC and It's Charact... <1%

109	Publication	Perkins, K.M.. "Corrosion fatigue of a 12%Cr low pressure turbine blade steel in ... <1%
110	Publication	Rajesh K Bhamu, Aakash Shukla, Satish C Sharma, S P Harsha. "Vibration Respons... <1%
111	Publication	Ritu Raj Singh. "Silicon Nanowire Optical Waveguide Sensors: Design and Analysis... <1%
112	Publication	Z XIAOPENG. "A new formula for estimating fatigue crack propagation rates", Int... <1%
113	Internet	duepublico.uni-duisburg-essen.de <1%
114	Internet	files01.core.ac.uk <1%
115	Internet	ir.jkuat.ac.ke <1%
116	Internet	journal.mtu.edu.iq <1%
117	Internet	konferencia.unideb.hu <1%
118	Internet	masing.masfak.ni.ac.rs <1%
119	Internet	sapphire.ph.utexas.edu <1%
120	Internet	worldwidescience.org <1%
121	Internet	www.amrita.edu <1%
122	Internet	www.apmiinternational.org <1%

123 Internet
www.i-scholar.in <1%

124 Internet
www.m.growingscience.com <1%

125 Internet
www.semanticscholar.org <1%

126 Internet
www.testinglaboratory.org <1%

127 Publication
"Proceedings of the 10th International Conference on Energy Engineering and En... <1%

128 Publication
A. Gomes Correia, Fernando E.F. Branco. "Bearing Capacity of Roads, Railways an... <1%

129 Publication
Abid Hossain Khan, Md. Shafiqul Islam. "Prediction of thermal efficiency loss in n... <1%

130 Publication
Ardeshir Sarmast, Jan Schubnell, Johannes Preußner, Manuel Hinterstein, Eva Car... <1%

131 Publication
Boris A. Rozenberg, Grigori M. Sigalov, Marina Z. Aldoshina, Yurii B. Scheck. "Hete... <1%

132 Publication
Chakherlou, T.N.. "Investigation of the fatigue life and crack growth in torque tig... <1%

133 Publication
E. Goli, H. Bayesteh, S. Mohammadi. "Mixed mode fracture analysis of adiabatic c... <1%

134 Publication
Edward Miller. "Plastics Products Design Handbook - Part B Processes and Design... <1%

135 Publication
Folker H. Wittmann, Desiderius G.H. Latzko, Brian Tomkins. "Structural Mechanic... <1%

136 Publication
Guanghui Yang, Guangcan Yang, Qingbo Chen, Tianen Cao, Shujie Hu. "Research ... <1%

137 Publication
Heping Xie, Yuehan Wang, Yaodong Jiang. "Computer Applications in the Mineral ... <1%

138 Publication
High Performance Computing in Science and Engineering 11, 2012. <1%

139 Publication
J A Hesketh. "Effects of Wetness in Steam Turbines", Proceedings of the Institutio... <1%

140 Publication
John P. Dakin, Robert G. W. Brown. "Handbook of Optoelectronics - Concepts, Dev... <1%

141 Publication
Jun Yin, Pengfei Li, Xiaodan Li, Feng Guan, Jiacheng Wu, Sailan Wang, Guang Yang... <1%

142 Publication
L. Patriarca, M. Filippini, S. Beretta. "Short-crack thresholds and propagation in a... <1%

143 Publication
Maktouf, Wassim, and Kacem Saï. "An investigation of premature fatigue failures ... <1%

144 Publication
Nan Guofang, Yao Xia, Yang Sirui, Yao Jingya, Chen Xu. "Vibrational responses an... <1%

145 Publication
Neil Petchers. "Combined Heating, Cooling & Power Handbook: Technologies & A... <1%

146 Publication
Pengfei Hu, Qingqiang Meng, Wei Fan, Weifei Gu, Jie Wan, Qi Li. "Vibration charac... <1%

147 Publication
Rajesh Kumar Bhamu, Aakash Shukla, Satish C. Sharma, S. P. Harsha, Pawan Kum... <1%

148 Publication
Roy Nichols, Genki Yagawa. "Structural Mechanics in Reactor Technology - Fractu... <1%

149 Publication
S. Can Gülen. "Gas Turbine Combined Cycle Power Plants", CRC Press, 2026 <1%

150 Publication
Sasaki Toshihiko, Toshiyuki Miyazaki, Hamiru Ito, Takashi Furukawa, Tsuyoshi Mi... <1%

151 Publication
Sayed A. Nassar, John H. Bickford. "Handbook of Bolts and Bolted Joints", CRC Pre... <1%

152 Publication
Schönbauer, Bernd M., Stefanie E. Stanzl-Tschegg, Andrea Perlega, Ronald N. Salz... <1%

153 Publication
Srinivasan Gopalakrishnan, Ramesh Babu Jangala. "Advanced Modeling Methods ... <1%

154 Publication
Takahito Goshima. "THERMOMECHANICAL EFFECTS ON CRACK PROPAGATION IN ... <1%

155 Publication
Thermal Spray Fundamentals, 2014. <1%

156 Publication
Unarine Ramakokovhu, Dawood Desai, Glen Snedden, Tamba Jamiru. "Significanc... <1%

157 Publication
V Giannella. "Fatigue crack-growth predictions for a railway axle under material ... <1%

158 Publication
V. Dakshina Murty. "Turbomachinery - Concepts, Applications, and Design", CRC P... <1%

159 Publication
V. Giannella, R. Citarella, M. Perrella, V. Shlyannikov. "Surface crack modelling in ... <1%

160 Publication
V. Shlyannikov, R. Yarullin, M. Yakovlev, R. Citarella, V. Giannella. "Mixed-mode cr... <1%

161 Publication
W Hu, H Miah, N.S Feng, E.J Hahn. "A rig for testing lateral misalignment effects i... <1%

162 Publication
Wei Guo, Ke Li, Zhigang Fang, Tao Feng, Tianwen Shi. "A sustainable recycling pro... <1%

163 Publication
Wu, D.Y.. "Self-healing polymeric materials: A review of recent developments", Pr... <1%

164 Publication
Xing Wang, Xuehui Zhang, Yangli Zhu, Xinjing Zhang, Wen Li, Haisheng Chen. "Eff... <1%

165 Publication

Y. Sakai. "Advanced geothermal steam turbines", Elsevier BV, 2022 <1%

166 Publication

Yasutomo Kaneko. "Mechanical design and vibration analysis of steam turbine bl... <1%

167 Publication

Zengzhi Wei, Xingyuan Liang, Lei Wang, Zhicheng Yuan, Lijun Wu. "Practical limit... <1%

168 Internet

assets-eu.researchsquare.com <1%

169 Internet

diva-portal.org <1%

170 Internet

dr.ntu.edu.sg <1%

171 Publication

du Toit, Ronald G.. "A Stochastic Hybrid Blade Tip Timing Approach for the Identif... <1%

172 Internet

etda.libraries.psu.edu <1%

173 Internet

hrcak.srce.hr <1%

174 Internet

hull-repository.worktribe.com <1%

175 Internet

iapws.org <1%

176 Internet

ijcsi.pro <1%

177 Internet

ijream.org <1%

178 Internet

ir.library.nitw.ac.in:8080 <1%

179 Internet

research-information.bris.ac.uk <1%

180 Internet

sig3.ecanews.org <1%

181 Internet

theses.fr <1%

182 Internet

www.biomaterials.org.in <1%

183 Internet

www.citethisforme.com <1%

184 Internet

www.e3s-conferences.org <1%

185 Internet

www.nature.com <1%

CHAPTER 1

INTRODUCTION

1.1 Motivation and Introduction

Thermal power plants are capable for producing majority of all the world's electricity as they generate constant, dependable, dispatchable, and base-load type power irrespective of climate conditions. Thermal power plants can produce high volumes of base-load type power due to availability of large reserves of fuel and using the established technology based on Rankine Cycle through steam turbines. Thermal power plants can provide consistent power and meet base-load requirements; these characteristics, along with the widespread availability of existing thermal power plant infrastructure, contribute to their continued dominance as the world’s primary source of electricity. Hence, thermal power plants are the predominant source of electricity due to their high reliability, long history of operation, and compatibility with the existing electrical grid.

Electricity serves as the backbone of modern industrialized economies, enabling technological innovation, facilitating large-scale manufacturing, laying the foundation of infrastructures including health care, transportation/mobility,

agriculture, information and communication technology, consumer house holdsand therefore, promoting economic and social development. In 2026, according to International Energy Agency (IEA), global electricity usage reached 29,000 TWh, indicating a worldwide trend toward increasing electrification among both established and developing economies. The IEA predicts that electricity demand will grow annually at a rate of 2-3% for the next 20 years due to expanding global population, urbanization, digitalization and increased utilization of electric vehicles and resource intensive industries.

Fig. 1.1 illustrates installed power generation capacity, a key indicator of India's transition from a predominantly conventional to a renewable energy mix. Thermal power plants based on coal fuel are the country's primary source of energy. At 221.6 GW, coal remains the leading form of energy, accounting for 47.2%, while oil/gas contributes only 5.5% of the total at 25.8 GW, primarily to support peak loads and serve as backup to other energy sources. The renewable energy sector has shown significant increases with Solar energy at 102.5 GW (21.8%), Wind energy at 48.6 GW (10.3%), and large hydro at 46.5 GW (9.9%). Biomass and Small hydro account for smaller amounts of decentralized energy generation, at 11.4 GW and 5.1 GW, respectively. Nuclear Power accounts for 8.2 GW of installed capacity, providing low-carbon base-load support on a much smaller scale than other energy sources. Fig.1.1 clearly indicates that India is highly reliant on coal-based thermal power to meet its increasing energy demands.

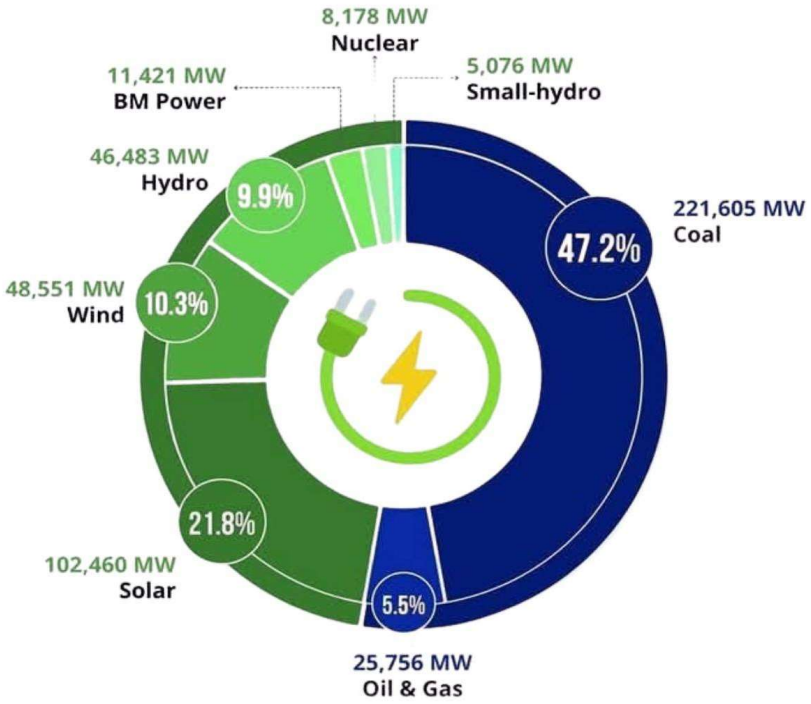

Figure 1.1: Share of electricity production by fuel type *(NITI Aayog, 2023)*

In steam turbines, its blades are the critical component as they experience the largest degree of centrifugal, vibrational, and thermo-mechanical loads among other turbine components.

184 The structural integrity of blades is essential to determine the overall performance, reliability, and safety of the turbine. Catastrophic failure of blades in steam turbine results in reduced operating efficiency of the unit and substantial financial losses. In Low-pressure blades of steam turbine, researchers have found that the primary mode

61 of failure is high cycle fatigue due to large number of vibration cycles. Therefore, it is essential to predict the fatigue failure mechanisms of the steam turbine blades in order to increase its fatigue life, optimize its performance and reduced the forced shutdowns of steam turbine due to blade failure, which results in huge economical losses.

Analysis of turbine blade failures has emerged as a rapidly developing field of interest to both researchers and industry professionals alike during the past few decades. Turbomachinery engineers have been working to identify and understand the underlying reasons for blade failures on all forms of turbines, and to implement practices that will reduce the occurrence of un-scheduled outages.

1.2 Review of Literature

An extensive literature is available in the form of journal articles, conference proceedings, review paper and technical books explaining the reasons of failure of steam turbine blades. The literature review is divided into four sections. The first section presents a comprehensive review of literature available in research papers and scholarly articles, focusing on identifying metallurgical investigations and failure mechanism in steam turbine blades by utilizing experimental techniques. The second section provides a critical review of journal articles and other archival literature, emphasizing experimental techniques employed to evaluate the residual stresses in steam turbine blades. The third section highlights the review of literature from journal articles and technical reports to assess the dynamic behavior of LP steam turbine blades by utilizing computational techniques. The fourth section provides the review of literature reported in journal articles and scholarly articles, for crack growth simulation and fatigue life prediction in LPST blades to identify the fatigue crack initiation and propagation in computational approach for crack growth simulation and fatigue life prediction in LPST blades.

1.2.1 Metallurgical investigation

To identify the causes of low-pressure (LP) steam turbine blade failure, interdisciplinary and multidisciplinary methodologies must be employed, combining materials science, mechanical response, and environmental interaction. Blades in the L-0 or last-stage region of LP turbines experience extreme environmental conditions, including high centrifugal forces, cyclic stresses, wet-steam erosion, and corrosive condensate. These stresses/forces cause complex failure mechanisms, including corrosion-fatigue, stress-corrosion cracking, erosion-corrosion, and creep-fatigue interaction, and therefore cannot be completely simulated using computer models.

Scanning electron microscope (SEM) is mostly used to examine and characterize the fractural topography including fatigue striations; inter-granular cracking; and pitting on the fractured surface. Energy-Dispersive X-ray Spectroscopy (EDS) is used for detailed compositional characterization and assist in identifying deleterious contaminants such as chloride, sulphide and oxide that contribute to localized corrosion. Further, metallography helps researchers to identify the effect of thermal and mechanical exposure on microstructure involving degradation at grain boundaries; increase in size of carbide precipitates; phase transformation.

Researchers employed metallurgical techniques to evaluate various causes of failure in turbine blades over the past several decades. Also, findings of these metallurgical investigations provide the basis for evaluating Fatigue life of turbine blades.

Das et al.,(2003) investigated a low-pressure final stage steam turbine blade through metallurgical techniques such as SEM & EDX. They found pits that serves as crack

initiation sites for inter-granular cracks, which progressed due to cyclic operational loads. They have resulted that the steam turbine blades failed due to a combination of crevice corrosion and mechanical fatigue.

Mukhopadhyay et al., (2001a) investigated the LPST blade to evaluate its failure mechanism using different techniques including SEM & EDX, Vickers indentation and three-point bend tests. They have found that the fretting occurred at the blade lacing interface results into weak spots for initiation of cracks, which propagate due to excessive vibration from fluctuating frequency conditions. It is resulted that the steam turbine blade failed due to poor brazing, corrosion and dynamic stresses.

Wang et al., (2007) studied a low-pressure turbine blade, which failed after 13,200 cycles. On visual inspection, it is observed that the cracks are originate at inner arc face of the suction side. They have concluded that these fatigue cracks are due to stress concentrations at various geometric features of the turbine blade. Therefore, they have suggested to change the tempering temperature and the curvature of the blades to prevent future failures.

Kubiak Sz. et al., (2007) examined the failure mechanism of a blade root of 350 MW steam turbine. On visual examination they identified the crack formed within the blade root area due to high localized stresses, which are generated from the root geometry of the blade as well as contact between the blade and rotor disc. It is deduced that the blade failure is due to investigated between the contact surface of the blade root and rotor fastening.

Mazur et al., (2008) collected a failed last-stage low-pressure turbine blade and analyzed it to find the root causes of its failure through different techniques including

SEM-EDS and finite element modeling. It is found that the primary cause of blade failure was high-cycle fatigue, aggravated by fretting wear at the blade root during resonant vibration. They concluded that combined effect of dynamic stresses and fretting wear resulting into failure of turbine blade.

Kim, (2011) identified the primary cause of crack initiation in the fourth-stage blade of a LPST blade. In this research, Non-destructive evolution methods, including ultrasonic testing and visual examination, were employed to assess the extent and severity of the cracks. The results indicate that combined effect of high-temperature interaction and mechanical stresses result in the formation of crack in turbine blade.

Katinić and Kozak, (2018) presented the fracture investigations of the two adjacent rotor blades through fractography and computational modeling. It is resulted that the primary cause for blades failure was corrosion-fatigue, arising as a result of synergistic effect of cyclic stresses and chloride induced corrosion pitting in the phase transition region.

Wei et al., (2020) presented the corrosion fatigue crack mechanism found in 17-4PH blade of low-pressure rotor of a steam turbine. They found that in a steam environment, potassium ions (K^+) and chlorine ions (Cl^-) interact physically, chemically, and electrochemically with the turbine blades to produce localized corrosion pits, which act as stress concentrators and site for crack initiation that propagate on further loading, resulting into failure of turbine blade.

Yang et al., (2021) investigate a failed last-stage turbine blade using optical microscopy, SEM, and mechanical testing to identify its failure mechanism. They concluded that microstructural in homogeneities, specifically coarse and fine

martensitic microstructures, which are developed due to poor heat-treatment processes. These microstructures in homogeneities act as localized stress concentrators that contribute to crack formation which propagates on further loading and results into failure of turbine blade.

Sarim Khan et al., (2022) investigated the failure mechanism of a failed LPST blade made of AISI 420 steel. They determined that the presence of shallow corrosion induced pits n and varied loading conditions resulting into formation of fatigue cracks at the regions of vulnerability that leads to the abrupt turbine blade failure.

Rivaz, et al.(2020) examined the 410 stainless steel blade which failed after operating life of 165000 hours through metallurgical techniques. They observed the corrosion pits that contain oxides and chlorides, which act as stress concentrator and provide site for crack initiation that propagate during cyclic loading. Additionally, inter-granular crack propagation and fatigue striations are observed that accelerate corrosion-fatigue fracture in turbine blade.

Rani and Agrawal, (2022) examined a 210 MW last-stage LPST blade undergoing 1,52,241 hours of working to identify the critical location of damages that leads to its failure. The blade is analyzed through visual examination, chemical analysis, metallurgical analysis and Non-destructive testing (NDT) techniques. It is determined that major cause of blade damage is water-droplet erosion near the blade edges that creates erosion pits, which act as stress concentrations regions and probable crack propagation sites, posing a high risk of catastrophic failure.

Graciano et al., (2023) developed a methodology integrating fatigue testing, numerical simulation, and modal analysis to estimate blade's life. This research demonstrated

that changes in natural frequencies and damping coefficient alarming the initiation of cracks that leads to failure of blade. A hybrid approach combining random vibration analysis and the Palmgren–Miner rule is used to predict cumulative fatigue damage of blade.

Gao et al., (2024) investigated the crack formation mechanisms and evaluated corrosion fatigue behavior in the last stage rotor blade of steam turbine using metallography, SEM analysis and rotary bending corrosion fatigue test. They found that crack initiation occurred at the erosion-corrosion pits and crack propagation occurred into two stages initial inter-granular propagation of crack was due to stress corrosion and later trans granular propagation of cracks was due to corrosion fatigue. Rotary bending testing further supported that high frequency induction quenching improved the micro hardness and water corrosion resistance of the surface material blade material.

1.2.2 Residual Stress Evaluation

Residual stresses have a significant influence on the assessment of blade failure. The residual stress is a key factor in influencing the formation and progression of cracks in turbine blades (You *et al.*, 2017). It affects the susceptibility of blades to fatigue and corrosion, which ultimately leads to fracture of blade (Bendeich *et al.*, 2006). Therefore, it is necessary to accurately evaluate the residual stresses for reliable design and maintenance of steam turbine blades. Researchers have employed X-ray diffraction technique to identify areas of high stress concentration, that act as site for crack initiation. After observing stress concentrated zones, researchers have

implemented targeted mitigation strategies such as stress-relief treatments or material modifications, which reducing the risk of crack initiation (Ramakokovhu *et al.*, 2021). In this research work, Residual Stresses of L-0 LPST blade made up of X10CrNiMoV12-2-2 a martensitic stainless-steel alloy is evaluated using X-ray Diffraction (XRD) with Cos α Method. Residual stresses induced during blade manufacture or developed over time during service are measure during X-ray Diffraction (XRD) with Cos α Method. These residual stresses often serve as initiators for crack development when they interact with environmental or operational loading conditions. This integrated methodology serves as a tool for the assessment of blade material degradation that leads to failure of the blade.

Gelfi et al., (2004) introduced a novel method for evaluating residual stresses by using Debye ring analysis for stress measurement (DRAST), to address the shortcomings of conventional XRD methods, such as longer measurement time, alignment errors and variation in penetration depth during stress analysis of thin films and complex geometries. The DRAST method focused on a two-dimensional XRD experiment, where strain is calculated from Debye ring distortion exhibits a similar linear relationship with $\sin^2\Psi$ as observed in the traditional XRD technique. They concluded that DRAST method presents a fast, reliable, and an effective way for residual stress measurements in both thin films and bulk materials.

LaRue and Daniewicz, (2007) highlighted the impact of residual stresses on fatigue crack growth using elastic superposition and closure-based modelling techniques including plasticity-induced crack-closure concepts. They identified significant uncertainties in the adjacent threshold crack growth region. They concluded that

fatigue crack growth prediction requires precise experimental evaluation near threshold regions and validation of these results to show the stability and reliability of different approaches used to evaluate fatigue crack growth.

James et al., (2010) investigated the effects of shot peening as a surface enhancement technique to introduce compressive residual stress in steam turbine blade material, thus improving their fatigue resistance. They employed X-ray diffraction techniques to quantitively asses the residual stress profiles created by shot peening technique. Their results revealed that shot-peening process effectively generated beneficial compressive residual stresses near the surface and subsequent cyclic loading under fatigue conditions produced time dependent stress relaxation, reducing the long-term effectiveness of the treatment.

Rossini et al., (2012) presented a comprehensive overview of recent advancements in methods for measuring residual stresses in components, to assist researchers in selecting appropriate techniques, including destructive, semi-destructive, and non-destructive approaches, based on their specific applications. They concluded that none of the technique alone is perfect because selection of any particular technique must be controlled by specific geometry of the component, depth of measurement and material penetration acceptable level and hence, suggested that hybrid approaches offered enhanced reliability.

Bhagi et al., (2018) investigated the effect of residual stress on a fractured L-1 LPST blade using a two-dimensional X-ray diffraction method with a portable μ-X360 FULL 2D X-ray residual stress analyzer. They observed that the turbine blade surface exhibited randomly oriented crystal grains, as indicated by uneven diffraction intensity

across the Debye ring. It is concluded from FWHM plot that a major contributing factor to blade failure is induced tensile stresses resulting due to vibrations occurred by operating the turbine at high RPM.

1.2.3 Static Structural and Dynamic Analysis

A steam turbine is exposed to critical dynamic forces which experiences unsteady flow and centrifugal forces. One of the prime factors of failure in the steam turbine blade is vibration persuasion fatigue *(Mohan et al., 2014)*. Fluid flow in the steam turbine blade induced vibrations. When the blade starts to vibrate with large amplitude, resonance occurred, resulting in catastrophic failure of turbine blade *(Sanvito et al., 2012)* Researchers have performed vibration analysis of steam turbine blade either computational or experimentally for finding the impact of vibrations on steam turbine blades (Zhao *et al.*, 2018a). The evaluation of blade's natural frequencies is a major concern for the safe functioning of the steam turbines. Campbell diagrams were used to determine the critical conditions for resonance when the exciting frequencies of turbine blades were close to their natural frequencies.

In this research, the static structural and dynamic analysis of a LPST blade has been done computationally through finite element-based software *ANSYS*®. Static structural analysis is performed to measure the stress distributions and locate the critical region susceptible to failure under operating conditions. Dynamic analysis of LP steam turbine blade is performed to evaluate the natural frequencies so that resonance conditions could be avoided during operation. Campbell diagram is drawn to find critical speed corresponding to the intersection of the fundamental frequency

with harmonic excitation lines to prevent resonance, hence prevent catastrophic failure of turbine blade.

(Saxena *et al.*, 2015) investigated the failure of low-pressure turbine blade through mechanical testing, metallographic analysis, and finite-element modeling. In this study, they found that cracks originated near the boss area along the concave face of the blade and continued to propagate downward along the root and into the pin areas. Their findings revealed that, excessive vibrational stresses and stress concentrations resulting into fatigue cracking. Also, combined effects of dynamic loading conditions and design characteristics contributed in the blade failure.

Shukla and Harsha, (2016) performed the dynamic analysis of normal and a cracked LPST blade to predict their dynamic behavior computationally using *ANSYS* software and experimentally by conducting NFT (Natural frequency test) and analyzing the harmonic spectrum obtained from the Natural frequency test Graph natural frequencies for different modes are obtained for normal and cracked blades. It is observed that some intermediate high peaks are observed prior to the third frequency mode particularly in case of cracked blade. These intermediate frequency peaks may be harmful. On comparing computational results of normal and cracked blade, they found that there is continuous reduction in natural frequency is observed in the cracked blade compared to normal blade across different modes and these change in natural frequency is more visible at higher modes.

Rani et al., (2019) performed vibration analysis of first stage gas turbine blade to detect its dynamic characteristics i.e modal frequencies, mode shapes and damping coefficients using vibration analyzer OROS and Global rational fraction polynomial

method (GRFP). Also, the blade is analyzed to extract its dynamic characteristics computationally. On comparing natural frequencies obtained experimentally and computationally they found that the natural frequencies ae almost same with an error percentage of 1%. They have also discovered that the areas of stress concentration observed on leading and trailing edges in the computational model of failed blade at the 6^{th} mode is well supported by the cracked region observed on leading and trailing edges of a real case failed turbine blade which offers grounds to infer that the blade has been failed due to resonance at 6^{th} modal frequency.

Zhao et al., (2018b) analyzed LPST blade of a nuclear power plant both theoretically and experimentally to predict its dynamic behavior. Natural frequencies and mode shapes of the blade are evaluated statically and dynamically by considering centrifugal force and steam flow forces using finite element *ANSYS* software. Further, the natural frequencies are valuated experimentally by performing vibration test. They discovered that the predicted values of finite element are close to the experimental natural frequencies. Also, fretting wear was observed along the concave root surfaces near the trailing edge of the blade, which can be attributed resonant vibration. Normal fatigue patterns are observed on the fracture surface of the cracked blade Based upon these observations, they resulted that the blade failure is primarily attributed to a combined influence of high cycle fatigue (HCF) and fretting wear.

Rodríguez et al., (2019) examined the LPST blade made up of martensitic stainless steel AISI 410 blade to find the reasons for crack initiation and propagation under normal operation and resonance conditions experimentally and computationally. A spectrum analyzer was used to perform the experimental test and *ANSYS* was used to

perform numerical simulations. On analyzing the results, it is claimed that under resonance conditions, the presence of crack reduces the natural frequency of the blade and increase displacement amplitudes, which promotes crack propagation over fewer cycles causing reduction in the fatigue life of the blade. The outcome showed that centrifugal loading, associated with high stress levels may lead to the creation and dissemination of crack.

Cano et al., (2019) analyzed the failure mechanism of the last stage (L-0) blade of a 110 MW output steam turbine by using numerical and analytical models of turbine blades based on mean stress correction, Strain life and Morrow and Smith Watson Topper (SWT). The findings demonstrate that high stresses induced by centrifugal loading promote initiation and growth under low-cycle fatigue(LCF) conditions. Further, they reported that SWT model provides more accurate predictions for damage detection in steam turbine blades.

Shetkar and Srinivas, (2021) purposed a structural modal approach using the Ryleigh-Ritz method for evaluating the vibration characteristic of FG (Functionally Graded) LPST blade. They found that vibrational analysis for standard FG (Functionally Graded) blade using FEM methods is costlier, whereas purposed structural model approach provides results with higher accuracy and at reduced cost. The results further indicated that increase in angular velocity leads to increases in the natural frequency of the FG blade in both flap wise and chord wise modes. A higher twist angle reduces chord-wise frequency and increases flap wise frequency.

Hafshejani et al., 2025) analysed L-2 stage LPST blade by simulating it in5-stages, to investigate its root causes of its failure. They used *ANSYS* CFX for simulating the blade

in 5-stages and the results of its relation are analysed using Navier-Stokes equations and conjugate heat transfer as the governing equations, together with the SST (shear stress transport) turbulence model. They observed that working at part-load conditions and at increased condenser pressure leads to vortex formation on the steam turbine blades. These vortices resulting into vibrations on the turbine blades, which can create cracks at the weak points of the blade that ultimately results into blade failure and considerable losses.

1.2.4 Fatigue Analysis

Fatigue analysis is vital to predict the fatigue life of the blade and used as a tool for finding the root causes in the reduction of the fatigue life of turbine blades. Conventional fatigue analyses rely on experimental techniques such as the stress-life (S-N) method, strain-life (ε-N) method, crack growth models *(Tulsidas, et al. 2014)* that are expensive and have material and sample constraints *(Měšťánek, 2008)*. Consequently, researchers switched on computational simulation methods such as finite element modeling (FEM) and extended finite element modeling (XFEM) to predict intricate behavior of turbo-machinery *(Bayesteh and Mohammadi, 2011, Chen et al., 2022)* Software tools such as *ANSYS* and ABAQUS are widely used to model the intricate stress distributions and thermal gradients experienced by turbine blades under operating conditions (Salehnasab and Poursaeidi, 2020). Simulations of turbine blades carried out using these software tools provide critical insights into crack initiation and its growth that ultimately leads into catastrophic failure of the turbine blade.

Perkins and Bache, (2005) inspected the failed specimen via optical and scanning electron microscopy (SEM) to identify the influence of inclusions such as oxides and sulphides on the fatigue life of a Low-pressure turbine blade made up of X12CrNiMoVNb steel which is designated as FV566. It is observed that the presence of inclusions causes the significant decrease in fatigue life of turbine blade.

Kovacs, Beck and Singheiser, (2013) performed the fatigue test under uniaxial stress at 20 kHz on ultrasonic fatigue testing machine to investigate the fatigue behavior of a martensitic steel X10CrNiMoV12-2-2 alloy at different loading conditions ranging from R = 1 to R = 0.7 at room temperature. They observed “fish-eye” fractures that forms due to the transition from surface to internal crack initiation at oxide inclusions. Further, it is stated that increase in mean stress results in the reduction of fatigue strength. Hence, it is suggested to include mean stress in turbine blade design as it has a significant impact on fatigue life of turbine blade.

Hu and Yao, (2013) proposed a novel numerical method to observe fatigue crack growth based on a combination of finite element modeling and analytical solutions for fatigue crack growth. They quote that their method was capable of simulating fatigue crack growth with high accuracy. It is concluded that this method used as a robust and computationally efficient tool, which is helpful to predict crack path of a specimen subjected to cyclic loading as well as its fatigue life.

Xue et al., (2014) analyzed a nuclear power plant's LPST blade metallurgic ally and computationally to find the root causes of its failure. They revealed that there was low clearance between the turbine blade and disk. This low clearance develops sliding motion and resulting into fretting wear during operation. Electron Dispersive

Spectroscopy(EDS) analysis detected the presence of micro-oxide particles at the crack initiation site that also confirms fretting wear of the turbine blade. Further, they analysed the blade computationally to evaluate the stress distribution by a non-linear elastic finite element analysis. It is found that crack initiation site did not aligns with the location of maximum von-misses stresses as crack initiation occurred due to combined effect of fretting wear and high localized stress. They concluded that the blade failed due to the fretting fatigue occurred at the root-disk interface.

Citarella et al., (2016) developed a combined Finite element method (FEM) and Dual Boundary Element Method (DBEM) numerical simulation methodology to demonstrate crack propagation within low-pressure turbine vane segments. The FEM method was utilized to obtain the global stresses, whereas the DBEM method was used to determine the local stress intensity factor values at each point along with the actual crack path. They concluded that the FEM/DBEM coupled solution is an efficient means for modeling three-dimensional mixed-mode crack propagation in turbine vanes as well as a viable analytical tool for predicting fatigue life and assessing the structural integrity of turbine vanes.

Plesiutschnig et al., (2016) analyzed LPST blade made up of martensitic stainless steel. It is observed that when the blade experiences combined centrifugal forces and bending load, the initiated crack at the corrosion pit propagates resulting into regressive vibrations (resonance) that results in severe structural failure of the blade.

Zhang et al., (2017) investigated the crack growth in a gear tooth subjected to experimentally and numerically. The fatigue crack growth experiments were carried out at room temperature employing a servo-hydraulic fatigue testing machine with a

maximum load capacity of 100 KN and torque capacity of 500 N. The numerical finite element simulations were performed using *ANSYS* and FRANC 3D (Fracture Mechanics Software) having same loading conditions as used experimentally. It is resulted that fatigue crack growth was primarily due to Mode I Stress intensity factor, and also observed that the stress intensity factor is directly proportional to the fatigue crack length. It is concluded that simulated crack growth results show good agreement with the experimental measured crack lengths. Both the simulated and experimental results indicate a gradual crack growth initially, followed by a rapid increase in crack propagation rate as approaches near 1,44,000 cycles confirming the validity of the simulation model.

Yang et al., (2017) proposed a linear elastic fracture (LEFM) based algorithm for simulating three-dimensional fatigue crack growth under non-proportional mixed-mode loading. Investigated the crack propagation behavior in thin-walled, hollow cylinders containing a notched specimen under combined non-proportional cyclic tension and torsion loading using finite element software ABAQUS together with the three-dimensional fracture analysis software FRANC 3D. Their results showed a change in fracture mode from tensile to shear with the crack path length lying between the predictions of Maximum Tensile stress criteria (MTS) and Maximum shear stress criteria(MSS). Fatigue life estimated using Paris law and effective stress intensity factors showed good agreement with experimental results at low loading levels. However, at higher loads the simulation slightly overestimated fatigue life due to faster crack growth observed experimentally near the notch region.

Escalero et al., (2018) proposed a methodology to inspect cracked wind turbine bearing rings. A hole created into 42CrMo4 steel plate experienced Mode-I cyclic loading. Different approaches as per BS 7910: 2013 fitness-for-service code were employed. The growth of a hole edge to crack was predicted analytically. By consider Failure Assessment Diagram (FAD) as a failure criterion, the result indicated fatigue life was over predicted by 3.96% in the best-case scenario, while the estimation of critical showed an error of less than 3%.

Kuželka et al., (2019) applied fracture mechanics approach for Fatigue Crack growth simulation (FCG). They used Paris Law, ΔK_{th}, K_{IC}, FCG based on ABAQUS for simulation of rotor section of a steam turbine. It is concluded that growth of crack in the rotor blade groove axial direction is more than two times than in rotor tangential direction.

Kocharla et al., (2022) developed a finite element model of low-pressure last stage steam turbine blade to evaluate model parameters and stress intensity factor under the influence of crack for critical loading. Further they plot Campbell diagram of the blade was analyzed to determine the resonance condition during start/stop operation of the turbine blade to estimate final crack length that occur during crack propagation before catastrophic failure of the blade. Further vibration-based condition diagnostic approach is employed to identify the crack prior to reach the maximum crack length at the blade root.

Yuan et al., (2026) analyzed the low-pressure rotor blade of the steam turbine cracked at fir tree part of the blade and subjected to 70,000 cycles to find reasons of its failure. The cracked blade examined to various metallurgical techniques including optical

microscopy, scanning electron microscopy and energy-dispersive spectroscopy also determined the mechanical properties of the blade including tensile strength and hardness of the blade were also evaluated. Further, computational model analysis of the blade is carried out to evaluate stresses, strains and vibrational characteristics. It is observed that the actual crack site resembles with the location of maximum stress. During the operation of steam turbine, a gap is created between fir tree part of the blade and rotor due to vibrations resulting into wear which leads to surface degradation in the contact region. Under the combined effects of multiple stress component and vibration, fatigue cracks initiate from the damage surface, propagate under further loading and eventually lead to fracture at the fir-tree part of the steam turbine blade.

Subramanian et al., (2026) investigated a last stage X20Cr13 turbine blade of a 600 MW thermo-electric plant subjected to 42000 cycles through mechanical and metallurgical techniques such as fractography, EDX analysis, tensile test, impact test, wet fluorescent magnetic particle inspection, Computational dynamic analysis to find the root causes of its failure. Fractographic results reveal tempered martensitic morphological structure It is concluded that fatigue cracks are created due to presence of various non-metallic inclusions material defects and not due to vibrations.

1.3 Research Gaps

After rigorously literature review, it is observed that numerous studies have been conducted to understand the failure mechanism of steam turbine blades using both mechanical and metallurgical techniques including fractography, computational analysis and simulation, experimental investigations. These techniques are used on failed blades to determine causes of blade's failure and to locate the regions of high

stress concentration. However mostly, these studies are focused mainly on crack initiation and stress distribution but a detailed prediction of fatigue crack propagation in complex geometries is often limited. Residual stresses have a substantial impact on the initiation and growth of cracks in turbine blades but in many studies their influence has not been thoroughly investigated using advanced techniques such as X-ray diffraction (XRD) with the cos-alpha method. This research provides experimental evaluation of residual stresses using X-ray diffraction (XRD) technique. As a result, the contribution of residual stresses on the failure of turbine blade is not always fully understood.

Conventional numerical investigations typically rely on finite element tools such as *ANSYS* to determine static and dynamic stresses in turbine blades. Despite their effectiveness in stress distributions and locating critical stress regions, but they have limited capability in simulating three-dimensional fatigue crack growth under cyclic loading conditions. As a result, accurate prediction of crack growth path and crack growth life solely based on finite element analysis is difficult.

Another limitation in the existing literature is the limited use of specialized fracture mechanics tools capable of accurately simulating crack growth. Software such as FRANC3D provides the capability to model three-dimensional crack propagation and to evaluate stress intensity factors, which are essential for fatigue crack growth analysis. However, its integration with conventional finite element simulations has rarely been applied in the analysis of LPST blade failures.

To address these gaps, the present study adopts an integrated experimental and computational approach for the analysis of a failed LPST blade. Experimental

techniques including SEM fractography, EDS analysis, and residual stress measurement using XRD (cos-alpha method) are used to locate the crack, its initiation and propagation mechanism, to understand the blade's material characteristics. Static structural and dynamic analyses of LP steam turbine blade are performed using *ANSYS,21* software to determine the regions of maximum stresses and strains, vibration characteristics including modal frequencies and mode shapes. Furthermore, a hybrid computational approach is employed using *ANSYS,21* and FRANC3D to simulate fatigue crack growth and predict crack propagation paths. This integrated methodology provides a more realistic understanding of the fatigue failure behavior of LPST blades.

However, a comprehensive review of the existing literature reveals several critical areas that remain insufficiently explored or inadequately addressed. These research gaps are summarized as follows:"

- While extensive research exists on the failure analysis of low-pressure steam turbines, but no research yet focused on to understand the failure mechanism Low-Pressure (LP) steam turbine blades manufactured from material X10CrNiMoV12-2-2 martensitic stainless steel.
- Only a limited number of researchers have evaluated and investigated the effect of residual stresses on the failure of LPST blades using the X-ray diffraction technique, specifically employing the "cos α" method.
- While numerous researchers have conducted computational analysis of steam turbine blades, but none of them focused on computational analysis of LPST

blade made up of material martensitic stainless X10CrNiMoV12-2-2 to locate crack, its initiation and propagation.

- Various researchers have proposed methodologies for the fatigue life assessment and enhancement of turbine blades; but there has been limited research on the fatigue analysis and life assessment of Low-Pressure (LP) steam turbine blade made up of material X10CrNiMoV12-2-2 martensitic stainless steel alloy.

1.4 Research Objectives

Based on a comprehensive review of the literature, the primary objectives of the research work presented in this thesis are as follows:

- To investigate the root cause of failure of an L-0 LPST blade experimentally with a real case.
- To evaluate residual stress for the fractured surface of a LPST blade and to examine its effect on the failure of the turbine blade.
- To design a computational framework to assess the dynamic behavior of a LPST blade.
- To study the fatigue analysis and life assessment of a LPST blade.

1.5 Contribution of the Present Research Work

This study integrates experimental investigation and advanced simulation to analyze fatigue failure mechanism in LPST blades of a 210 MW thermal power plant. The collected failed blade is from the 29th stage and made up of stainless material martensitic stainless steel. The cracked blade is examined through

different metallurgical techniques comprising visual inspection, optical microscopy, scanning electron microscopy (SEM) with energy-dispersive spectroscopy (EDS) and mechanical techniques including to evaluate hardness of the blade on Vickers hardness testing machine, evaluating residual stresses on PULSTEC, μ-X360 machine using X-ray diffraction (XRD) cosα method.

Static structural and dynamic analysis of a LPST blade is carried out using finite element-based software *ANSYS* to determine regions of maximum stresses and strains, vibration characteristics including modal frequencies and mode shapes. Static structural analysis used to evaluate stress distributions and identify locations prone to failure under operational loading conditions. Dynamic analysis of LP steam turbine blade is performed to determine the natural frequencies and assessed potential resonance conditions that could be avoided during operation. Campbell diagram is constructed to identify critical speed at the intersecting fundamental frequency with the harmonic's lines to avoid resonance, hence prevent catastrophic failure of turbine blade.

In this research work, a hybrid simulation approach integrating *ANSYS* and FRANC 3D software is introduced and applied to investigate fatigue crack growth behavior of a crack in LPST blade. In this approach, the stress intensity factors K_I, K_{II}, K_{III} are evaluated and stress intensity factor (K_I) is considered as the parameter for checking the stability of the crack. When the stress intensity factor (K_I) exceeds the material toughness (K_C), the crack becomes unstable and start propagating on its own till the catastrophic failure of the blade happen. This research highlights and utilized different mechanical and metallurgical

methodologies to investigate the failure mechanism of a failed LPST blade. Further these methodologies may also be used to provide foundation for predictive maintenance, enhancement of fatigue life and optimization of design parameter of turbine blades.

1.6 Organization of the Thesis

The chapter of the thesis outlines as follows. *First chapter* provides the introduction and background of the research along with a comprehensive review of previous studies pertaining to failure of turbine blades. In addition, the chapter include research gaps, objectives and contribution of this research work. *Second chapter* presents a comprehensive overview of steam turbines including their classification, construction and working principles. The chapter also discusses the fundamental aspects associated with the failure of low-pressure (LP) steam turbine blades and methodologies adopted to understand the failure mechanism. The third chapter focuses on the investigation of root causes of failure of a failed L-0 LPST blade made up of material X10CrNiMoV12-2-2 collected from a 210 MW thermal power plant. Failure analysis includes detailed metallurgical examinations by using Scanning Electron Microscopy (SEM) and Energy-Dispersive X-ray Spectroscopy(EDX*). Fourth chapter* presents the assessment of residual stresses of LPST blade using non-destructive technique X-ray diffraction (XRD) based on cos α method. *Fifth chapter* deals with the static structural and dynamic analysis of LP steam turbine blade through *ANSYS* software to identify the stress concentrations regions vibration characteristics including modal frequencies and mode shapes that may contribute to blade failure. *Sixth chapter* focuses on fatigue crack growth behavior of a crack in LP steam turbine blade. A hybrid simulation

approach integrating *ANSYS,21* and FRANC 3D is introduced and applied to investigate fatigue crack growth behavior of a crack in LPST blade and for checking the stability of the crack. *Chapter Seven* concludes the thesis and presents the scope and impact of the research.

turnitin Page 44 of 178 - Integrity Submission Submission ID trn:oid:::29034:134939416

CHAPTER -2

REASONS OF FAILURE OF LPST BLADE

2.1 Fundamental and background of steam turbine

Steam turbines are recognized as a major advancement in engineering, playing a crucial role in modern power generation and energy conversion system. The major function of a steam turbine is to generate mechanical rotational energy from the thermal energy contained within high-pressure, high-temperature steam. The mechanical energy generated by a steam turbine is transformed to electric energy via a synchronous generator.

Steam turbines are also the primary source of mechanical power as thermal power plants produces approximately 60-65% of the world's total generated electrical energy. Apart from conventional thermal power plants, steam turbines are the crucial component in nuclear power plants and combined cycle diesel power *plants (Darwish, et al., 2010)*. The modern concept of the steam turbine was pioneered by Sir Charles Parsons in 1884, marking a major advancement in power machinery *(Guy and Parsons, 1939)*.Steam turbines eventually replaced reciprocating steam engines

because they offered significantly better thermal efficiency, smoother operation, and a much higher power-to-weight ratio. Since that time, they have been relied upon as the primary source of power due to their mechanical efficiency and reliability of operation over long periods, as well as their ability to provide large amounts of base-load power. The basic principles governing the operation of a steam turbine are based on both thermodynamic and fluid-dynamic processes *(Lesiuk, 2020)*.

A coal-fired thermal power plant is shown in Fig. 2.1, the steam generated in the boiler is heated to a temperature of around 500-5500C before being supplied to the turbine. When this superheated steam hits the turbine blades, it transfers its energy to the turbine *(Chaplin, 2009)*.

A steam turbine is composed of multiple stages formed by a sequence of stationary (stator) blades and rotating (rotor) blades arranged alternatively along the flow of steam path. The stator blades, mounted on the turbine casing, guide the steam and increases its velocity, ensuring that it strikes the rotor blades at the desired angle for effective energy transfer. On the other hand, rotor blades convert the energy of the steam into rotational motion of the rotor. The stator blades not only guide and control the steam flow, but also facilitate in the conversion of pressure energy into steam energy, ensuring that the steam reaches the next rotor stage with required velocity for efficient operation. The rotor contains multiple stages of moving blades that engage with high-energy steam guided by stationary nozzles, thereby producing the torque required for driving the generator *(Neilson, 1908)*.

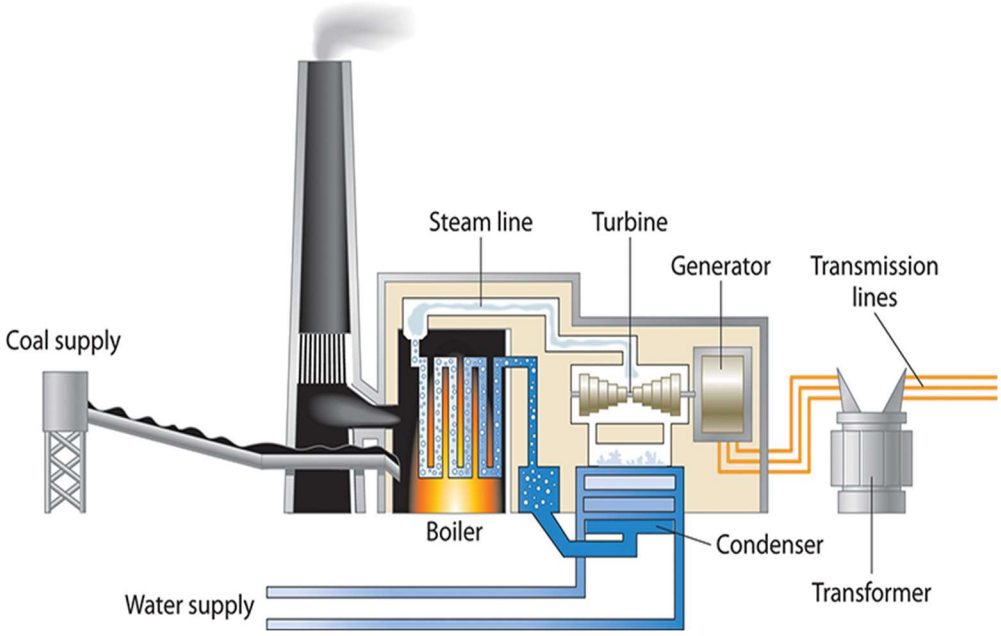

Figure 2.1: Schematic representation of coal-fired thermal power plant (*Fedorova*, 2018)

As the steam enters the turbine it undergoes expansion which resulted in gradual reduction of temperature and pressure, along with the corresponding increase in specific volume. To handle the increasing volumetric flow of steam, the blade height is progressively increased in the further stages of turbine. As a result, a considerable variation in blade geometry is observed between the initial high-pressure stage to later final Low-pressure stages *(McCloskey, 2003).*

Turbine blades operate under extremely demanding conditions, as they are subjected to a complex combination of mechanical, thermal, and environmental loading in all parts of a turbine (Navinesh *et al.*, 2020). Therefore, their operation reliability, structural integrity, and the duration of maintenance downtime are all crucial factors. The overall efficiency and safety of a steam turbines are directly related to the mechanical integrity and aerodynamic design of the turbine blades *(Ruchert, 20*

et al., 21). During operation, the blades experience significant centrifugal stresses due to high rotational speeds, along with the fluctuating aerodynamic loads resulting from continuous interaction with high-velocity steam flow *(Bhagi et al., 2018*). Thermal transients result in thermal gradient-induced stresses. Additionally, aggressive chemical environments exist in the low-pressure area of the turbine, where many corrosion-causing elements are present. Therefore, blades degrade rapidly through various mechanisms, including fatigue, corrosion fatigue, stress corrosion cracking, erosion, and fretting (Niu *et al.*, 2018). Blade failure can result in the complete loss of generating capacity for extended periods, and even cause secondary damage to other equipment in the system, leading to very costly losses (Yang *et al.*, 2021). This chapter provides a basic understanding of steam turbines including the operating environment of steam turbine and classification of steam turbines. This chapter presents an overview of various stages of steam turbine and discusses the characteristics of the materials used in each stage. The primary reasons for LP turbine blade failures are then discussed in detail. The final part of this chapter describes the methodologies used for investigating LP turbine blade failures. These methodologies are the basis for the experimental and analytical work presented in the further chapters of this thesis.

2.2 Classification of Steam Turbines

Steam turbines can be classified on the five principle bases, (a) According to the mode of steam action (b) According to the direction of flow of steam (c) According to the exhaust conditions (d) According to the number of stages, (e) According to the steam pressure, as shown in Fig. 2.2 given below

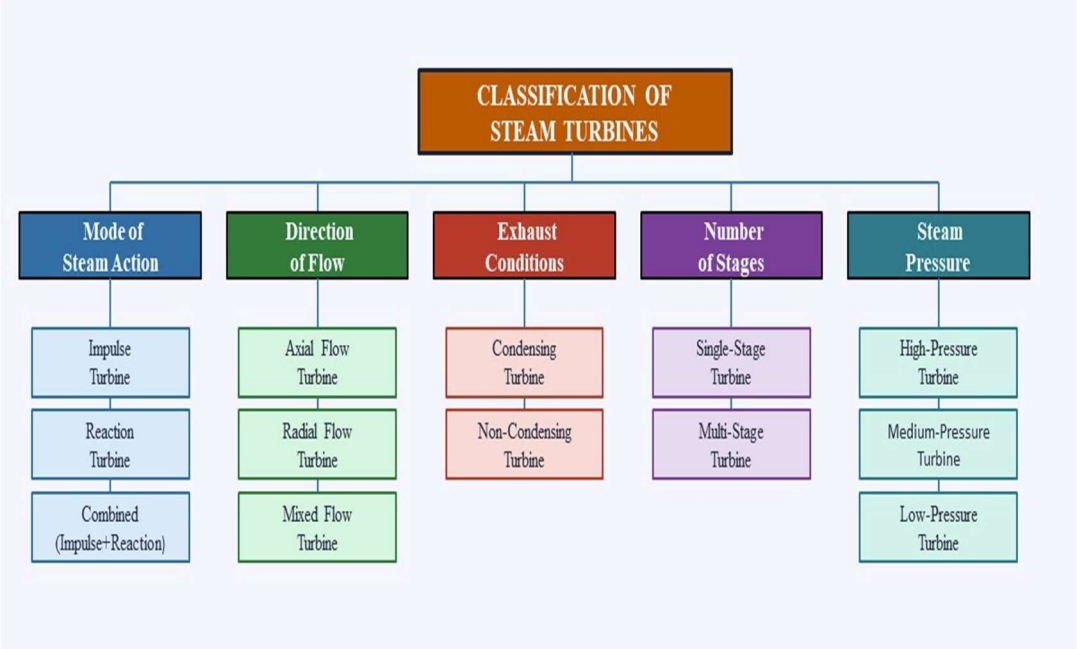

Figure 2.2: Classification of steam turbines

Steam turbines are generally divided into two broad types according to the manner in which the steam expands and gives up its energy to the rotor blades.

2.2.1 Impulse Turbines and Reaction Turbines.

(a) Impulse turbine: In the case of an impulse turbine, all of the pressure drop of the steam takes place in the stationary nozzles prior to entering the rotating (moving) blades *(EMS Machines, 2024)*. The nozzles transform the thermal energy of the high-pressure steam into high-velocity kinetic energy. Then, once the high-speed steam jet impacts the rotating blades, it changes the blades' momentum, generating an impulsive force that turns the rotor.

The pressure of the steam flowing over the rotating blades remains relatively unchanged while its velocity changes. The rotating blades are symmetrically designed

and primarily function as flow deflectors, bearing no significant pressure loads. As a result, because there is little to no pressure drop across the rotating blades, the passages through the blades are not completely sealed; therefore, the turbine does not require a pressure-tight casing surrounding each row of blades. Due to their mechanical simplicity and ability to operate effectively in high-pressure, low-mass-flow applications, impulse turbines are ideal for smaller-scale turbines as well as the high-pressure stages of larger-scale power-generating units *(Luthman Jr, 2017)*. However, due to the extremely high velocity at which the steam travels, impulse turbines suffer significant erosion and losses, limiting their efficiency as a means of producing large amounts of electricity on their own.

(b) Reaction turbine: A Reaction Turbine works using the continuous expansion of steam through stationary and moving blades, which causes a decrease in pressure through each row of blades. Torque is generated by a combination of Impulse and Reaction forces due to changes in steam momentum and pressure as it passes through the moving blades. The turbine features alternating rows of stationary blades, fixed to the casing and acting as nozzles, and moving blades attached to the rotor drum. Uniform steam admission is provided over the entire annular path, providing equal energy distribution over the length of the blade span *(Peng, 2007)*. As steam passes through each stage of the turbine, its pressure continues to drop while its specific volume increases. As this occurs, the height of the blades and the rotor diameter for subsequent turbine stages will also need to be increased to accommodate the greater steam volume. Because the steam continues to expand through all the various stages of the turbine, which can have multiple stages, the reaction turbine can achieve very high efficiencies and is therefore used extensively in the lower- and mid-pressure areas

of large steam turbines used for electrical generation *(Chaplin, 2009)*. Reaction turbines, especially those in the LP area of the turbine, have the most complexity in terms of stress (pressure loading, wet steam, etc.) and fatigue potential as compared to the other areas of the turbine due to the combined effect of these factors (Singh *et al.*, 2020) .

A comparative view of these types of systems is appropriate for the practical application of power plants, as modern steam turbines do not operate solely on either impulse or reaction type. As such, they use combinations of each: impulse (high-pressure) and reaction (intermediate- and low-pressure) type blades. The combination of both types enables the best possible energy recovery over a broad range of pressure and flow rates, providing an optimal balance between the turbine's efficiency, structural integrity, and blade life *(Mazur et al, 2009)*.

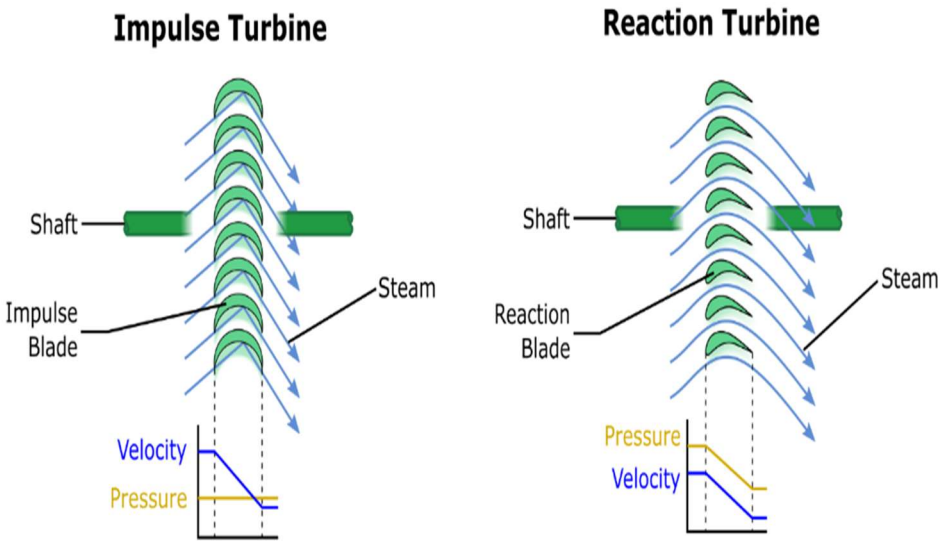

Figure 2.3: Flow behavior of steam: Pressure and velocity changes in Impulse and reaction turbine *(Chaplin et al., 2009)*

2.2.2 According to steam pressure

The primary division of a modern steam turbine includes the low-pressure (LP), intermediate-pressure (IP), and high-pressure (HP) turbine stages. The primary reason for these divisions is to capitalize on the significant differences in steam pressure, temperature, and specific volume as it expands continuously from boiler conditions to a condenser vacuum *(Leyzerovich, 2021)*.

2.2.2.1 High Pressure (HP) turbine

The initial turbine stage is the high-pressure (HP) turbine stage, which receives hot, superheated steam at high pressure and temperature. Since the specific volume of steam is relatively small at this stage, the height of the blades is short, and the flow area is compact. The primary purpose of the HP stage is to begin converting the energy of the steam and maintain control over thermal growth and stress *(Binner et al., 2013)*. Blades in the HP stage are thick and heavy-duty in order to support extreme thermal gradients and high steam forces. Although thermal stress and creep are the major design issues with respect to HP blades, fatigue failure is less likely, as there is significantly less blade length and therefore less amplitude of vibration *(Tanuma, 2022)*

2.2.2.2 Intermediate pressure (IP) turbine

Steam is expanded partially in the HP turbine, and is then usually reheated and sent into the intermediate-pressure (IP) turbine stage. Steam pressure and temperature are reduced, yet remain high compared to the LP stage. The reheating process enhances overall cycle efficiency and reduces the amount of moisture formed in subsequent

stages. As steam flows through the IP turbine, the specific volume of the steam increases significantly, which requires longer blades and larger flow areas. The IP stage will experience a combination of thermal, centrifugal, and dynamic loading, making blade vibration an increasingly important concern (Chen *et al.*, 2009) Therefore, the intermediate-pressure (IP) forms a transitional zone were aerodynamic performance and structural dynamics, demands a balanced approach.

2.2.2.3 Low-Pressure (LP) turbine

The low-pressure (LP) stage is the final and most critical region of the steam turbine blade. In the LP stage, steam undergoes expansion to very low-pressure, close to vacuum pressure level and is subsequently directed to condenser. At this stage, the steam occupies high specific volume per unit mass, making it necessary to employ longer and wider blade to efficiently extract the remaining energy. Therefore, LP blades rank among the largest turbine components, and are subjected to complex loading and high centrifugal forces because of their extremely large size and high rotational speed (*Bhamu, et al., 2021)*. Secondly, the wet steam in LP stage also implies some difficulties like droplet impingement that may result in the erosion of blade surfaces and gradual erosion of blade materials *(Azevedo et al.,2009)* All these factors render the LP stage highly vulnerable to fatigue, corrosion. To enhance operational safety and reliability, advanced design features such as shrouds, snubbers and damping mechanism are incorporated *(Bhagi et al., 2017*).

To conclude, the HP-IP-LP staging design allows effective recovery of energy and it is able to accommodate the large variation in the steam properties over the turbine as shown in Fig. 2.4. The major concern of the HP stage is thermal *(Binner et*

al., 2014) the IP stage is both thermal-mechanical and dynamic effects, and the LP stage is vibrational, fatigue, and moisture-based damage. Such a multi-stage arrangement plays a crucial role in ensuring high-efficiency, extended service life and dependable structural performance in large steam turbine.

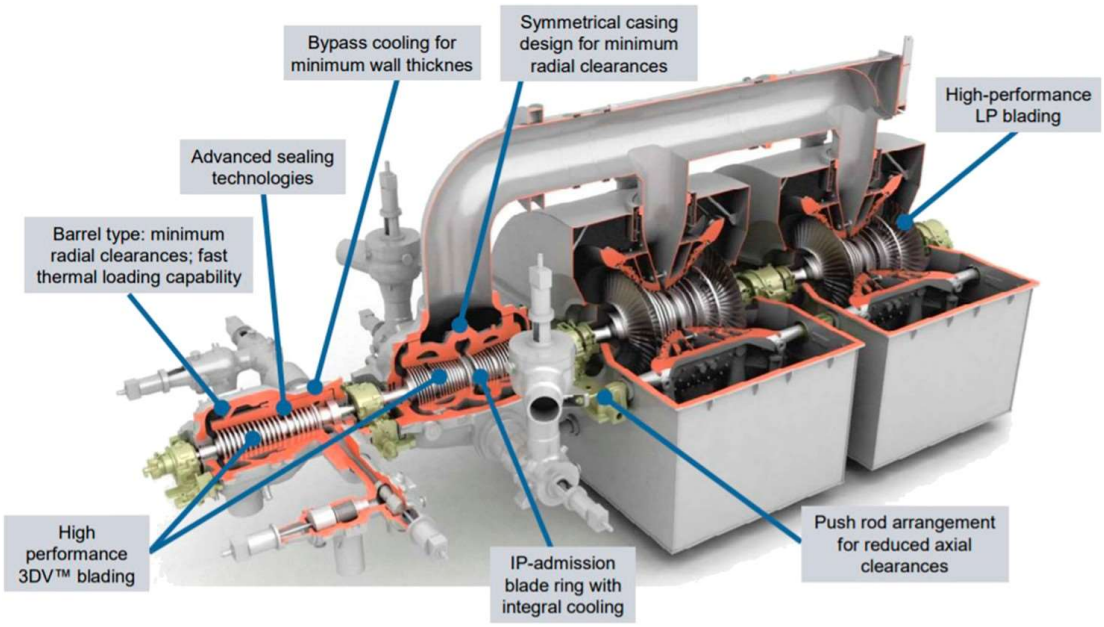

Figure: 2.4 Different stages of steam turbine HP, IP, and LP stages (Cziesla *et al.*, 2009)

2.3 Geometric configuration of LP steam turbine blade

The blade of a turbine may be sub-divided into three major areas: the root, the aerofoil (profile), and the tip as shown in the Fig. 2.5. This is particularly relevant to the design of these areas in the low-pressure (LP) stages since at this point the steam increases significantly in volume as it expands. To deal with such conditions, the aerofoil is extended in length and frequently a gradual twist across the span is taken to provide good interaction with the flow of steam (Liu *et al.*, 2022). The root section has been designed in such a way that it firmly attaches the blade to the rotor and can withstand

the centrifugal forces that are high in the process (He *et al.*, 2020). The tip is modelled in a way to minimize loss and enhance overall performance. It is worth understanding the purpose of each of these areas; thus, the next few sections explain the blade root, aerofoil and tip in more detail.

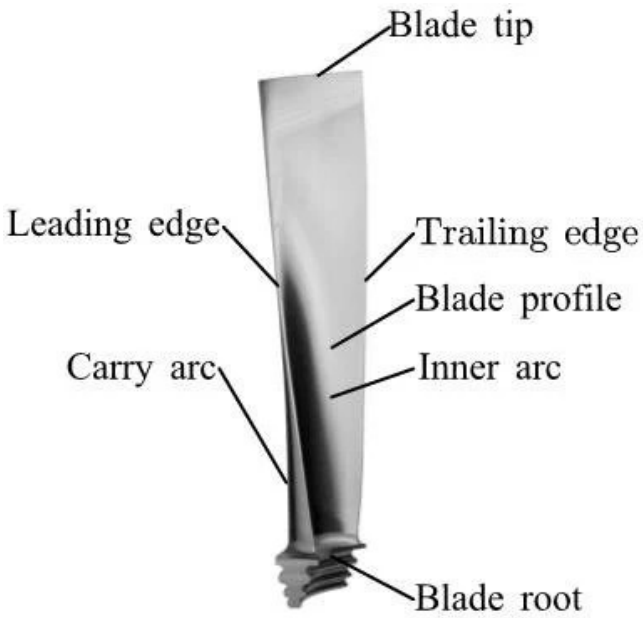

Figure 2.5: Geometric configuration of a twisted Low-pressure steam turbine blade (Ding *et al.*, 2019)

2.3.1 Blade root:

The blade root constitutes the lower portion of the blade and provides the interface for attached to the turbine rotor. It is employed with the attachment configurations such as called as fir-tree, dovetail or T-root which provides secure mechanical interlocking (Shankar, et al. 210). The root region plays a crucial role in transferring centrifugal forces and aerodynamic loads from the blade to the rotor disc. Due to the presence of geometric discontinuities and stress concentrations, this region is particularly

susceptible to crack initiation and requires careful design consideration (Kubiak Sz *et al.*, 2009).

2.3.2 Blade Aerofoil

The geometry of steam turbine blades is based on aerofoil theory, a fundamental principle in both aeronautical engineering and turbomachinery's. The aerofoil region is the main working portion of the blade where steam flows over the curved blade profile, a pressure difference is created, resulting in high static pressure on the concave (pressure) face of the blade, while a comparatively low-pressure region is formed on the convex (suction) side of the blade *(Tanuma, 2017)*. This pressure difference generates a lift force acting perpendicular to the direction of steam flow and this lift force causes the turbine to rotate. The blade has a leading edge which is smoothly rounded to ensure gradual steam entry to minimize the shocks, while the trailing edges is comparatively sharp to allow smooth exit of steam and reduce wake formation *(Shlyannikov, et al. 2014*).

2.3.3 Blade Tip

8

The blade tip is located at the outermost radius and plays an important role in reducing leakage losses between the blade and casing as shown in Fig. 2.4. However, due to the large size of blade, the tip experience maximum peripheral velocity and dynamic loading. From previous studies it has been found that both experimental observation and analytical investigations indicate vibration amplitudes are maximum near the tip of the blade and making it susceptible to resonance-induced damage and fatigue failure *(Mohan, et al. 2014).* In addition, exposure to wet steam results in erosion and pitting

at the tip of the blade, which further acts as a stress raiser and facilitate crack initiation and propagation (Zhang *et al.*, 2017)

2.4 Characteristics and Significance of LP steam turbine blade

The low-pressure (LP) steam turbine is the final and most critical component in the complete steam turbine; it is the part of the turbine where steam undergoes an extreme expansion from intermediate pressures down to vacuum conditions prior to entering the condenser. One of the main characteristics of the LP turbine is the enormous specific volume of steam at low pressure. This means that LP turbine blades are typically much longer and slimmer than those found in the higher-pressure sections of the turbine. Also, the area of the annulus between adjacent blades increases progressively along the flow path. Therefore, LP turbine blades – especially the last stage or "L-0" blades – are the longest moving parts in the turbine. While they may be relatively cool compared to other parts of the turbine, they are subjected to extreme centrifugal force, large amounts of steam deflection, and considerable vibrational stress, creating significant challenges to the design of LP turbine blades *(Mukhopadhyay et al., 2001).*

52

A further characteristic of the LP turbine is the existence of wet steam in the latter stages. As the steam continues to expand into the two-phase region, water droplets will continue to develop and hit the blade surface, resulting in erosion, corrosion, and corrosion-fatigue. The presence of wet steam, combined with the long length of LP turbine blades and their relatively low stiffness, makes them particularly susceptible to high-cycle fatigue, resonance, and cracking at the roots, shroud, or

attachments (*Jonas*, 1985). To counteract some of these problems, LP turbines often employ advanced design techniques, including shrouded blades, snubbers, lacing wires, and damping systems, in addition to carefully selecting the natural frequency of the turbine to prevent vibration due to flow-induced forces *(Kaneko et al., 2022)*.

The importance of the LP steam turbine stems from both its ability to generate energy and its impact on the overall reliability of the turbine. The LP turbine operates at low pressure; however, it extracts a significant fraction of the remaining thermal energy available in the steam. In a number of large electric power-generating stations, the last LP stage accounts for 10–15 percent of the total power generated by the turbine. The improved efficiency of the LP turbine has a direct impact on the pressure inside the condenser (i.e., backpressure) and, consequently, on the overall thermal efficiency of the Rankine cycle (*Gülen*, *2021*). A small loss of flow in the LP section of the turbine results in a corresponding decrease in electrical generation and an increase in heat rate. From a reliability and maintenance standpoint, the LP turbine is the most failure-prone component in the steam turbine. The combination of long blades, the cyclic loading they experience, vibration, and the wet-steam environment encountered by LP blades results in the majority of reported blade failures in power plants occurring in the LP stages. Therefore, detailed studies of the aerodynamics, structural dynamics, fatigue behavior, and residual stresses in LP turbine blades are necessary for their design and the prediction of their remaining useful life.

2.5 Material used in Steam turbine blades

Steam turbine blades operate under a wide range of thermo-mechanical stresses and environmental conditions. Therefore, the selection of optimal material for steam

turbine blades is a challenging task, as it involves the optimization strategy encompassing material strength, resistance to creep, resistance to corrosion, process ability and cost feasibility *(Rivaz, et al. 2020)***.** Over the past few decades, advancement in material engineering have resulted in the development of high-performance alloys designed for stage-specific operating conditions. Among these, martensitic stainless steels have been widely adopted material for LPST blades due to their optimal combination of mechanical strength, fracture toughness and corrosion resistance *(Ruchert et al., 2024)*.

2.5.1 Engineering material used in steam turbine blades

The material employed in steam turbine blades can be broadly categorized and selected on the basis of their material composition and operational conditions of different turbine stages are tabulated in table 2.1

Table 2.1 Material used in different stages

Turbine stage	**Operating conditions**	**Common material used**	**Properties required**	**Applications**	**Reasons of failure**
High Pressure (HP) stage	High Temperature (500-600^{0}c), High Pressure (100 – 250 bar),dry steam	Ferritic–martensitic steels (9–12% Cr steels, Nickel-based superalloys, Austenitic stainless steels	High creep strength, High temperature stability, oxidation resistance	Initial stages of utility and thermal power plant turbines	Creep deformation due to prolonged exposure to high temperature; thermal fatigue caused by start-stop cycles; oxidation-induced

					material degradation
Intermediate pressure stage (IP)	Moderate Temperature range (350–500°C), Moderate Pressure (20 – 100 bar)	Martensitic stainless steels (11–13% Cr)	High strength, good fatigue resistance, moderate corrosion resistance	Centre stages of steam turbine	Creep–fatigue interaction, thermal fatigue and oxidation-assisted degradation, with vibratory stresses contributing to fatigue damage
Low-Pressure (LP Stage	Low Temperature (30–300°C), Low-Pressure (0.05–20 bar)	Martensitic stainless steels, Advanced martensitic steels	Erosive wear resistance, corrosion resistance, high fracture toughness, reduced material density	Low-pressure (LP) stages of large-scale steam turbines, thermal and nuclear power plants	Liquid droplet erosion, Corrosion and erosion interaction, high centrifugal stresses and fatigue under combined centrifugal and vibratory stresses, corrosion fatigue, stress concentration

129

The material selection and design of steam turbine blades differ considerably in high-pressure (HP), intermediate-pressure (IP), and low-pressure (LP) stages. Mainly due to expansion of steam and variations in thermal and pressure conditions. As steam undergoes expansion from high-pressure to low-pressure regions, a significant increase in its specific volume occurs. As a result, larger blade dimensions are

required, along with changes in geometry, structural characteristics, and material requirements.

2.5.1.1 Types of material used in High-Pressure (HP stages) steam turbine blades

Blades in the high-pressure (HP) stage, are comparatively short in length and compact, as the steam entering this stage possesses high pressure and temperature but low specific volume. In HP stages materials are required to have creep resistance, oxidation resistance, and ensure microstructural stability under prolonged service conditions. Accordingly, the materials employed in this stage are carefully selected to provide high-temperature strength along with resistance to thermal degradation. Generally, the choice of the materials to be used in the HP stage is determined by their capacity to withstand severe thermal and mechanical loading conditions and resist creep deformation, oxidation and thermal fatigue to provide dependable operation over the most demanding thermodynamic condition in the turbine (Hurd *et al.*, 2005). Below are the materials used in HP stage of a steam turbine

(a) ATI 720 Alloy: ATI 720 is a nickel-based high strength, precipitation-hardening alloy that was originally developed as industrial gas turbine blades. (Aruna Prabha *et al.*, 2023) It was considered as a candidate of HP steam turbine blades in this study due to its high tensile and fatigue strength at high temperatures.

(b) Waspaloy: Waspaloy is a nickel-based superalloy that has a high thermal stability, creep resistance, and oxidation resistance in the high operating temperature with precipitation hardening. (Aruna Prabha *et al.*, 2023) discovered that Waspaloy was the best thermal and fatigue-resistant material of all materials considered in their study,

including ATI 720 and Inconel 725, as it performed better under high operating conditions due to its thermal stability and creep resistance *(Ahmed et al., 2022)*.

(c) Molybdenum TZM (Titanium-Zirconium-Molybdenum): TZM is a molybdenum alloy that has a higher recrystallization temperature, creep strength and tensile strength compared to pure molybdenum, typically made by either powder metallurgy or arc-casting (Aghajani Derazkola *et al.*, 2025). It has been chosen due to its outstanding high temperature mechanical stability.

(d) INCOLOY® Alloy 903: INCOLOY® alloy 903 (UNS N19903) is an age-hardened nickel–iron–cobalt alloy having high strength with a consistent low coefficient of thermal expansion and modulus of elasticity (Liu *et al.*, 1995). Its thermal cycling stability in dimensions renders it applicable in HP blade applications.

(e) INCONEL® Alloy 725: INCONEL® alloy 725 (UNS N07725) is a corrosion-resistant nickel–chromium–molybdenum–niobium alloy that may be age hardened to achieve exceptionally high strength (Aruna Prabha *et al.*, 2023). Its corrosion resistance and age-hardenability enable it to be a good candidate in high-pressure steam applications.

2.5.1.2 Types of materials used in intermediate-pressure (IP) stage

With the growth and release of steam to the intermediate-pressure (IP) stage, the pressure decreases and the specific volume increases, and results in a moderate increase in the length of the blade relative to the HP stage. The middle-pressure (IP) in the steam turbine is an operating zone being at the condition of reheated steam, and the temperatures are relatively high, although the pressure is decreased compared to

the high-pressure one. This means that the materials to be employed in this stage have to offer a balanced creep resistance, fatigue strength and oxidation resistance and also structural reliability at the cyclic thermal and mechanical load.

Cr -Mo -V low alloy steels are among the most commonly used types of materials in the IP stage. These steels have been historically used as they possess reasonable high-temperature strength, good toughness and the cost-effectiveness. Chromium is better at increasing oxidation resistance and molybdenum at increasing creep strength and higher temperature resistance to softening. Vanadium also enhances strengthening of the precipitation by the formation of stable carbides which enhances overall mechanical performance. In modern turbine designs, 9–12% chromium martensitic steels have increasingly replaced conventional low alloy steels. These materials exhibit superior oxidation resistance, improved creep strength, and better resistance to creep–fatigue interaction (*Dudova*, 2022). The presence of a tempered martensitic structure, strengthened by a uniform distribution of fine carbides, ensures improved microstructural stability during long-term operation at higher temperatures and under repeated cyclic loading.

Moreover, modified or enhanced martensitic steels with refined alloy compositions are also being employed in order to enhance performance across the IP stage further (*Lucacci*, *2017*). Additions of tungsten and niobium lead to improvement of creep resistance and microstructural stability and refined and stable microstructure is guaranteed by controlled heat treatment processes. These materials are especially applicable in the high-efficiency turbine when the service conditions are adverse.

In general, the material employed during the IP stage has to be chosen in order to provide a good balance of high-temperature strength, creeping-fatigue interaction resistance, and oxidation resistance to allow the reliable functioning in the intermediate thermodynamic conditions.

2.5.1.3 Types of Materials Used in Low-Pressure (LP) stage

The low pressure (LP) turbine blades responsible for extracting a significant portion of energy from the steam flow are more prone to failure than those in intermediate pressure (IP) and high pressure (HP) blades. As the steam passes from HP to LP, the volume expands to 150 times so that's why LP turbine blades are large in size. LP blades are generally 1m long, highly twisted and slender, with large tip diameters. They are subjected to substantial centrifugal forces due to their length and rotational speed. These blade operate in a moist steam environment, typically around 120°C while rotating at 3000 rpm. LP blades must possess high toughness, excellent corrosion resistance, and resistance to liquid droplet erosion (*Adnyana*, 2018) . The most widely used materials in this stage are martensitic stainless steels containing 10–13% chromium, which provide a favourable combination of strength and environmental resistance.

Also, titanium alloys are employed in particular Low-pressure (LP stage) turbine blades, especially in large size thermal power plants and nuclear power plants (Gialanella *et al.*, 2020). The characteristics of these materials include low density resulting in less centrifugal loading in long blades and high ratio of strength to weight that allows an increase in structural performance. Titanium alloys are also noted to have good resistance to corrosion and erosion in moist and saline environments as a

result of the formation of protective and stable oxide coating *(Agripa et al., 2019)*. Moreover, they possess titanium blades which are resistant to fatigue and are also stable to mechanical integrity when subjected to cyclic loading. The above properties make titanium alloys to be very appropriate in the latter stages of turbines where the blade length and content of moisture are high (Bhattacharjee, Saha and Williams, 2017). Their relative expensiveness and complexity in manufacture, however, restrict their very extensive use in comparison with the martensitic stainless steels.

Overall, the materials to be used in the LP stage are chosen according to their strength against the erosion, corrosion and fatigue in the moisture-saturated environment where the advanced martensitic stainless steels alloy like X10CrNiMoV12-2-2 are the most commonly adopted materials, with titanium alloys being used in the specialized applications where lightweight and excellent corrosion resistance property of the solution is required.

2.6 Root Causes of Failure in Low Pressure Turbine Blades

The damage of LP steam turbine blades is controlled by the interaction of mechanical, environmental, material and operational factors, of which corrosion fatigue and vibratory stresses are the most significant. Damage is generally critical at stress concentrations such as the blade root, leading edge and joints, where cracks are likely to initiate and propagate (Graciano *et al.*, 2023). Table 2.2 shows the summary of LPST Blade Failure: Causes, Signs and Locations

Table 2.2 Summary of reasons of LP steam turbine blade failure

Failure reasons	**Root cause/ Primary**	**Key Parameters**	**Critical regions of the blade**
Corrosion-fatigue	Interaction of cyclic stresses with wet steam containing chlorides, oxygen, impurities	Corrosion pits, inter-granular cracks, reduced fatigue life, fatigue striations with corrosion marks	Leading edge, trailing edge, blade surface, root regions
High-cycle Fatigue (HCF)	Vibratory stresses due to resonance, aerodynamic excitation, flow instability	Fine fatigue striations, crack initiation without plastic deformation, sudden fracture	Blade root-fillets, shroud attachments, mid-span regions
Low-cycle fatigue	Thermal cycling, star-stop operations, load fluctuations	Plastic deformation marks, crack initiation at high-stress zones, shorter fatigue life	Blade root, hub, connection areas
Erosion/ Erosion-fatigue	Droplet impingement, high moisture, poor steam quality	Surface material loss, pitting, thinning of leading edge, rough surface texture	Leading edge, blade tip, outer periphery
Stress-corrosion cracking (SCC)	Tensile stress combined with aggressive chemical environment	Brittle, Inter-granular cracks, little plastic deformation, branching crack patterns	Blade root, stress concentration zones, attachment regions
Material defects/metallurgical issues	Inclusion, improper heat treatment, microstructure inhomogeneity	Crack initiation at inclusions, brittle fracture, Irregular grain structure	Internal regions, root section, forged zones
Design/ geometric effects	Stress concentration due to sharp corners,	Crack initiation at geometric discontinuities,	Fir-tree root, keyways, holes,

	notches, poor geometry	localizes high stress regions	shroud, connections
Operational factors	Off-design operation, poor steam chemistry, overload, frequent cycling	Accelerated wear, corrosion deposits, unusual vibration behaviour, reduced service life	Entire blade, especially high stress and high-moisture regions
Deposition/fouling	Salt oxide deposition from steam impurities	Deposition on blade surface, imbalance, increased vibration, efficiency loss	Blade surface, especially near leading edge and mid span

2.6.1 Corrosion fatigue

Blade degradation of low-pressure steam turbines by corrosion fatigue is a complicated mode of attack that arises from the combined effects of both cyclic mechanical stresses and a corrosive wet steam environment. Later, during the steam expansion, water condensation leads to the formation of dissolved oxygen, chlorides and other contaminants, which favour the development of localised electrochemical reactions on the surface of the blade. These reactions contribute to the formation of corrosion pits that act as stress concentrators and are potential sites for cracks initiation during the cyclic loading (Yang *et al.*, 2021). The cyclic loading is important as it makes the oxide film to break and expose new fresh metal to the corrosive environment, enhancing the localized attack. The cracks, after initiation, propagate with the combined effect of mechanical and environmental factors - often inter-granular, because of the low strength of grain boundaries (Katinić *et al.*, 2019). Other rapid crack propagation processes, which significantly shorten the fatigue life, include anodic dissolution and hydrogen embrittlement (Schönbauer, Salzman and Zhou, 2011). In addition,

impurity, wet dry cycling and microstructure increase the susceptibility to corrosion fatigue. The interaction of environmental degradation and applied loads governs the failure process leading to premature and often catastrophic failure of the blade under loads lower than the design load.

2.6.2 Stress corrosion cracking (SCC)

In the power plant applications, LPST blades commonly fails due to Stress corrosion cracking (SCC). Three factors are required for SCC to occur: a vulnerable material, a corrosive environment and a tensile stress. All three conditions are met in the LP turbine blades *(Lynch, 2019).* The susceptible materials are 12% Cr martensitic stainless steel and 17-4PH precipitation hardened stainless steel, both of which are vulnerable to cracking in the presence of chlorides and sulphides ions (Wei *et al.*, 2020). The dissolved contaminants - chlorides, sulphates and caustic species created by leakage from the steam condensers, contamination in the make-up water and steam impurities are concentrated in the moisture transition zone of the LP turbine by evaporation and condensation in orders of magnitude higher than the concentration in the bulk steam, to create a corrosive environment.

The natural stress on the blades due to centrifugal and bending force is the tensile stress, and it is concentrated at geometrical discontinuities. The initiation of SCC is largely confined to the stress concentration sites - serration flanks of the blade root, shroud tenons, lacing wire holes, pitting corrosion sites and machining marks *(Jones, 2003*). Unless the SCC cracks are detected during routine inspections, they may grow to a critical size where upon a sudden fast fracture may occur under the current centrifugal stress to produce a fragment of the blade, which may have

catastrophic downstream consequences *(Sieradzki et al., 1987)*. It is avoided by both proper control of steam chemistry, i.e. chloride content below 1-5 ppb and oxygen content below 10 ppb, and, in new power plants, the use of chloride-resistant titanium alloys as last stage LP blades.

2.6.3 Erosion induced failures

The erosion-dominated processes and its interaction with fatigue and corrosion, particularly in the moist region of the last stages contributes significantly in the failure of the blades in low-pressure steam turbines. In this region, accelerated water droplets and entrained solids result from the expansion process and continuously impact the blade surfaces. Water droplet erosion is an erosion process due to impinging large water droplets, accelerated to speeds comparable to the blade tip, which impact the blade surface and cause very large stresses and repetitive plastic deformation of the material and subsequent abrasion of the surface (Zhang *et al.*, 2021). On the other hand, solid particle erosion, which can be caused by oxide scales (such as magnetite) formed in the boiler tubes, is a source of additional surface erosion caused by abrasive impact, especially in zones of high steam velocity and turbulent flow.

The result of these erosion processes is surface irregularities in the form of pits, grooves and roughing that serve as stress concentrators and greatly decrease the fatigue strength of the blade material. These degraded areas with time are favoured locations of crack initiation under cyclic loading to cause erosion fatigue failure, where the cracks grow out of eroded surfaces and propagate under varying stresses during operation. Under these circumstances, corrosion increases the rate of material removal and increases the rate of crack propagation by making the material weaker at a

microstructural level. Therefore, the total failure mechanism does not originate in one factor but is the result of synergistic and reinforcing influences of droplet erosion, solid particle erosion, cycle fatigue loading and corrosive attack (Ahmad, Schatz and Casey, 2018). The outcome of this synergistic interaction is a progressive surface damage, crack formation at local weak locations and eventual catastrophic failure of the LPST blades.

2.6.4 Fatigue Failure

Fatigue failure is a progressive degradation of materials which is a result of cyclic or variable loading and is usually at stress levels less than the yield strength. It is known to be the leading cause of mechanical breakdowns in engineered elements, which is the cause of a significant proportion of in-service failures. The failure begins by the development of microscopic cracks near the areas of stress concentration like surface discontinuities, inclusions or geometric discontinuities (Mazur, García-Illescas and Hernández-Rossette, 2009) . The cracks accumulate with the increasing number of loading cycle until they attain critical size, and then they suddenly fracture without any considerable deformation.

Three factors mainly determine the fatigue behavior of a material and these include the maximum tensile stress intensity, amplitude of the stress variation, and the total number of loading cycles. Increased stress and greater stress variations increase the rate of crack initiation and propagation, and small stresses has the potential to cause failure when repeated with a large enough number of cycles. Other variables like surface condition, microstructure, residual stresses and environmental influences are also added to the *(Banaszkiewicz, 2018)*. Fatigue is a serious factor to be taken into

account during design and reliability analysis of the components that are loaded dynamically, especially in task like blades in steam turbines, because it is cumulative and is not readily noticeable.

2.6.4.1 High-Cycle Fatigue

Following are the characteristics of High Cycle Fatigue.

- It occurs under relatively lower stress amplitudes.
- Deformation in high cycle fatigue predominately elastic.
- It exhibits comparatively extended fatigue life.
- A very high number of loading cycles is required to initiate failure.
- High cycle fatigue generally corresponds to fatigue lives exceeding 10^4 to 10^5 cycles ($N > 10^4$ to 10^5 cycles).

2.6.4.2 Low-Cycle Fatigue

Following are the characteristics of Low Cycle Fatigue:

- It occurs under relatively under high stress levels, often approaching or exceeding yield strength
- Each loading cycles involves both elastic and plastic deformation.
- It is characterized by a relatively short fatigue life.
- Low cycle fatigue typically occurs for fatigue lives below 10^4 to 10^5 cycles ($N < 10^4$ to 10^5 cycles).

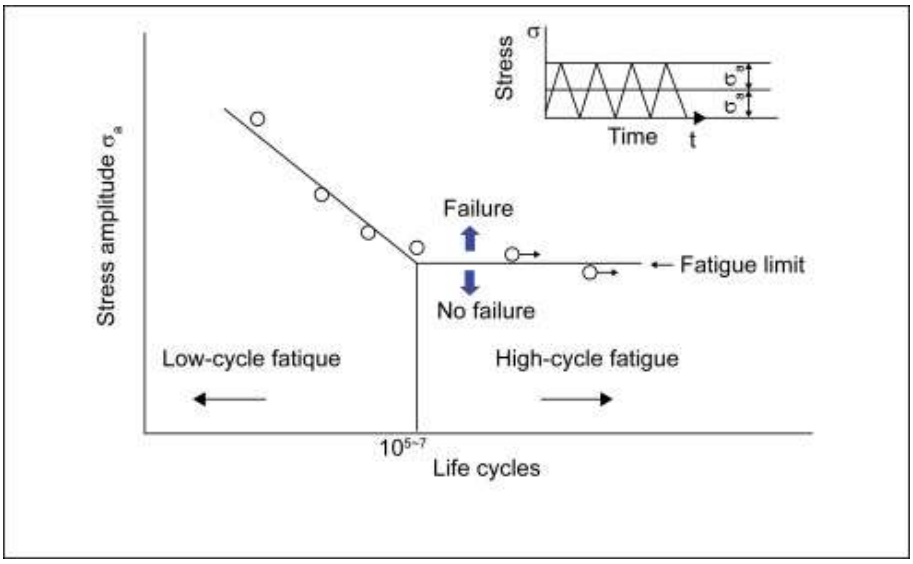

Figure: 2.6 Low cycle and High cycle fatigue *(Farhat, 2021)*

2.7 Research Methodology

This chapter introduces a structured and in-depth research methodology to effectively address the four key objectives of the present study. The research incorporates experimental techniques, non-destructive residual stress measurement, computational structural analysis, and advanced fatigue crack growth simulation in order investigate the failure analysis of the last-stage (L-0) LPST blade made of X10CrNiMoV12-2-2 martensitic stainless-steel alloy.

2.7.1 Research Methodology Framework

A summary of overall research workflow is provided in Table 2.3, mapping each of the investigative stages to its objective, experimental or computational tools and deliverables.

Table 2.3 Research workflow

S. No	Phase	Methodology
1	Problem identification	Collection of fractured blade, visual examination and microstructure characterization
2	Experimental Investigation	Microstructure, fractographic and mechanical characterization
3	Residual stress Evaluation	Assessment of residual stresses using X-ray diffraction (XRD) cos α method
4	Computational analysis	Static structural and dynamic analysis using finite element-based software ANSYS® and vibration characteristics including modal frequencies and mode shapes
5	Fatigue crack growth simulation	Investigated fatigue crack growth behavior of a crack in LPST blade using hybrid simulation approach integrating ANSYS and FRANC 3D.

2.7.2 Description of blade material

The turbine blade examined in this paper is made up of X10CrNiMoV12-2-2 martensitic stainless steel, a high-alloy steel that is largely used in LPST last-stage turbine blades due to its good fatigue characteristics, high strength and corrosion resistance in wet steam service. The chemical composition and mechanical characteristic the blade material is tabulated in are Table 3.2 in the further chapters.

Phase I: Problem identification, Collection of fractured blade, visual examination and microstructure characterization

The last stage steam turbine blade of the L-0 row is collected from 210 MW thermal power plant. High levels of noise and vibration at the LP zone during operation caused the unit to shut down and one of the blades from the 29^{th} stage was found to be fractured on opening the turbine casing. The fractured blade is made of

X10CrNiMoV12-2-2 a martensitic stainless-steel alloy. The cracked region of the blade was identified using preliminary visual inspection and specimens were prepared from this region using a precision abrasive cut-off machine with continuous water-cooling to avoid thermal damage and maintain the microstructural integrity of the material. Metallographic specimens were prepared by standard procedures which include rough grinding using silicon carbide abrasive papers of increasing number of grinding lines, i.e., 120, 240, 400, 600, 800, 1200 and 2400 grit, and then polished to a mirror-like surface finish by fine polishing using 6 μm and 1 μm diamond suspension, and finally 0.05 μm colloidal silica suspension on a vibro-polisher. To ensure no contamination, specimens were ultrasonically cleaned in ethanol after each step in preparation. Chemical etching for microstructural revelation was done using Glycergia etchant which is recommended reagent for martensitic and ferritic stainless steels. The composition of the etchant included hydrochloric acid (HCl), nitric acid (HNO_3), and glycerol in the right proportions. Etching was performed by swabbing the polished surface for a controlled amount of time and then immediately rinsing with ethanol and drying under warm air.

Phase 2: Experimental Investigation of failure mechanism

To investigate the root cause of failure of a LPST blade, following experimental methodology have been adopted.

(i) Optical microscopy

The characterization of the microstructure of the blade material was preliminary done using the optical microscope. By etching the specimens with glyceregia reagent, the specimens were systematically investigated to present the important microstructural

characteristics, such as the morphology of the grains, phase distribution, tempered martensitic lath structure, and the precipitation behavior of carbide. Special focus was on the detection of the microstructural anomalies including non-metallic inclusions, elemental segregation, and potential heat-affected areas. In order to have a representative appraisal, various areas of the blade cross-section in different places were evaluated and recorded to be able to analyze any microstructural gradients of the surface to the core.

(ii) Fractographic analysis (SEM/EDS)

Detailed fractographic analysis was conducted using a VEGA3 TESCAN scanning electron microscope in order to study the failure characteristics of the blade with high resolution. The fracture surface was studied in its as-received state without any further preparation so as not to alter the initial fracture features and the surface morphology. Secondary electron (SE) imaging was used for acquiring high-resolution topographical data about the fracture surface. The analysis focused on locating critical features such as the crack initiation site and crack propagation behavior and final fracture region. Specific fractographic features such as fatigue striations, beach marks, river patterns and cleavage facets were meticulously studied to discriminate between fatigue, brittle and mixed mode fracture mechanisms. Furthermore, the nature of fracture (inter-granular or transgranular) was determined to understand the failure mode.

172

Energy Dispersive Spectroscopy (EDS), integrated with the SEM system, was used in order to determine the elemental composition at selected areas of interest on the fracture surface. Point analysis and area scans were performed at inclusions, deposits and crack initiation areas in order to detect compositional heterogeneities. In

120

addition, elemental mapping was performed to assess the distribution of key elements in space. Particular attention was given to the detection of corrosive species such as chlorine, sulphur and oxygen that are known to contribute to stress corrosion cracking and corrosion fatigue interactions in steam turbine environments. The combined SEM-EDS analysis led to important information of the fracture mechanisms, environmental effects and material degradation mechanisms that are responsible for the failure of the L-0 LPST blade.

(iii) Hardness measurement

Micro hardness measurements were made with a Vickers hardness tester under an applied load of 0.5 kgf (4.9 N) and a dwell time of 10 sec, per the methods of the ASTM E384 standard. A hardness traverse was performed from the surface of the blade to the core to check for any hardening of the surface, decarburization, or any localized softening from overheating or phase transformation. A minimum of 10 indentations were made at each location and the average hardness value and its standard deviation were reported

Phase 3: Residual Stress Evaluation

To evaluate the residual stresses in LP steam turbine blade using X-ray diffraction (XRD) cos α method following methodology was adopted:

Residual stresses are self-equilibrating internal stresses that will not disappear in a component once manufacturing processes/ operational loading is completed without external forces. The tensile residual stress present on the surface, or in the near-surface of the steam turbine blades, are especially deleterious because they are additive, in

effect, to the cyclical stresses caused by service, which drives an increase in the mean stress and accelerates fatigue crack initiation and growth. Compressive residual stresses on the other hand are desirable since they prevent crack-opening. The precise definition of the residual stresses in the fractured blade is thus necessary in order to comprehend stress conditions existing at the fracture origin.

(i) Residual stresses measurement using cos α method

To assess the residual stresses in a failed L-0 low pressure steam turbine blade, following methodology was adopted.

i. A 2-D detector test was applied on the failed specimen of L-0 LPST blade using PULSTEC μ-X360 FULL 2D portable machine.

ii. Unlike the traditional $\sin^2\psi$ method, Cosα method uses a two-dimensional (2D) X-ray detector that simultaneously records the entire Debye-Scherrer diffraction ring in one exposure, it includes 30 sec X-ray exposure and 90 sec to display all the results, which has made it possible to achieve quick determination of residual stress without specimen tilting to several different ψ angles.

iii. Characteristic X-ray of Cr Kα radiation and 311-diffraction were used. The Fitting Lorentz method was employed for to analyse the peak with 15752 measurement counts. Measurements of the lattice plane spacing for Fe (311) was carried out at three different directions to evaluate the normal stress component.

iv. The diffraction of X-rays from the crystal lattice of the specimen being examined produces circular patterns known as Debye rings. The 2D and 3D views of the

Debye-Scherrer ring image from the turbine blade sample, created using diffraction line 311 with Cr Kα radiation at a 35º angle to the z-axis.

v. The angle of diffraction and the radius of the resulting Debye ring are analyzed to assess the blade's characteristics.

vi. The resulting stress data (residual σ and τ)) will reveal whether tensile or compressive stresses were locked in the material, which could accelerate crack initiation or retard propagation

Phase 4: Computational framework to determine the stress distribution and dynamic response of LPST blade

Static structural and dynamic analysis of LPST blade were performed using following methodology.

i. The three-dimensional CAD model of the blade was produced via a 3D laser scanning process in order to capture the exact shape and size of the blade by using a line of laser light.

ii. The 3D cad model of the scanned blade is converted to a solid model by finite element software *ANSYS*®a triangular surface meshing is generated.

iii. The fixed support is provided at the fir-tree part of the blade as its boundary condition. The operating speed of the turbine blade is considered to be 3000 rpm.

iv. To analyse the deformation behavior and stress distribution in a LPST blade, Static structural analysis has been performed. This analysis highlights potential regions that are prone to failure.

v. Modal analysis is carried out to determine the natural frequencies of the blade, thereby preventing resonance during operation. Further, the first six natural frequencies for 0 rpm, 500 rpm, 1000 rpm, 1500 rpm, 2000 rpm, 2500 rpm and 3000 rpm have been evaluated.

vi. The critical speeds are found by the intersection of the harmonics line with the frequency line which can be represented by a Campbell diagram. Campbell diagram facilitates in identifying safe operational regions to prevent resonance.

Phase 5: Fatigue crack growth behavior in LPST blade

To investigate the fatigue crack propagation behavior in LPST blade following methodology was adopted.

i. Created a 3D cad model of the LPST blade in *ANSYS*
ii. Performed meshing and apply boundary conditions
iii. Performed static structural analysis in *ANSYS* to determine the deformation and von-misses stresses in the blade
iv. Exported the stress results to FRANC 3D
v. Developed a sub model of the blade critical region
vi. Defined a crack location and introduced 2 mm edge crack
vii. Performed meshing around the crack front
viii. Computed SIF (K^I, K^{II}, K^{III}) and Crack propagation was controlled by two primary factors: $\Delta K \geq \Delta K_{th}$ and $K_{equiv} < K_C$
ix. The simulation proceeded as long as the stress intensity factor range (ΔK) remained greater than the threshold value (ΔK_{th}) while the equivalent stress intensity factor was lower than the critical fracture toughness value (K_C.). the

analysis was automatically terminated when ΔK dropped below ΔK_{th} or K_{equi} reached or surpassed K_C.

2.8 Chapter Summary

The chapter has presented a five-phase step wise step methodology to determine the reasons of failure and fatigue crack growth behavior of LPST blade. Phase 1: involves the problem identification, collection of fractured blade, visual examination and microstructure characterization of the LPST blade to indicate the underlying material degradation and crack formation Phase 2: determines of root causes of failure of a failed L-0 LPST blade by using detailed metallurgical examinations, Scanning Electron Microscopy (SEM) and Energy-Dispersive X-ray Spectroscopy (EDX) techniques. Phase 3: evaluated the residual stresses in L-0 LPST blade using X-ray diffraction (XRD) method based on cosα method as a non-destructive and accurate method of measuring stresses that are presented in critical rotating parts. Phase 4: presented the computational framework to determine the stress distribution and dynamic response of LPST blade. Phase 5: presented a hybrid simulation approach integrating *ANSYS* and FRANC 3D software to investigate fatigue crack growth/propagation behavior of a crack in a LPST blade. Further these methodology and objectives are covered in Chapters 3 to 6 respectively and Chapter 7 provide the conclusion and future scope of the research work.

CHAPTER-3

Investigation of Failure Mechanism and Root Cause Analysis of a Failed L-0 LPST Blade

The previous chapter highlighted the fundamental concept of steam turbines including their working and classifications and discusses the major reasons and methodology to determine the failure reasons of LPST blade. Based on that this chapter presents an investigation of root causes of failure of a failed L-0 LPST blade by using detailed metallurgical examinations, Scanning Electron Microscopy (SEM) and Energy-Dispersive X-ray Spectroscopy (EDX) techniques.

3.1 Introduction

LPST (Low-pressure Steam Turbine) blades are the critical components in power generation systems, where they facilitate the conversion of steam energy into electrical power. These components are designed to endure elevated temperature and extreme pressure conditions, making them essential for reliable and efficient operation of

power plants. In a steam turbine, there are multiple stages through which steam passes before it enters the turbine, including HP (high pressure), IP (intermediate pressure), and LP (low pressure) zones *(Perkins & Bache, 2005b)*. Steam turbine blades are more prone to failure at LP than the HP and IP blades, as LP blades capture the major part of the energy from the flowing steam compared to IP and HP blades *(Saxena et al., 2015)*. However, despite their robust construction, turbine blades are susceptible to various forms of damage, which can lead to failure and, in some cases, catastrophic consequences from repeated stress cycles due to operational or loading conditions, leading to blade cracking or fracture *(Das et al., 2003; Mazur et al., 2008; S. Rani et al., 2017)*.

Low-pressure turbine blades may fail due to various factors, including mechanical stress *(Kim et al.,1999)*, corrosion *(Ebara, 2010; Perkins & Bache, 2005a)*, erosion *(Ahmad et al., 2013)*, fatigue *(Shlyannikov et al., 2014)*, and vibration *(Zhao et al., 2018)*. Excessive vibration, misalignment or poor balancing can cause mechanical stress, thereby causing blade deformation, creep, thermal distortion, and in the process cracking of the blade. Corrosion can be caused by the contaminants in the steam or condensate and lead to blade pitting or corrosion fatigue. Erosion may be caused by the action of solid particles or droplets in the steams causing erosion or wear to the blade surface, resulting in fatigue failure of the blade.

Recent studies have been dedicated to the understanding of how failure occurs in steam turbine blades primarily composed of martensitic steel and paying particular attention to the contribution of corrosion pits, fatigue cracks, inter-granular failure and corrosion fatigue failure. The fatigue corrosion is the major cause of the failure of the

LPST blades used in the industry. Corrosion fatigue is a kind of material degradation that is a combination of mechanical stress and corrosion. The fact that corrosion pits form on the surface of the material is evidence that the corrosion fatigue process has begun, which are stress concentrators. The cracks form at the location of the corrosion pits as the material is subjected to cyclic loading and may continue to extend through the material thus causing the material to fail

Bhagi et al., (2013) analysed the failed L-1 LPST blade to understand its failure mechanism. They noted that corrosion fatigue is enhanced by cyclic stresses and environmental influences. They have decided that the most likely cause of the blade failure is corrosion fatigue which occurred due to trans granular cleavage fracture. *P. Rani et al., (2022)* presented the failure investigations of 210 MW last-stage LPST blades after 1,52,241 hours of working. They have performed mechanical analysis, metallurgical analysis and Non-destructive testing (NDT) of the blade and discovered that the water-droplet erosion at the edges of the blade forms erosion pits that causes the blade to fail.

Based on extensive literature review, it is evident that appropriate preventive measures are required to minimize crack initiation and reduce the risk of blade failure thereby enhancing the fatigue life of the blade. There are different methods to enhance the blade's fatigue life, like shot peening *(James et al., 2010; Pant et al., 2013; You et al., 2017)*, coating the blade *(Abdulwahab et al., 2022; Navinesh et al., 2020)*, and providing dampers between the blades *(Bhagi et al., 2017)* in order to reduce the failure rate of the blade.

This chapter presents an investigation of root cause of failure of a L-0 LPST blade; a fracture event occurred in one of the L-0 blades of the 29^{th} stage of a 210 MW

low-pressure steam turbine. Prior to this event, the turbine had been in operation for many years and exhibited excessive vibration and unusual sounds while in operation. Upon emergency shutdown and subsequent inspection, a transverse fracture was discovered in the vicinity of the leading edge of the blade approximately 350 mm from the blade tip. The fractured blade was made up of material X10CrNiMoV12-2-2 a martensitic stainless-steel alloy commonly used for the fabrication of the final-stage blades due to its high tensile strength, good creep resistance, and acceptable corrosion resistance. Although the desired properties of the alloy are advantageous, the harsh operational environment experienced by the low-pressure stages (i.e., high moisture content, contaminants in the condensed water, and variable stresses) can compromise the performance of the alloy over time, resulting in premature fatigue failure.

The primary aim of this research is to determine the root cause of the fracture event to evaluate whether the failure resulted from a material defect, overstressed operation, environmental corrosion, or a combination of these mechanisms. To accomplish this, an experimental approach was developed and implemented that included:

• Visual and macroscopic examination of the fracture region, crack initiation zone(s), and general failure morphology.

• Verification of chemical composition to ensure conformance with the design specification.

• Tensile and hardness testing to evaluate the residual strength and degradation of the material resulting from service.

• Optical microscopy (OM) to evaluate the grain structure, heat treatment uniformity, and micro-structural changes near the fracture surface.

• Scanning electron microscopy (SEM) to perform high-resolution fractography to reveal fatigue striations, dimples, and other microscopic details related to the failure.

• Energy dispersive spectroscopy (EDS) to map the elements and detect corrosion products or inclusions on the fracture surface.

The experimental data generated using the above techniques provide evidence that relates the applied stresses, material microstructure, and fracture morphology, thereby providing insight into the failure process. Additionally, the conclusions drawn from the experimental analysis will serve as a basis for developing computational models and predicting the fatigue life of similar blades, which are discussed in detail in subsequent chapters. Ultimately, the findings of this study are intended to improve the reliability, durability, and design of LPST blades that operate in aggressive wet-steam environments.

3.2 Experimental details

The last stage steam turbine blade of the L-0 row is collected and investigated fractographically to determine the main reasons for its failure. A transverse crack was noticed on the blade's aerofoil-leading edge at a distance of 350 mm from the blade's tip, as shown in Fig. 3.1. The samples were prepared from the cracked region of the blade as shown in Fig. 3.2. The specimen was prepared using standard metallographic techniques for fractographic analysis, and the prepared sample's microstructure was revealed using glycergia etchant through an optical microscope. For crack

morphology, scanning electron microscopy of the prepared sample is carried out on VEGA3 TESCAN model accompanied with energy dispersive spectroscopy (EDS). Further, the hardness of the blade material was evaluated using the Vickers hardness test at a force of 0.5 kg for 10 seconds. And a tensile test was conducted to assess the mechanical properties of the blade material.

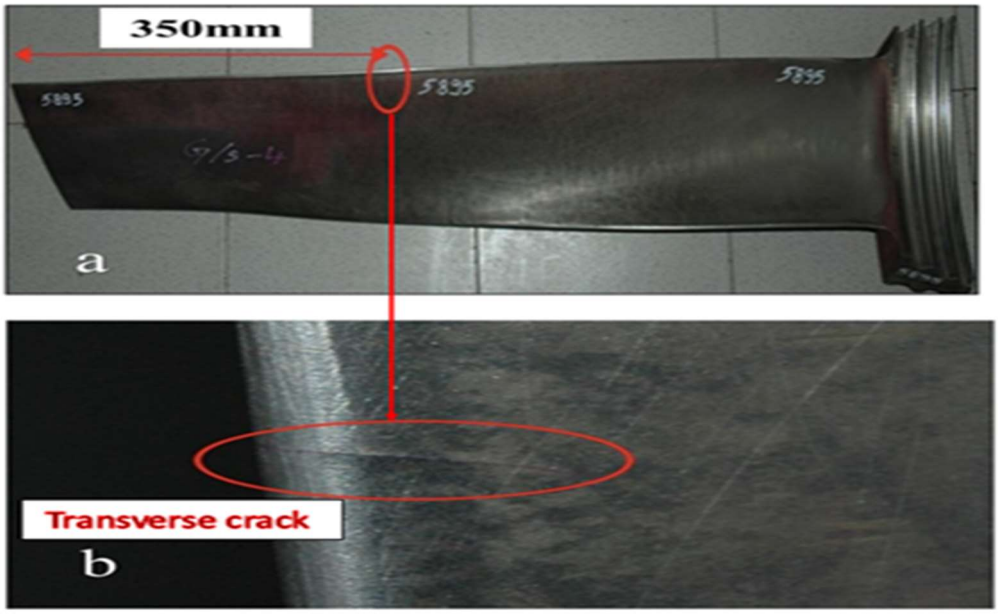

Figure 3.1: Transverse crack on the aerofoil-leading edge of the steam turbine blade

3.3 Results & discussion

3.3.1 Visual observations

On visual examination, a transverse crack of around 20 to 25 mm is observed at a distance 350 mm away from the blade's tip, which propagates from the leading edge towards the trailing edge as shown in Fig. 3.1. Regions of black patches i.e. iron oxide (Fe_3O_4) are also found on the blade's surface from tip to root of the blade as shown in Fig. 3.2 and presence of iron oxide (Fe_3O_4) can make the blade material weak and

ductile. Further, water droplet erosion creates erosion pits on the aerofoil-leading edge but these are away from the transverse crack as shown in Fig. 3.3, which concludes that the erosion pits are not the reason for the failure of the blade.

Figure 3.2: Black patches (Iron Oxide (Fe_3O_4) observed on the blade's surface

Figure 3.3: Erosion pits at the blade aerofoil-leading edge.

3.3.2 Chemical analysis

An optical emission analyzer was used to identify the chemical makeup of the blade material. The result of the chemical composition of blade material X10CrNiMoV12-2-2 is tabulated in Table 3.1. Chemical testing results reveal that the turbine blade material corresponds with AISI 410-grade martensitic steel.

Table 3.1: Chemical composition of turbine blade material

Composition	C	Cr	Mo	Ni	V	Mn	Si
Measured Weight-%	0.21	12.69	1.95	2.73	0.32	0.97	0.46

3.3.3 Microstructure analysis

In order to explore the microstructural properties of the blade material, optical microscopy was used. The micrographs of the blade material in 100x and 200x magnifications are provided in Fig. 3.4(a) and 3.4(b), respectively. The metallographic observation was conducted through the routine sample preparation methods, such as sectioning, mounting, grinding, and polishing with proper etching to bring out the microstructural features of the material in a clear manner.

The microstructure that is observed is made up mainly of hardened and tempered martensite that is evenly distributed all over the material matrix. This even distribution means that the material of the blade has been subjected to heat treatment and thus, the microstructure is fined, which promotes the strength and toughness. Tempered martensitic structure is also sought after in the steam turbine blades since it

180

is considered a good combination of high strength, good fatigue, and reasonable ductility.

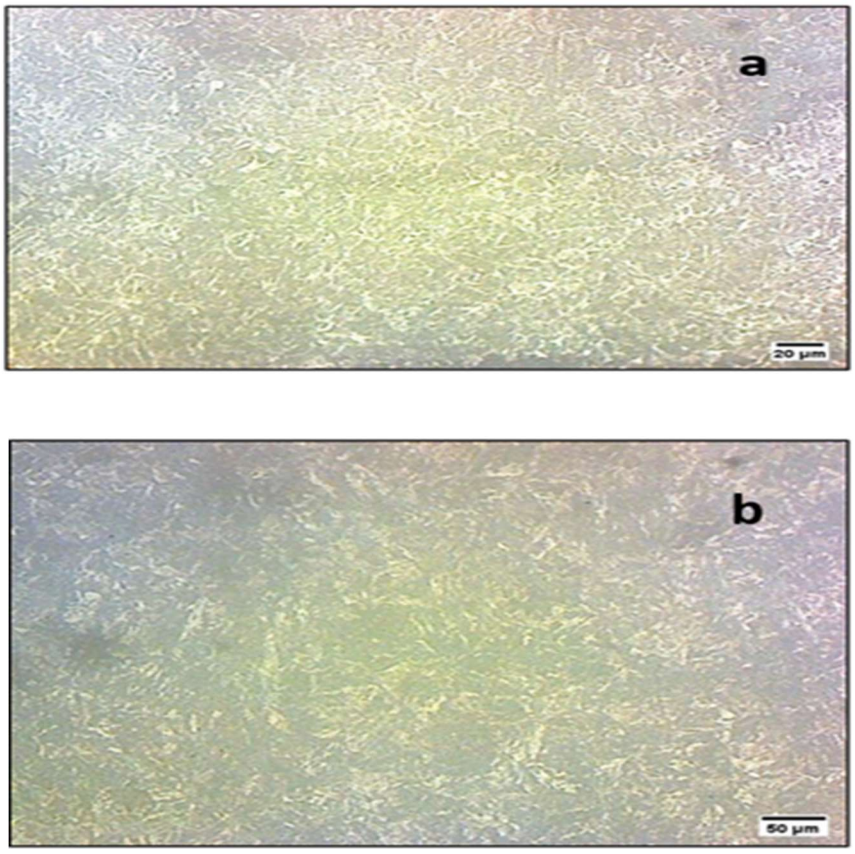

Figure 3.4: Optical micrographs showing the tempered martensitic microstructure (a) Microstructure at 100x (b) Microstructure at 200x

Even a close inspection of the micrographs shows that there are no evident traces of micro-structural degradation including carbide coarsening, weakening grain boundaries, micro voids, or phase changeover. The lack of such deterioration would indicate that this material has not been subjected to the adverse influence of service induced thermal or mechanical exposure and that it has still maintained its metallurgical integrity. Moreover, the presence of micro cracks, inclusions, and abnormal grain development was not detected in the studied areas, which means that

the material was of high quality and showed consistency in its manufacture. Consistency in the microstructure also means that there are little segregation and a constant phase distribution that is necessary to guarantee consistent performance under a cyclic loading condition.

3.3.4 SEM Analysis

In the case of Scanning electron microscopy (SEM) the specimen was a cut off section of the broken part of the steam turbine blade a in Fig. 3.5(a). SEM of the specimen was performed with the help of VEGA3 TESCAN MODEL with an EDS facility. In the case of fractographic analysis, the specimen is cut into three parts viz. R1, R2 & R3 as shown in Fig. 3.5(b). The fractographic results of region R1 are shown in Fig. 3.6, which depicts corrosion pits. The cracking of the LP steam turbine blades as aided by the environment typically initiates at the corrosion pits. The corrosion pits are stress concentrators or stress raisers; when a blade is operating, it undergoes cyclic loading as a result of the rotating forces as well as the flow of steam. The local stress concentrations may result in small cracks being initiated at the corrosion pits because of these cyclic loads. Such cracks may develop over time and ultimately cause a disastrous failure of the blade. Corrosion pits may also decrease the fatigue life of the blade by decreasing the thickness of the material at the pit. This thinning may raise the stress level in the material in the pit, which may make it more vulnerable to crack initiation and propagation.

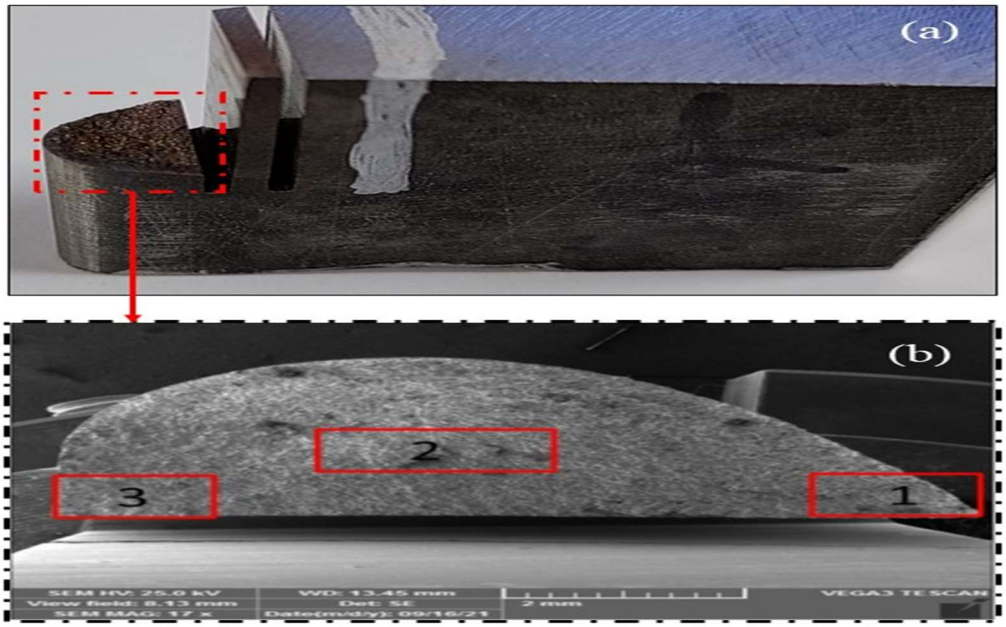

Figure 3.5: (a) Macro-morphology of the cracked part of the blade, (b) Micro-morphology or SEM view of the rectangular portion divided into three different regions R1, R2, and R3 for fractographic analysis.

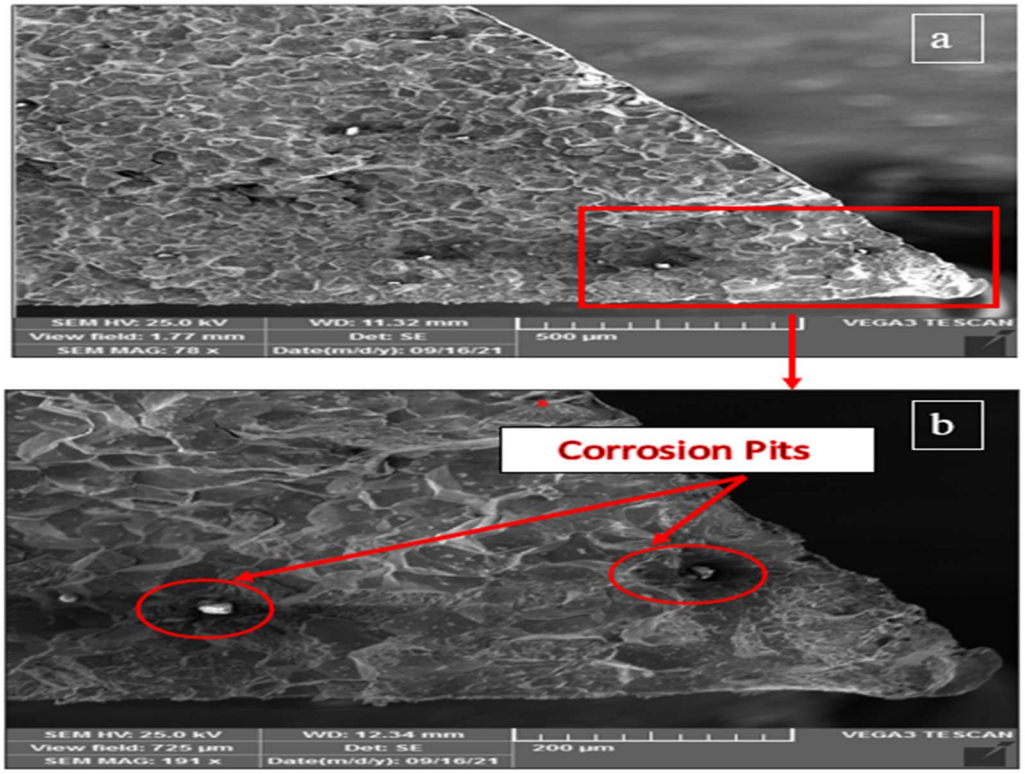

Figure 3.6: SEM fractography of R1 region depicts corrosion pits. (a) Normal view (b) Shows the magnified view of the corrosion part

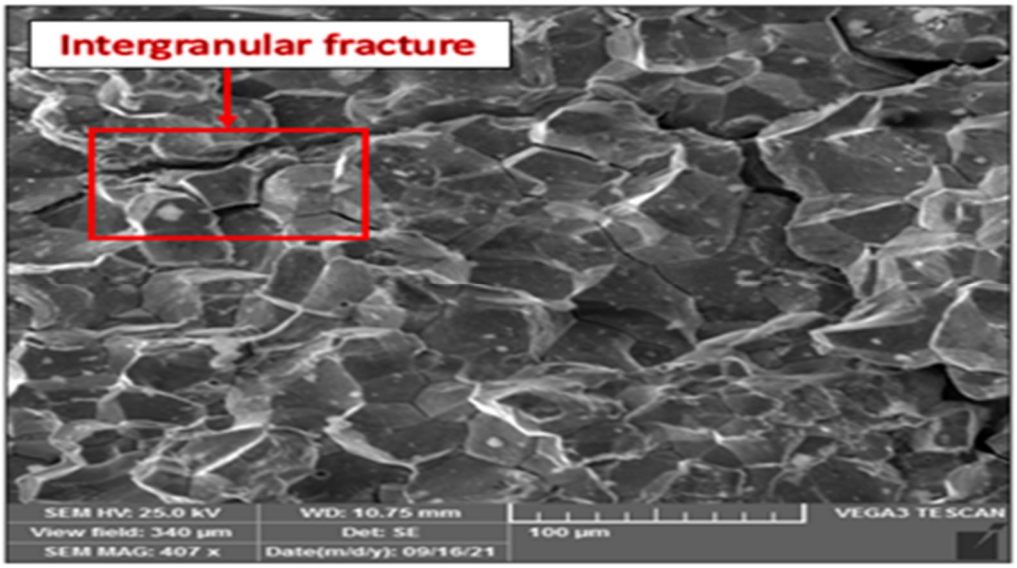

Figure 3.7: SEM fractography of region 2 showing the inter-granular fracture

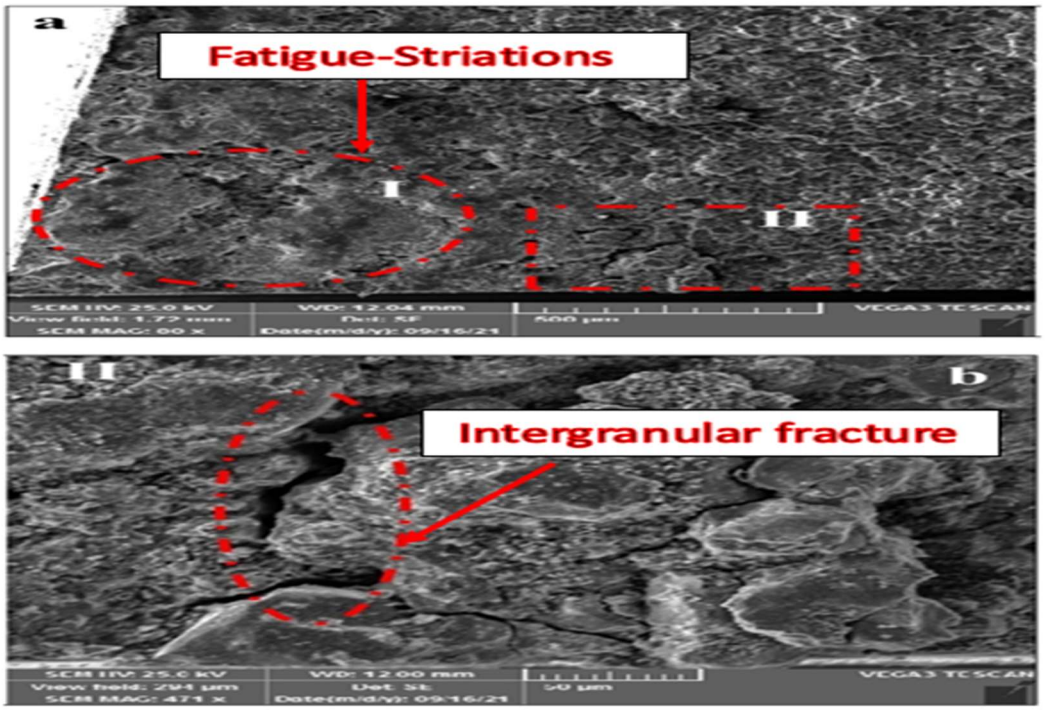

Figure 3.8: (a) SEM analysis of the R3 region represents the beach marks and fatigue striations followed by the inter-granular fracture. Fig. 9 (b) shows the magnified view of inter-granular fracture.

The SEM analysis result of the R2 region shown in Fig. 3.7, depicts the inter-granular failure mode. The SEM analysis of the R3 region has been presented in Fig. 3.8(a) and3.8(b) which depict the beach marks and fatigue striations respectively and then the inter-granular fracture. Fatigue striations are microscopic lines or ridges that form on the surface of a material as a result of repeated cycles of stress. A number of factors such as material defects, stress concentrations, and cyclic loading may cause fatigue striations and inter-granular fractures on a LPST blade. The fatigue striations also indicate the crack moves towards the trailing edge of the blade.

3.3.5 EDS analysis

EDS analysis done on the R1 region (Fig. 3.9) The EDS results reveal the existence of chlorine, silicon, oxygen and other corrosion promoting products. The particles of SiO2 are formed by combining silicon and oxygen and repeatedly strike the blade material to form deposits that cause grooves/pits in the blade material and deform the steam passage. The pits were penetrated into the material resulting in localized stress concentration, which resulted in fatigue cracks. The fact that there were foreign particles in the steam also contributed to the problem by giving it more stress concentrations. The Corrosion fatigue cracks often start at corrosion pits, particularly in the presence of chlorine and oxygen and propagate at cycling loading. The above findings indicate clearly that corrosion fatigue could be the cause of blade failure.

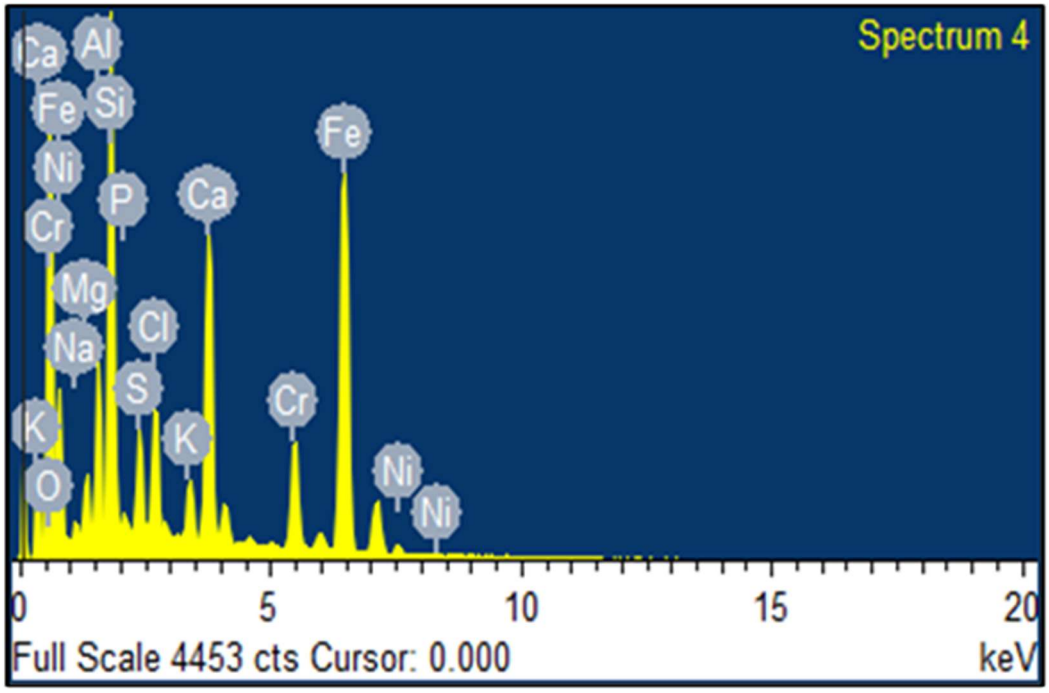

Figure 3.9: EDX analysis of the fractured surface of the blade for the R1 region.

3.3.6 Hardness

A hardness test was performed on a Vickers hardness testing machine close to the failed part of the blade. The surface of the blade material was subjected to a force of 0.5 kg in 10 seconds as in Fig. 3.10. The results of the hardness test are tabulated in Table 3.2. and plotted graphically (Fig.3.11). It is noted that the hardness is much greater on the fracture surface of the blade. The increase in hardness of the blade material may be due to strain hardening, Improper heat treatment, contamination & aging factor that can make the material more brittle and could potentially reduce the fatigue strength of the blade material that leads the blade more prone to cracking or fracture under stress or cyclic loading.

Table 3.2: Hardness values (HV) at a different location on the blade surface.

Distance from the fracture surface (mm)	Hardness (HV)
0.5	492.43 HV0.5
1	466.63 HV0.5
1.5	416.89 HV0.5
2	395.08 HV0.5

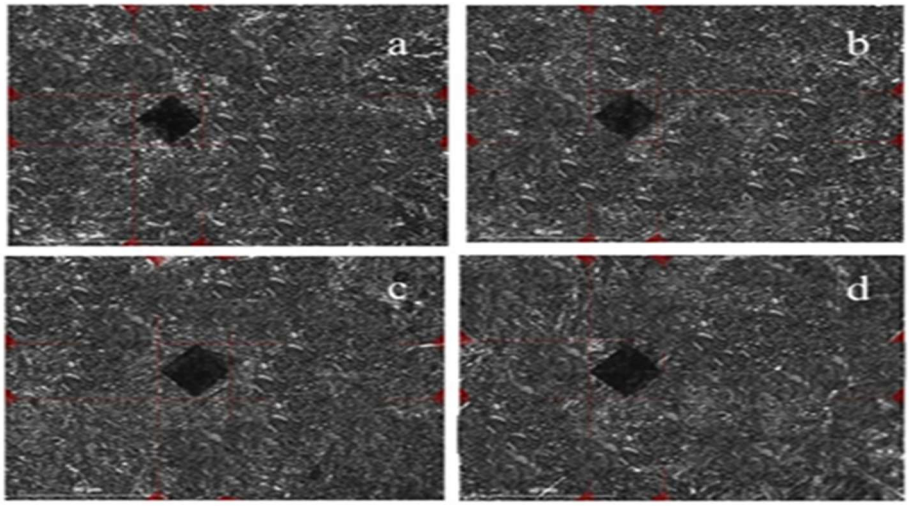

Figure 3.10: Vickers hardness test of the blade material at a force of 0.5 kg for 10 seconds

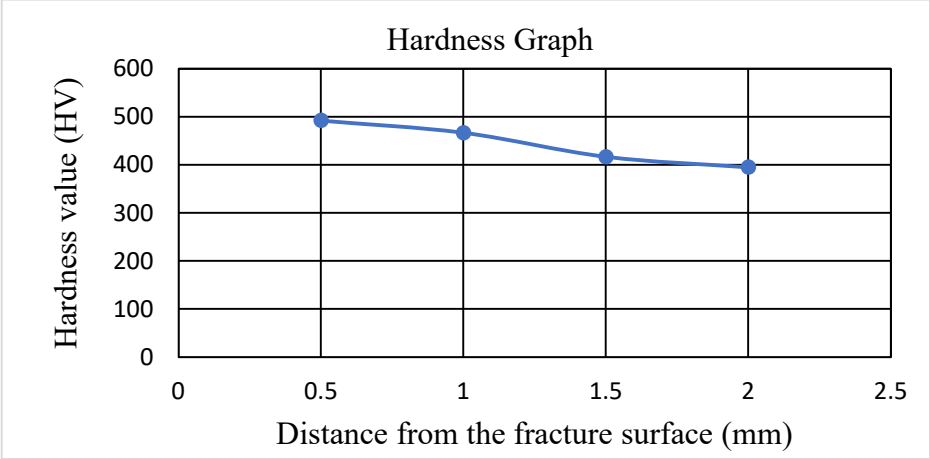

Figure3.11: Graphical plot of hardness value vs distance from the fracture surface.

3.3.7 Tensile test

Tensile tests were conducted on the blade's failed and un-failed regions of the blade. The stress-strain curve is shown in Fig. 3.12. The un-failed region of the blade has a yield strength of 530 MPa and an ultimate tensile strength of 865 MPa, while the failed region has a yield strength of 343 MPa and an ultimate tensile strength of 680 MPa. The reason for the lower value of the failed region is as it has undergone significant deformation and damage & which reduces the strength and ductility of the material.

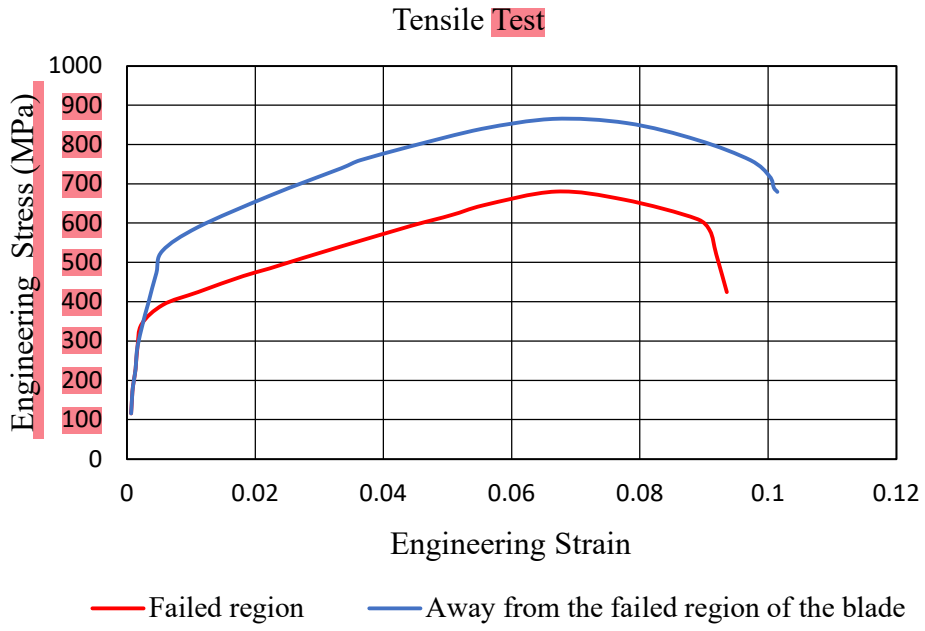

Figure 3.12: Stress-strain curve for the failed and the un-failed region of the blade

3.4 Conclusions

This chapter investigated the root cause of failure of a fractured L-0 LPST blade by using the experimental techniques such as visual examination, optical microscopy, SEM, EDS, and mechanical testing methods. The micro-structural analysis found that the blade material had a stable and well dispersed tempered martensitic microstructure,

which ruled out the existence of material defects and microstructure discontinuities as the cause of failure. Despite the presence of surface degradation in the form of water droplet erosion along the leading edge, but it was away the region of fracture, which denotes that it was not decisively involved in crack formation. The results of mechanical tests showed that the material's mechanical properties had deteriorated, with the material being more brittle due to an increase in hardness and a fall in ultimate tensile and yield stresses, respectively. In addition, SEM and EDS analysis revealed that there were corrosive impurities that included chlorine, oxygen, and silica particles deposited on the blade. The repetitive deposition and accumulation of SiO_2 particles produced pits and grooves on the surface that would serve as a localized source of stress concentrators. Such pits caused by corrosion acted as preferential sites of crack genesis under cyclic loading, which resulted in the gradual propagation of the crack to the trailing end. Inter-granular fracture characteristics and fatigue striations were the ultimate determinants of corrosion fatigue as the dominant failure mode through fractographic evidence.

The next chapter will describe the experimental evaluation of residual stress in L-0 LPST Blade using X Ray Diffraction (XRD) with Cos α Method as residual stresses have been considered as significant technique in determining the vulnerability of blades to fatigue, corrosion and fracture.

turnitin Page 98 of 178 - Integrity Submission Submission ID trn:oid:::29034:134939416

CHAPTER 4

EXPERIMENTAL EVALUATION OF RESIDUAL STRESS IN LPST BLADE

In the previous chapter, the root causes of failure of a fractured L-0 LPST blade is investigated by using experimental techniques such as visual examination, optical microscopy, SEM, EDS, and mechanical techniques. The results identified that inter-granular fracture characteristics and fatigue striations were the ultimate determinants of corrosion fatigue that dominant to failure mode. In this chapter, effect of residual stresses on a cracked LPST blade is analysed using PULSTEC, μ-X360 machine using X-ray diffraction (XRD) cos α method.

4.1 Introduction

Turbine blades experience considerable thermal and mechanical stresses during service, resulting in material damage and failure (*Mukhopadhyay et al.*, 2001b). Accurate knowledge of the residual stress state in turbine blades is important to enhance their performance, maintain safe operation and extend their fatigue life.

Residual stresses can be generated during manufacturing by various processes, such as machining processes e.g., grinding, milling, and turning, thermal processes (e.g., welding, casting, forging, and heat treating) and cold-working techniques e.g., shot peening, laser shock peening, ultrasonic peening, hammering, burnishing, low plasticity burnishing, rolling (Huang, Liu and Xie, 2013). The XRD is a non-destructive method of measuring the residual stresses on structures and turbine components. It measures a thin layer near the surface (a few microns) and multiple measurements can be made across a surface to produce depth profiles (Gelfi *et al.*, 2004). XRD technique is particularly attractive when near-surface residual stress measurements are required, and it is most useful for evaluating residual stresses from machining, shot and laser peening, heat treatment, and similar processes (Shajari *et al.*, 2023). It measures the surface residual stresses to depths of up to 30µm by measuring the material's inter-atomic spacing. The inter-planar spacing, d, of the diffraction planes are evaluated by measuring angles at which the maximum diffracted intensities occur using Bragg's law *(Rossini et al., 2012, Ao et al., 2020).*

The types of residual stresses that found in XRD (X-ray diffraction) are either compressive or tensile residual stresses. The presence of surface compressive residual stress is generally beneficial, as it contributes to improved fatigue performance, delays crack growth, and enhance resistance to degradation mechanism such as stress corrosion cracking and hydrogen assisted damage. On the other hand, tensile residual stress at the surface of the component is generally undesirable, as it decreases fatigue strength and fatigue life, increases crack propagation, and lowers resistance to environmentally assisted cracking *(Newby et al., 2014 ,Raj et al., 2009)*. Specifically,

residual stresses have been considered to play a significant role in determining the vulnerability of blades to fatigue, corrosion and fracture (Bendeich *et al.*, 2006).

Thus, proper evaluation and identification of residual stresses are the keys to the robust design and maintenance of blades of steam turbine. X-ray diffraction method is used by researchers to pinpoint the regions of high stress concentration and apply alleviating measures, including stress relief treatment, or changing the material, to minimize the potential risk of crack development and growth (Bendeich *et al.*, 2006). One of the key factors affecting the initiation and development of the cracks in the turbine blades is the residual stress (You *et al.*, 2017) and hence it is essential to evaluate residual stress for preventive maintenance and avoiding severe accidents.

In this chapter, the residual stress on a failed L-0 LPST blade is assessed using the X-ray diffraction (XRD) technique based on the cosα method. The residual stresses are a factor of paramount importance to the structural integrity, fatigue life, and failure behavior of turbine blades especially in the last-stage blades which are subjected to extreme mechanical loading and corrosive wet steam environments. It is important to correctly assess these stresses to understand the mechanism of crack initiation and propagation in the components that are subjected to fatigue loading or service conditions.

The method does not require multiple sample tilts and is thus especially appropriate to complicated geometries like turbine blades. The cosα technique has the benefit over the traditional $\sin^2\psi$ techniques of shortening measurement time, enhancing accuracy, and the capability to conduct localized stress analysis in small areas. It is useful in assessing stress levels in vital arears such as blade root, leading

edge, and the fatigue crack initiation regions. The residual stress measurement was done at selected critical points of L-0 blade to determine the magnitude and distribution of the stresses evolved during the manufacturing process and exposure to service.

4.2 Fundamentals of X-ray Diffraction (XRD)

When X-rays are incident on a metal sample, some grains, which satisfy Bragg's law ($n\lambda = 2d\sin\theta$), diffract X-rays in a continuous circular pattern called a Debye ring. The Debye ring connects the wavelength of the X-rays used, the angle of diffraction and the distance between the crystal planes. The ring can be used to determine the crystal structure and grain orientation and variation in Debye ring is also used to measure residual stresses (Miyazaki *et al.*, 2015). Residual stress can cause the spacing between the crystal planes to change, which in turn affects the angle of X-ray diffraction. This will result in variations in the Debye ring's position, shape or intensity. By accurately measuring the Debye ring using a 2-dimensional X-ray detector and examine the changes in the diffraction pattern of the Debye ring. its results can be used to determine the impact of residual stress on the crystal structure of material (Zhu *et al.*, 2019). The changes or deformations in the Debye ring due to the strain associated with residual stresses can be used to infer the level and nature of residual stresses present in the metal. The cos α method used to measure residual stresses by XRD utilized the correlation between the diffraction angle (α), inter-planar spacing (d) and the strain (ϵ), which is caused by the stresses in the material.

Through careful calibration and analysis, the cos α method enables the accurate determination of residual stresses in both surface and subsurface regions of turbine

blades (Tanaka, 2017). Four distinct strains on the same Debye ring are evaluated as shown in Eq.4.1 The strain at the central angle of α is represented as ϵ_α while the strains at angles -α, ($\pi + \alpha$), and ($\pi - \alpha$) are denoted as $\varepsilon_{-\alpha}\ \epsilon_{\pi+\alpha}$, $\epsilon_{\pi-\alpha}$ respectively (Gupta *et al.*, 2020).

$$\varepsilon_{\alpha 1} = \frac{1}{2}\{(\varepsilon_\alpha - \varepsilon_{\pi+\alpha}) + (\varepsilon_{-\alpha} - \varepsilon_{\pi-\alpha})\} \quad (4.1)$$

$$\varepsilon_{\alpha 2} = \frac{1}{2}\{(\varepsilon_\alpha - \varepsilon_{\pi+\alpha}) - (\varepsilon_{-\alpha} - \varepsilon_{\pi-\alpha})\} \quad (4.2)$$

$$\sigma_x = -\frac{E}{1+v}\cdot\frac{1}{\sin 2\eta}\cdot\frac{1}{\sin 2\psi_0}\cdot\left(\frac{\partial\varepsilon\alpha_1}{\partial\cos\alpha}\right) \quad (4.3)$$

$$\tau_{xy} = \frac{E}{2(1+v)}\cdot\frac{1}{\sin 2\eta}\cdot\frac{1}{\sin\psi_0}\cdot\left(\frac{\partial\varepsilon\alpha_2}{\partial\sin\alpha}\right) \quad (4.4)$$

The "cosα" method, is employed in a two-dimensional imaging technique to evaluate the stress ($\sigma_x$and τ_{xy}) by interpreting the radii of the Debye ring.

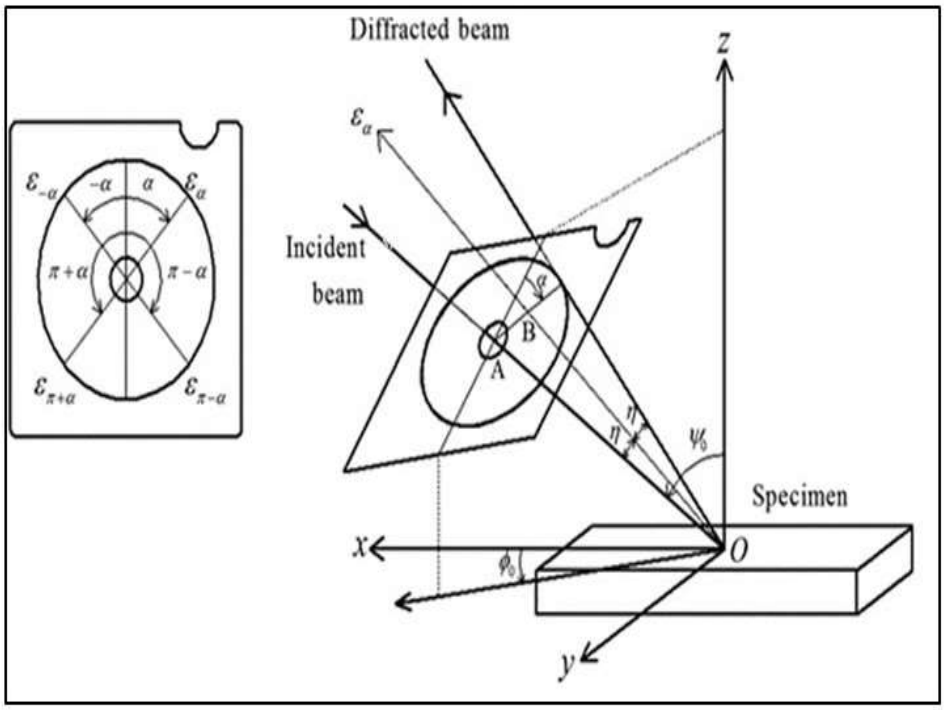

Fig. 4.1: Debye-Scherrer ring captured on a 2-D detector with a single X-ray exposure (*Miyazaki et al., 2015*).

4.3 Measurement of residual stresses by X-ray diffraction (XRD) using the cos α method

In order to evaluate the residual stress of the of L-0 LPST blade, 2-D detector test was performed on the advanced μ-X360 FULL 2D portable X-ray residual stress analyzer as shown in Fig. 4.2, which has taken 30 sec for X-ray exposure and 90 sec for displaying all results (excluding settling time). Table 1 presents all the measurement parameters of the 2-D detector *(Bhagi et al., 2018)*.

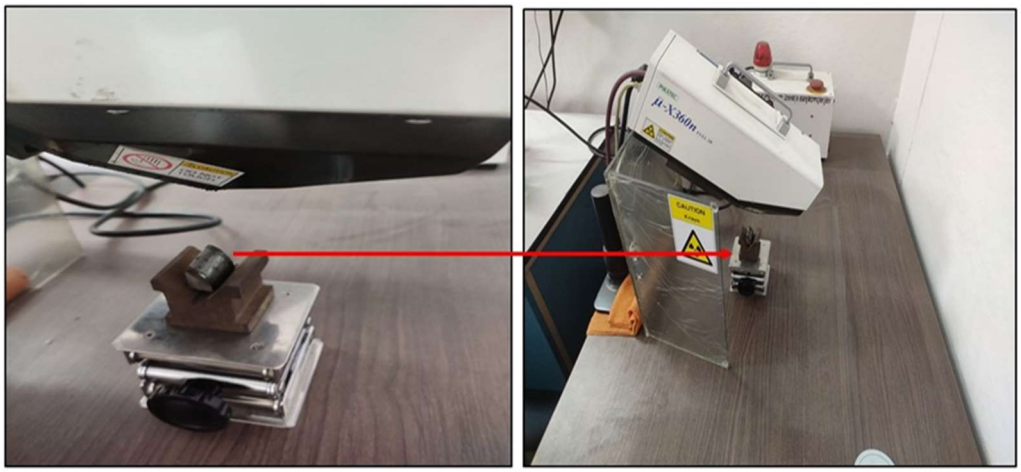

Fig. 4.2: Specimen of a L-0 low pressure steam turbine blade mounted on the μ-X360 machine

The specimen of a L-0 low pressure steam turbine blade mounted on the μ-360 machine as shown in Fig.4.2. Characteristic X-ray of CrKα radiation and 311-diffraction were used. Fitting Lorentz method was used for peak analysis with 15752 measurement counts. The lattice plane spacing of the Fe (311) was measured in three different angles with three different directions to calculate the normal stress component. Lattice plane specific elastic constants Young's modulus, E = 213 GPa and

Poisson's ratio, ν = 0.3 were used for all measurements and stress calculations. The established sample coordinate system follows as: X represents the longitudinal direction, Y indicates the transverse direction, and Z corresponds to the vertical direction *(Gupta et al., 2019)*, as depicted in Fig. 4.1.

Table 4.1. Sample information and Measurement condition of X-ray residual stress measurement

Characteristic X-ray	CrKα
Measurement Area	3.00-30,000 (mm^2)
Diffraction line, hkl	αFe (311)
X-ray Tube voltage	30 (kV)
X-ray Tube current	1.00 [mA]
X-ray Incidence angle	35.0 (Deg)
Pitch	50 (μm)
Sample distance (Monitor)	34.000 (mm)
Sample distance (Analysis)	25.991 mm
X-ray wavelength (K-Alpha)	2.29093 (A)
X-ray wavelength (K-Beta)	2.08480 (A)
Total measurement count	15752
Oscillation measurement count	70
X-ray irradiation time (Setup)	90 (sec)
X-ray irradiation time (Meas.)	90 (sec)
X-ray irradiation time (Max)	120 (sec)

17

The diffraction of X-rays from the crystal lattice of the specimen being examined produces circular patterns known as Debye rings. Fig.4.3 and Fig. 4.4 represents the

2D and 3D views of the Debye-Scherrer ring image from the turbine blade sample, created using diffraction line 311 with CrKα radiation at a 35º angle to the z-axis. The angle of diffraction and radius of the obtained Debye ring are examined in order to evaluate the structural characteristics of blade.

4.4 Results and discussion

An analysis of the diffraction intensity has been conducted from the centre of the Debye ring to its outer perimeter. Observations indicate that the diffraction intensity exhibits a gradual and uneven variation along the Debye ring. This variation is attributed to the differing depths of X-ray absorption caused by the varying properties of the blade surface. The Debye ring displays a 'spotty' distribution across its surface, suggesting the presence of coarse and randomly oriented crystal grains on the blade surface, indicating an inhomogeneous deformation of the blade.

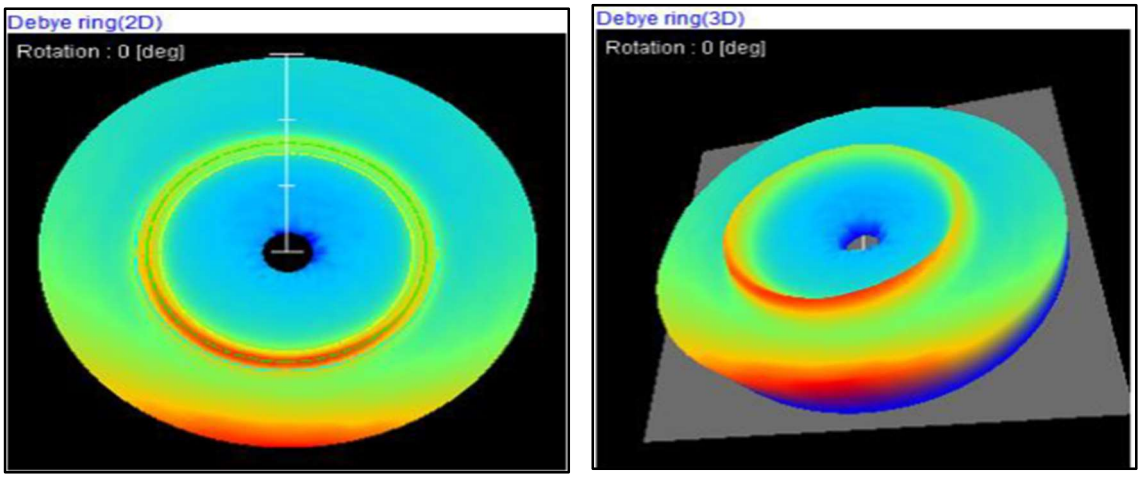

Fig. 4.3: Debye-Scherrer ring in 2 Dimensions and 3 Dimensions

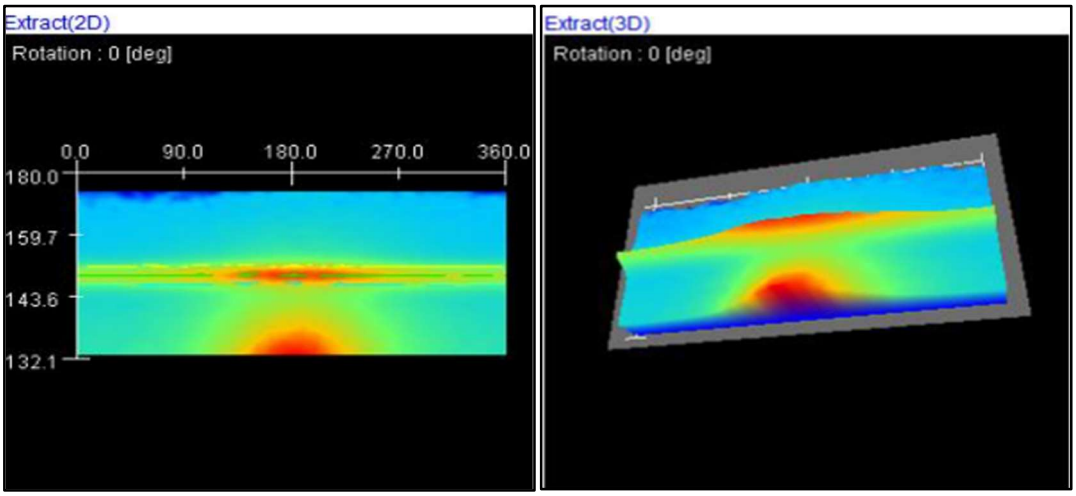

Fig. 4.4: Open Debye-Scherrer ring in 2 Dimensions and 3 Dimensions

Fig. 4.5 displays the plots of ϵ_{a1} - *cos* $\alpha$and ϵ_{a2} - *sin* α, which have been analyzed to ascertain the residual stress (σ_x) and shear stress (τ_{xy}) in MPa. The red line in the ϵ_{a1} - cosα and ϵ_{a2} – *sin*α diagrams represent the collinear approximation used to determine the slope, which is the variation in a1 concerning cos α and variation in a2 concerning sin α. These slopes have been utilized to calculate the residual stress and shear stress using Eqn. 4.3 and 4.4. Table 4.2 presents the results of the stress measurement using the μ-360 equipment. It is evident that the Residual stress (σ_x) and shear stress (τ_{xy}) are 46 MPa and -225 MPa, respectively, indicating the presence of non-zero residual stresses in the volume where X-rays are diffracted. The positive value of residual stress suggests that it is tensile in nature.

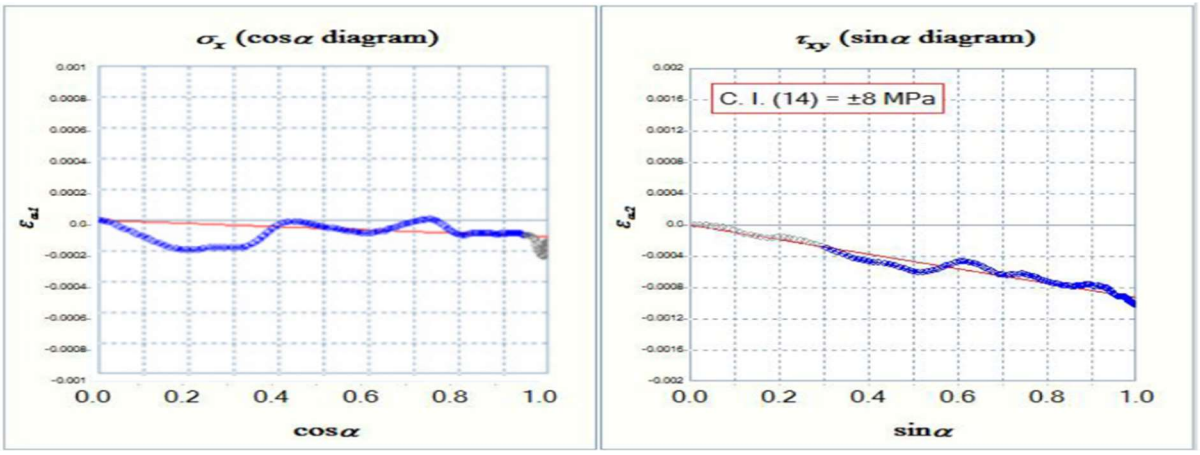

Figure 4.5: Stress analysis results for (cos α) and τ_{xy}) (sinα) diagram

Table 4.2: Measured Stresses

Slope (ϵ_{a1}-cosα diagram)	Residual Stress (σ_x)MPa	Slope (ϵ_{a2} -sinα diagram)	Shear Stress (τ_{xy}) MPa
- 0.000051	+ 46	-0.000941	- 225

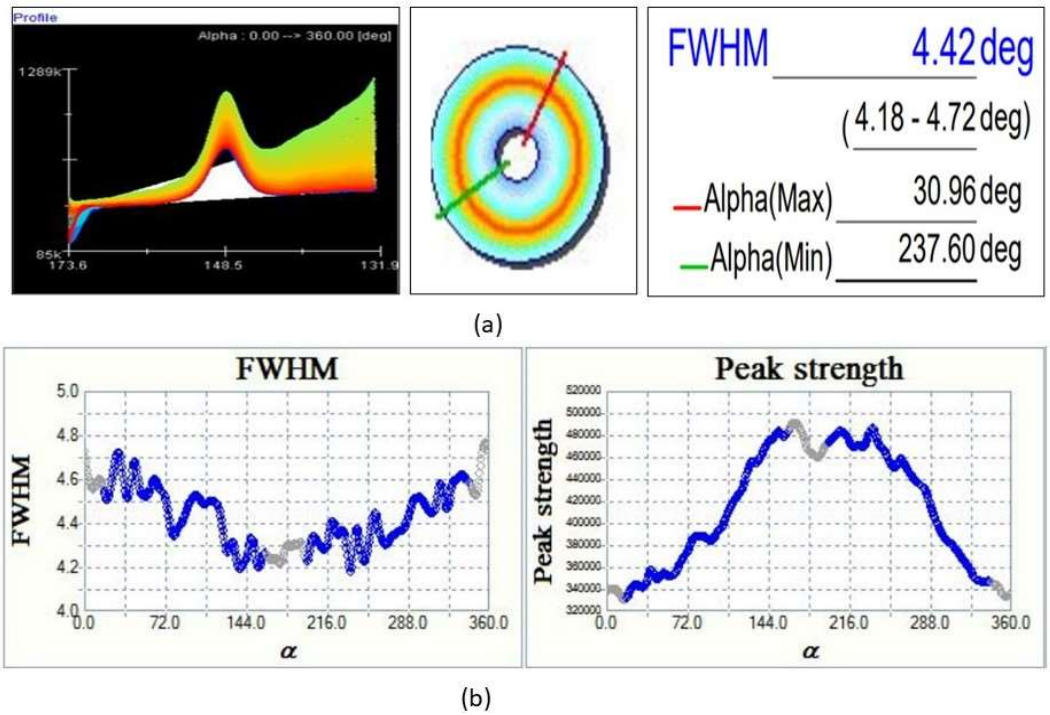

Figure 4.6(a): Profile image and intensity distribution of Debye ring (b): FWHM and Peak strength

The profile image presented in Fig. 4.6 depicts the intensity distribution as a function of the Bragg peak at 148.5°. The total diffracted energy, or integrated intensity, is calculated from the area under the diffraction intensity image. The peak width is usually measured by its Full Width at Half Maximum (FWHM). The Full Width at Half Maximum (FWHM) measures the broadening of a specific peak in the diffraction pattern and provides information on crystallite size and structural distortion, if present. Micro-distortions arise from stresses due to deformation, such as stacking faults or orientation variations, resulting in changes in inter-planar spacing that influence the

FWHM. The variation in FWHM and peak intensity is compared to the variation in integrated intensity. Factors that lead to an increase in peak maximum intensity can keep the integrated intensity constant. This consistency has been noted in the FWHM, as shown in Figure 4.6 (b), which was derived from 2D analysis of the failed turbine blade.

As shown in Figure 4.6 (b), the FWHM varies with maximum of 4.72 degree at α_{max}= 30.96 deg and with minimum of 4.18 degree at α_{min}= 237.60 deg, with an average of 4.45 degrees. This variation in FWHM suggests that the blade is subject to micro stresses caused by changes in inter-granular spacing, which result from high rotational speeds and extended usage. These factors are likely contributed to the blade's failure.

4.5 Conclusion

This chapter has provided a way to evaluate and analysis of residual stresses in L-0 LPST blade using X-ray diffraction (XRD) technique based on cos α method, which is a non-destructive and accurate method of measuring stresses that are presented in critical regions of rotating components. The experiment was able to develop the potential of the XRD cos α method of determining the residual state of stress with precision thus asserting its applicability in-service inspection and failure prevention measures. It was found that the blade surface is made of crystal grains, randomly oriented, and causes the non-uniform diffraction intensity along the Debye ring, reflecting the non-uniform stress distribution at the micro-structural level. In addition, the analysis of full width at half maximum (FWHM) showed that tensile residual

stresses were mainly on the blade surface. These tensile stresses are significant as they can greatly increase the rate of crack initiation and propagation due to cyclic loading under corrosive conditions, therefore become a contributing factor to fatigue and corrosion fatigue failure. The prime result of the chapter is that it was able to match the measurements of the diffraction with stress state of the blade material and this gives a good idea of the surface integrity and its role in structural reliability. The results address the significance of the inclusion of residual stress assessment in routine inspection and maintenance procedures to ensure high operational safety and longer service life.

Next chapter is dedicated to the static and dynamic analysis of the LP steam turbine blade using finite element simulation in *ANSYS*. The investigation focuses on identifying the critical stress concentration zones using static structural analysis, and analyzing the dynamic response of the blade using modal analysis and Campbell diagram to evaluate the natural frequency and corresponding mode shape of the blade at the operating conditions.

CHAPTER 5

COMPUTATIONAL FRAMEWORK TO DETERMINE THE STRESS DISTRIBUTION AND DYNAMIC BEHAVIOR OF LP STEAM TURBINE BLADE

In the previous chapter, critical analysis of residual stresses in L-0 low-pressure steam turbine blade was carried out using X-ray diffraction (XRD) technique based on cosα method. This approach provides a non-destructive and reliable means for accurately measuring residual stresses in critical turbine components. In this chapter, the final-stage low-pressure steam turbine blade is analyzed through both static structural and dynamic analysis using finite element approach. Primary aim is to locate the stress concentration regions and dynamic behavior of the low-pressure steam turbine blade responsible for its failure.

5.1 Introduction

For many years, the power generation industry has faced a serious problem with the breakdown of low-pressure steam turbine blades. According to the latest data from the Ministry of Power, Government of India, thermal power plants contribute to around 62% of the total electricity generated in India. Due to the sudden failure of turbine blades, the steam turbine stops working; such failure results in huge economic loss

(Wang et al. 2007). One of the most critical challenges in power plant operations is the failure of rotor blades, which causes premature failure of steam turbines and its other internal components. The Steam turbine comes under contact with severe dynamic forces subjected to unsteady flow and centrifugal forces *(Bhagi et al. 2018)*. Low-pressure steam turbine blades are more vulnerable to failure than high-pressure (HP) and intermediate pressure (IP) because LP blades derive a large portion of energy from the passing stream flow *(He et al. 2020)*. Low-pressure (LP) turbine blade failures can occur due to various factors, with a significant proportion of failures associated with fatigue, stress corrosion cracking (SCC), and corrosion fatigue *(Schönbauer et al. 2011)*. One of the prime factors of failure in the steam turbine blade is vibration persuasion fatigue *(Sanvito et al. 2012)* the fluid flow in the steam turbine blade excites the blade vibrations, and it becomes dangerous when resonance occurs as it starts to vibrate with large amplitude and result in catastrophic failure of blade *(Mohan et al. 2014)*. Multiple investigators have performed vibration analysis to scrutinize the cause of failure in low-pressure steam turbine blades.

Modal analysis and harmonic analysis are identified as efficient techniques for examining the vibration or dynamic characteristics of blades *(Shukla et al. 2016)*. A steam turbine blade must pass several critical speeds at distinct operating and dynamic conditions. These blades are designed to operate above and pass through from different critical speeds safely. The blade natural frequency investigation is a big concern for the safety of the steam turbine. The Campbell diagram is used to identify potential resonance conditions, which occur when the machine's rotational speed matches with one of its natural frequencies *(Kshirsagar et al. 2019)*.

Bhat et al., (1996) have determined the natural frequencies of the fourth and fifth stage of a low-pressure (LP), 235 MW steam turbine blade, two-blade disc system, and three-blade disc system using the Finite element method, dual-channel FFT analyzer, Campbell diagram. They have found that the natural frequencies decrease when the number of blades increases. Also, their conclusion indicates that a model with a single-blade disc provides a more precise prediction of the natural frequencies.

Rani et al., (2017) identified the failure mode and the exact location of the crack on the first-stage gas turbine blade. The investigation involved experimental modal analysis using *OROS*® vibration analyzer, and numerical analysis that employs finite element analysis (FEA) methodology using *ANSYS*® software. On comparing results obtained from experimental and numerical techniques, it is concluded that the findings of experimental modal analysis aligned with those of the computational analysis. Additionally, the study revealed that resonance at the sixth modal frequency was the underlying cause of the blade failure.

Prabhunandan et al., (2018) have performed the dynamic analysis of a single blade made of titanium material and for the assembly of rotor blades at two different speeds, 8500 rpm, and 19000 rpm. They have observed that at 8500 rpm, the blade is safe, but critical speed of the blade is obtained when the assembly of blades runs at 19000 rpm. Based on their findings, it was concluded that in order to prevent resonance, the turbine must operate at a speed below the critical threshold.

This Chapter focuses on the comprehensive computational analysis of the final stage low-pressure steam turbine blade. The study involves conducting static structural and dynamic analysis of steam turbine blade using finite element model, employing the *ANSYS,19* software as the primary tool. This research aims to locate the stress

concentration regions responsible for low-pressure steam turbine blade failure. Furthermore, the resonant frequencies of the steam turbine blade are ascertained by subjecting the blade to a modal analysis. The operational condition of the steam turbine may induce resonant vibrations in the blade, and they can be predicted with the help of the Campbell diagram.

5.2 Computation Analysis of an LP Steam Turbine Blade

The blade is collected from the 29th stage of 210 MW thermal power plant. The low-pressure steam turbine blade is made up of X10CrNiMoV12-2-2 alloy. Visual examination shows that the blade has a hairline crack in the transverse direction at a distance of 350 mm from the blade's tip.

To obtain the precise shape and dimensions of the blade, a 3D laser scanning process was conducted to create a three-dimensional CAD model of the blade using a laser light line. Scanning was done with the latest blue light scanning technology by Solutionix C500 structure blue light scanner. By utilizing the static structure analysis toolbox of *ANSYS 19*, the solid model of the scanned blade was created through the transformation of its 3D CAD model as shown in Fig.5.1.

Fig. 5.2 illustrates, the mesh model of the blade depicting a triangular surface mesh created initially, followed by volumetric meshing using the auto meshing capabilities of *ANSYS 19* software. The generated finite element modal has a total number of nodes as 50478 and a total number of elements as 28996. The fixed support is provided at the fir-tree part of the blade as its boundary condition, as shown in Fig. 5.3. The turbine blade has fixed supports at the root. The operating speed of the turbine blade is taken

as 3000 rpm. The rotation of the blade induces centrifugal forces resulting in a stiffening impact on the blade as shown in Fig. 5.4.

The centrifugal force acting on the blade evaluated by using Eq. 5.1

$$F \text{ (centrifugal force)} = \rho A \omega^2 (R_2^2 - R_1^2)/2 \quad 5.1$$

ρ is Material density = 7850 kg/m^3

A is the cross-section of turbine blade = 0.00097m^2

$R_1 = (R_2$ - Length of the turbine blade) = (1.6-0.9) m

R_2 is blade tip radius of the blade = 1.6m

ω is rotational speed of the turbine blade = 314.2 rad/s

The calculated centrifugal force is 778 KN/blade.

5.2.1 Chemical Composition

The material of the blade is characterized as X10CrNiMoV12-2-2 martensitic stainless steel alloy, which is a martensitic stainless steel. It is commonly employed in the steam turbine applications because it possesses great combination of high strength, corrosion resistance and good fatigue at high temperatures. The addition of alloying elements like chromium (Cr), nickel (Ni), molybdenum (Mo) and vanadium (V) increases hardenability, increases oxidation and corrosion resistance and helps to maintain microstructural stability in the course of long service exposures. To make a clear conception on the material characteristics, the chemical composition of the blade's material is tabulated in Table 5.1. This chemical compositional analysis becomes the foundation of correlating material characteristics with failure mechanism.

Table 5.1 Chemical Composition of X10CrNiMoV12-2-2 Alloy *(Ritz et al. 2018)*

Element	C	Cr	Ni	Mo	Mn	V	Si
Weight-%	0.117	11.4	2.70	1.64	0.70	0.31	0.23

5.2.2 Mechanical Properties

The mechanical properties of the turbine blade material X10CrNiMoV12-2-2 alloy are tabulated in Table 5.2. It is a high strength martensitic stainless-steel alloy that was specifically designed to be used in the steam turbine blades in which it gives an excellent combination of strength, toughness, corrosion resistance, and creep resistance in the higher temperature conditions. Critical parameters that determine the resistance of a material to centrifugal and aerodynamic high loads without plastic deformation and fracture are the yield strength and ultimate tensile strength of the material.

The material has a relatively high strength that ensures structural integrity at very high stresses of operation found in the end stage low-pressure turbine blades. Young's modulus (elastic modulus) controls the rigidity of the blade material and contributes greatly to the behavior of the material when it is loaded. This is an important parameter especially in the finite element analysis because it directly affects the stress distribution and displacement properties. The Poisson ratio is an indication of the behavior of the material in the lateral direction of the deformation and is crucial in the reliable prediction of 3D stress states using computational simulations. Besides the strength and stiffness, the elongation and reduction in the area also give an understanding of the ductility of the material that is important in crack initiation and propagation resistance in the presence of cyclic loading conditions. Sufficient ductility

will aid in delay of fatigue failure which is a prevailing failure mode in the turbine blades. The alloy hardness implies its ability to resist any surface deformation and wear, particularly, in the conditions when erosion caused by moisture and any impact on particles are common in the low-pressure stages. Moreover, the material demonstrates great fatigue strength and fracture toughness, which are necessary in the long-term reliability in varying stresses and vibratory loading. These characteristics will render material (X10CrNiMoV12-2-2) a good option when it comes to a rotating component that is critical like a steam turbine blade. Overall, the mechanical properties in Table 5.2 are the input parameters in the finite element modelling and are essential in the correct prediction of the stress-strain behavior, and the failure vulnerability of the blade when subjected to service conditions.

Table 5.2: Mechanical Properties of Turbine Blade Material

Young Modulus (GPa)	Tensile Yield Strength (MPa)	Ultimate Tensile strength (MPa)	Elongation at fracture	Contraction at fracture	Vickers Hardness (HV)	Density (Kg/m3)	Poisons ratio
213	843	1001	17.7%	58%	334	7850	0.3

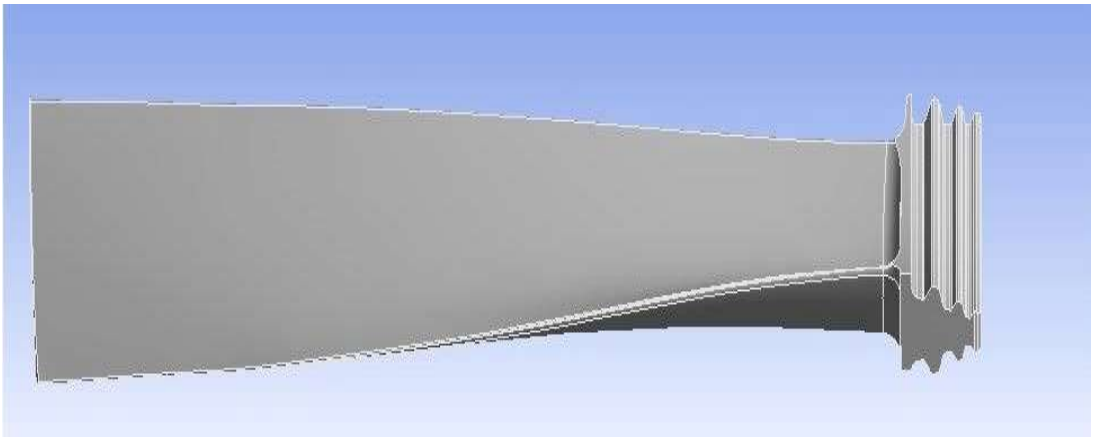

Figure 5.1: 3-D CAD Model of LP steam turbine blade

5.2.3 Boundary conditions

The boundary conditions that have been taken in the current analysis are designed to realistically depict the operational conditions of the turbine blade. Fig. 5.3 shows that a fixed support at the fir-tree root of the blade is used to simulate the rigid attachment of the blade to the turbine disc. The assumption limits any degree of translation and rotation at the root and thus simulating the actual mounting condition of the blade in service conditions.

The L-0 low-pressure steam turbine blade is analyzed at an operating speed of 3000 rpm as depicted in Fig 5.4, similar to the optical conditions of a steam turbine. A high centrifugal force is produced at this rotational speed because of the weight of the blade. These forces act radially outward and create tensile stresses in the span of the blade and the centrifugal loading effect results in the stiffening effect of the blade also known as centrifugal stiffening, which increases the structural rigidity of the blade and affects the dynamic characteristics of the blade, such as the natural frequencies and deformation.

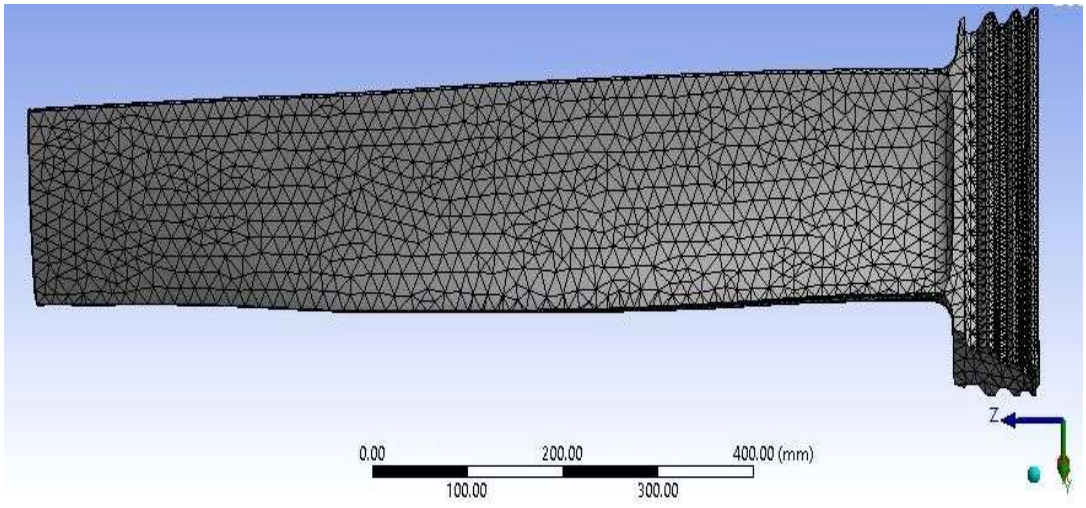

Figure 5.2: Mesh Model of LP steam turbine blade

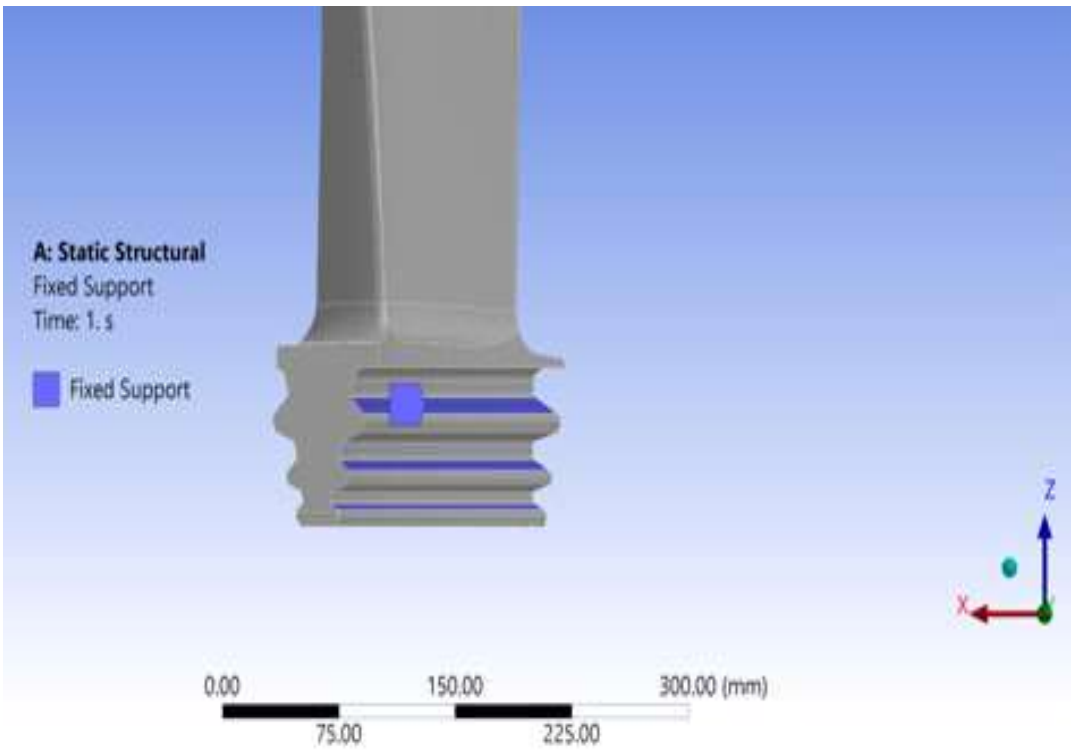

Figure 5.3 Blade is fixed at the fir-tree part of the blade

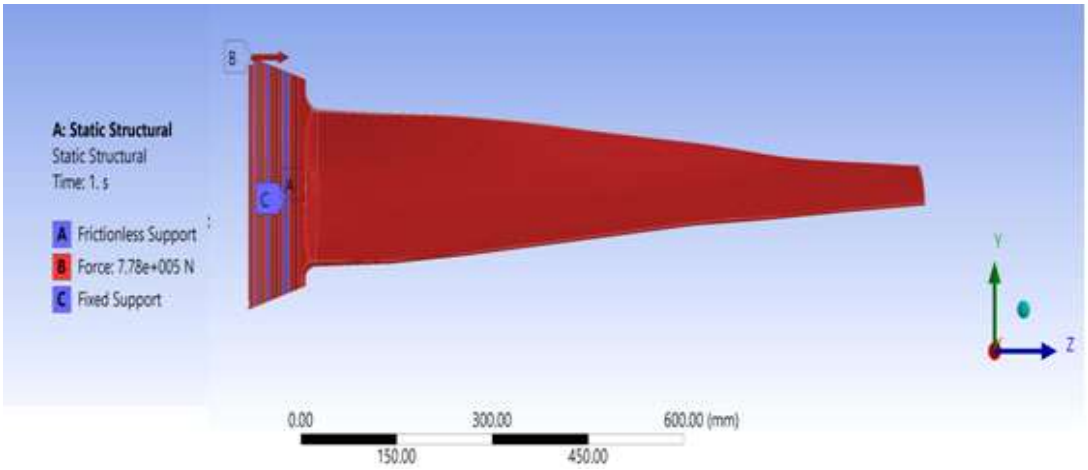

Figure 5.4: Centrifugal force applied on the blade

5.3 Static Structural Analysis of Blade

Static structural analysis has been performed to identify the deformation and stress distribution in a Low-pressure steam turbine blade. This analysis allows us to identify

the potential risks and areas that are critical and could fail during operation. The study is conducted with a numerical approach, and the software used is *ANSYS®19*. The maximum deformation of 47 mm was observed near the blade's tip (Fig. 5.5). This shows that the area near the tip or at the blade's tip is critical for failure. The Maximum Principal Stress, Maximum Principal Strain and Shear stress induced in the blade have a maximum value of *713.81 MPa, 0.00318 MPa,* and *83.203 MPa,* respectively (Fig. 5.6-5.8). The Von-Mises stress induced in the blade is near the concave side of the root and has a maximum value of *678 MPa* and a minimum value of *0.465 MPa* (Fig. 5.9).

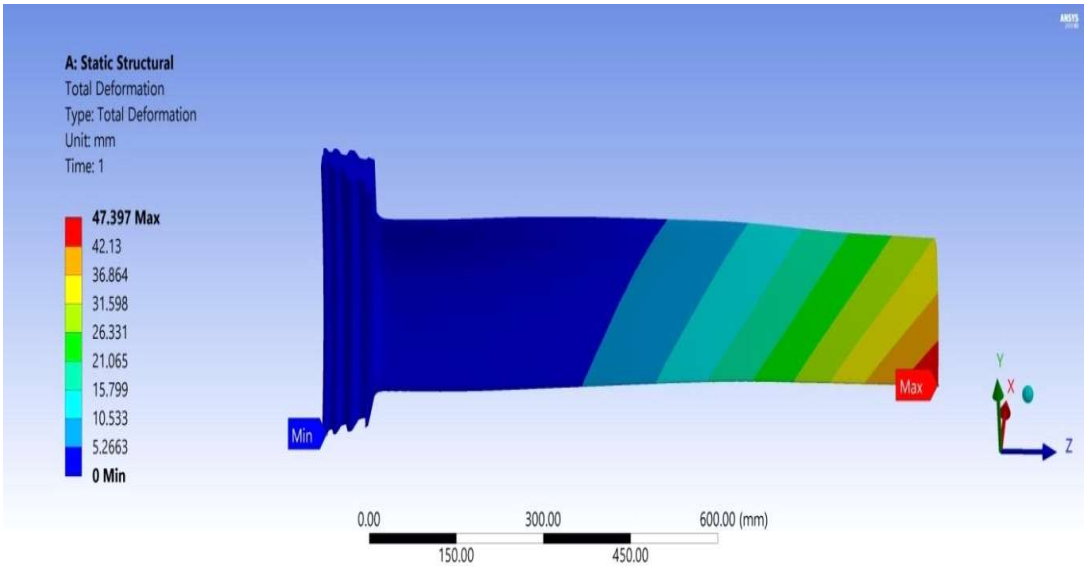

Figure 5.5: Maximum deformation of the LP steam turbine blade

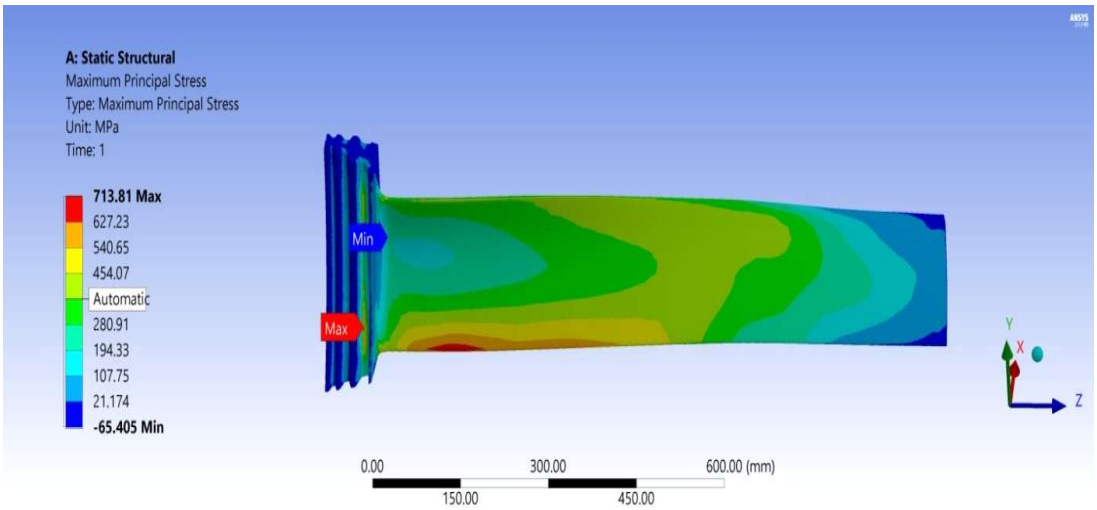

Figure 5.6: Maximum Principal Stress of the LP steam turbine blade

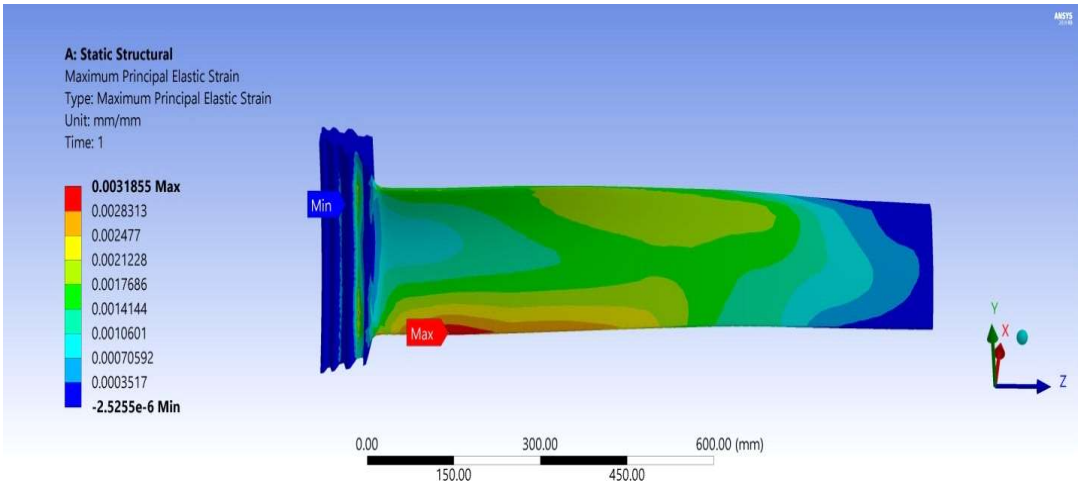

Figure 5.7: Maximum Principal Elastic Strain of the LP steam turbine blade

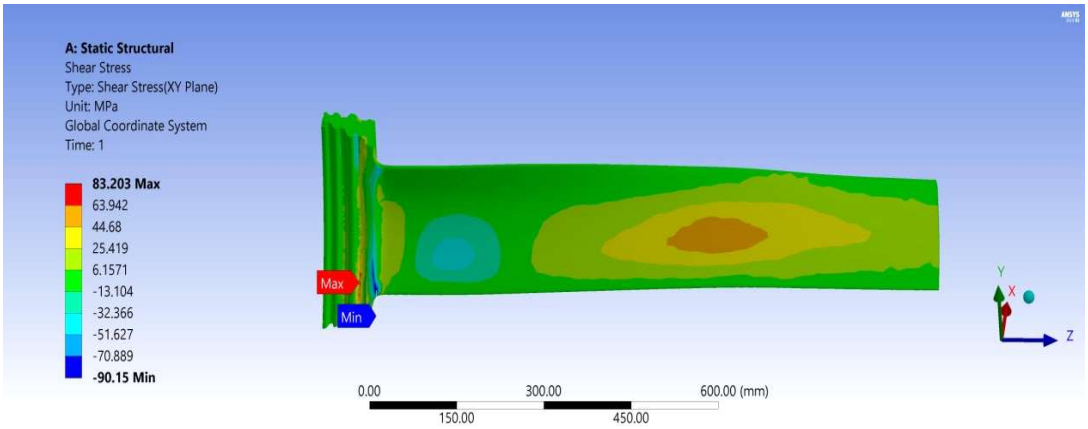

Figure 5.8: Maximum Shear Stress of the LP steam turbine blade

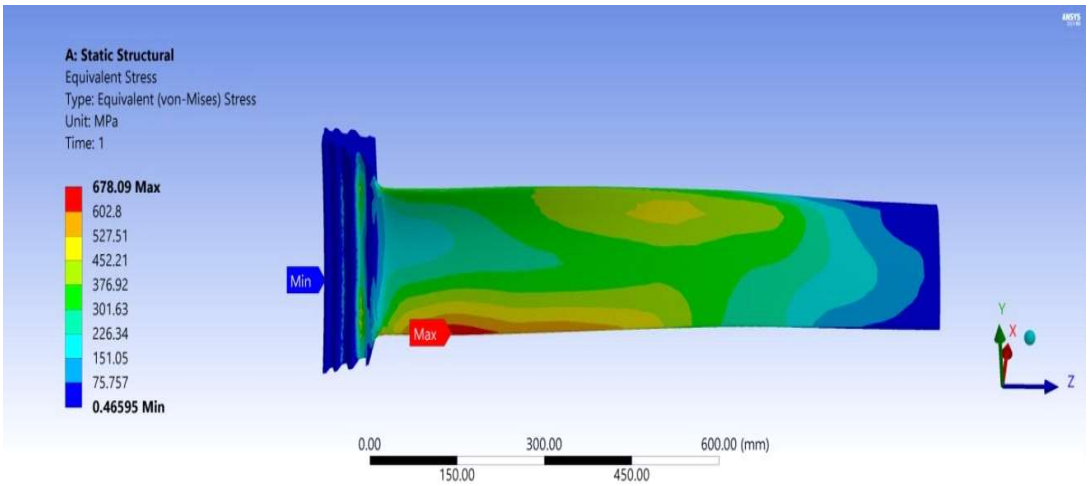

Figure 5.9: Maximum Von-Mises Stress of the LP steam turbine blade

5.3.1 Dynamic Analysis of LP Steam Turbine Blade

A finite element approach is employed to perform dynamic analysis of an LP steam turbine blade. The three-dimensional model of the blade is created and analyzed on *ANSYS*® software. The first six modal frequencies are obtained as *45.984 Hz, 108.62 Hz, 192.75 Hz, 240.2 Hz, 318.54 Hz* and *394.54 Hz.* The first six natural frequencies and their respective mode shapes are shown in Fig. 5.10 -5.15.

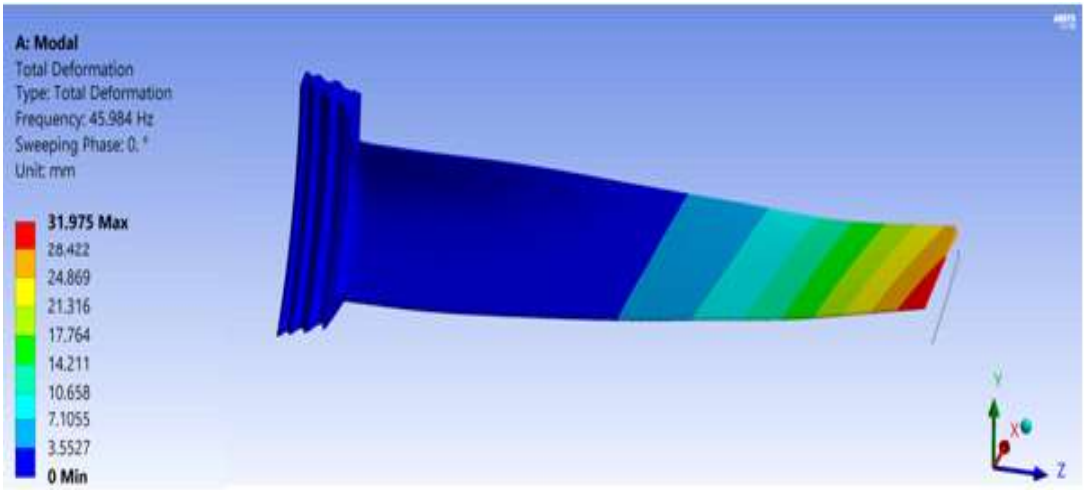

Figure 5.10: Mode 1 (Bending) of the blade at frequency 45.984 Hz

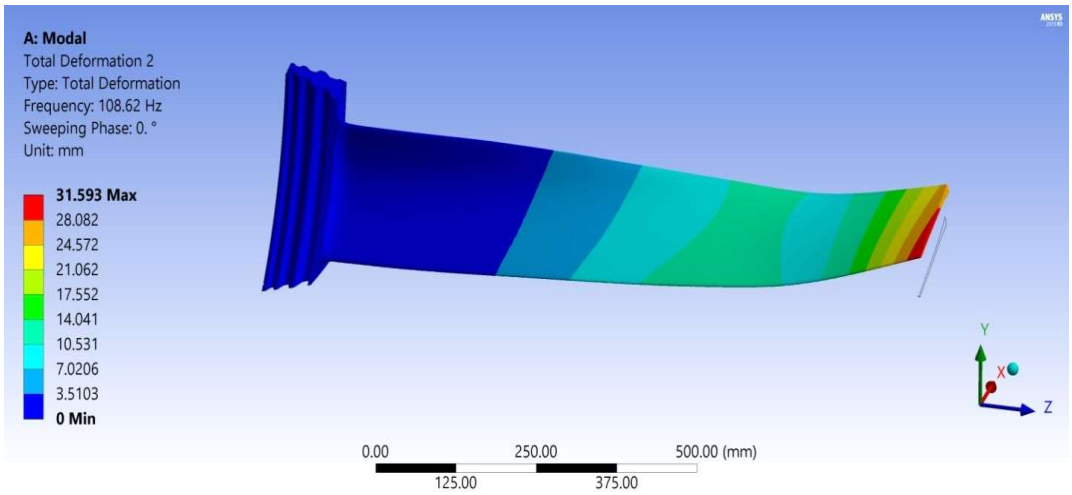

Figure 5.11: Mode 2 (Bending-Torsion) of the blade at 108.62 Hz

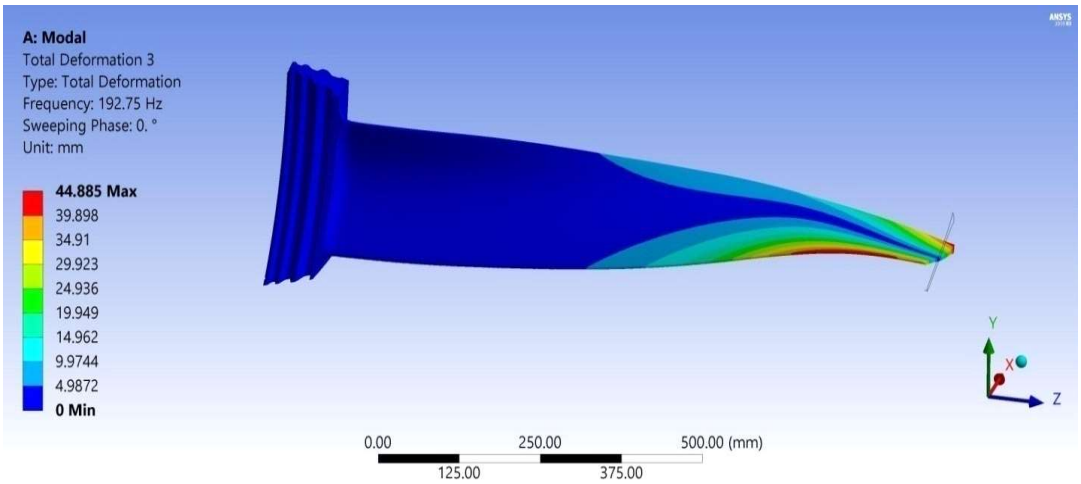

Figure 5.12: Mode 3 (Torsion) of the blade at 192.75 Hz

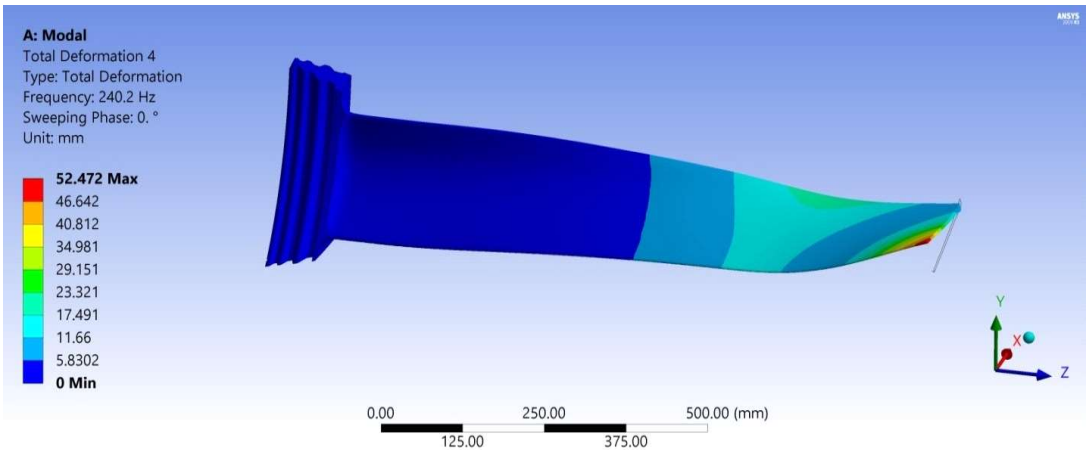

Figure 5.13: Mode 4 (Bending-Torsion) of the blade at 240.2 Hz

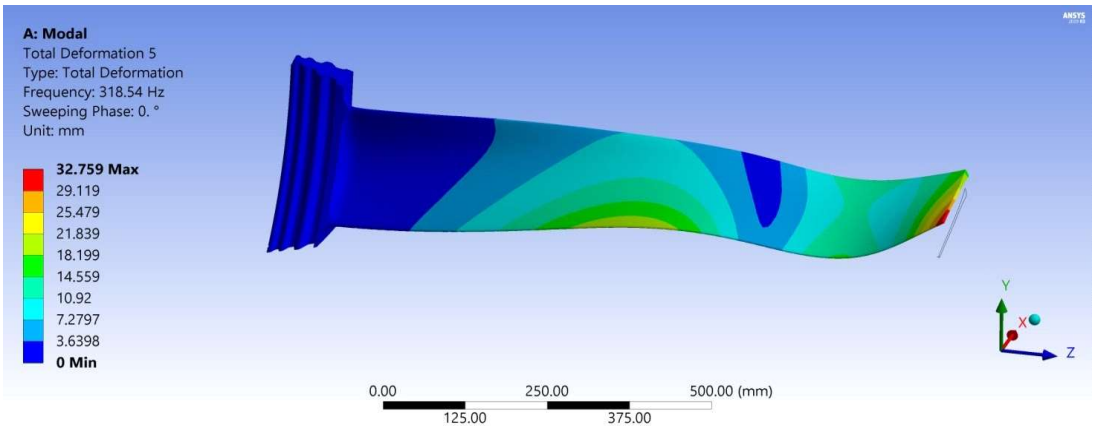

Figure 5.14: Mode 5 (Bending-Torsion) of the blade at 318.54 Hz

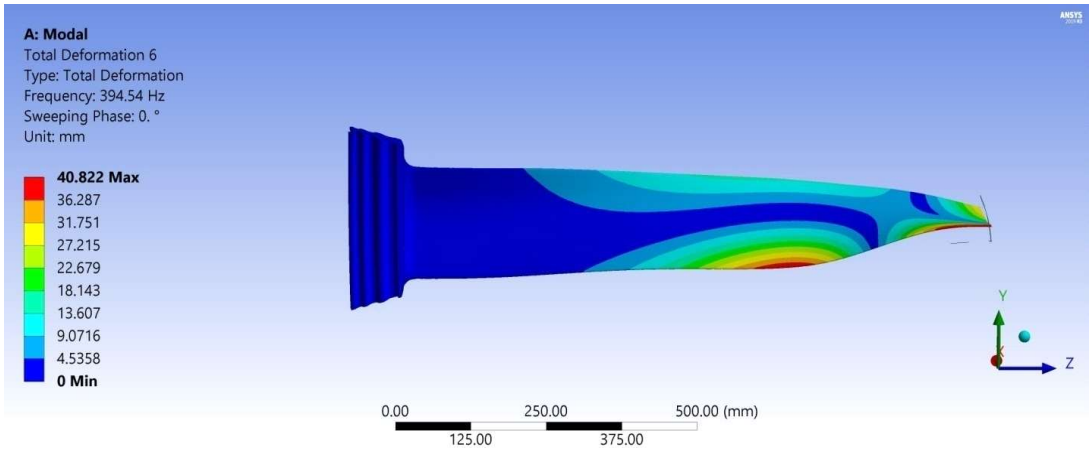

Figure 5.15: Mode 6 (Bending-Torsion) of the blade at 394.54 Hz

5.4 Campbell Diagram of LP Steam Turbine Blade

The Campbell diagram is a graphical representation that displays the relationship between blade rotational speed and frequency and is utilized to predict potential resonant conditions during blade operation. It becomes necessary to determine the component's critical speed at the intersecting fundamental frequency. The Campbell diagram is drawn on the Graph Pad software to draw harmonic lines. Three harmonic lines were graphed on Graph Pad software, with each line starting from the zero point and sloping upwards toward the right of the vertical axis. Within the operational speed

range, the point where the natural frequency lines and the harmonic lines meet signifies the likelihood of blade resonances. According to the manufacturer's operation guide, the operating speed range for low-pressure steam turbines is 2880 rpm to 3000 rpm. The first six natural frequencies of the blade at different rotational speeds are obtained by dynamic analysis of the blade and tabulated in Table 5.4

Table 5.4: Natural frequencies of the blade at the different rotational speed

Mode	0 rpm	500 rpm	1000 rpm	1500 rpm	2000 rpm	2500 rpm	3000 rpm
First Natural frequency	45.984 Hz	39.788 Hz	30.006 Hz	22.884 Hz	18.173 Hz	14.964 Hz	12.676 Hz
Second Natural frequency	108.625 Hz	102.642 Hz	96.375 Hz	91.390 Hz	86.275 Hz	80.810 Hz	75.211 Hz
Third Natural frequency	192.752 Hz	208.534 Hz	201.284 Hz	186.963 Hz	174.446 Hz	164.892 Hz	157.960 Hz
Fourth Natural frequency	240.199 Hz	255.954 Hz	294.068 Hz	302.082 Hz	304.015 Hz	304.776 Hz	305.157 Hz
Fifth Natural frequency	318.538 Hz	324.219 Hz	372.317 Hz	465.675 Hz	548.790 Hz	625.429 Hz	703.505 Hz
Sixth Natural frequency	394.538 Hz	411.251 Hz	453.053 Hz	528.410 Hz	636.922 Hz	764.685 Hz	898.966 Hz

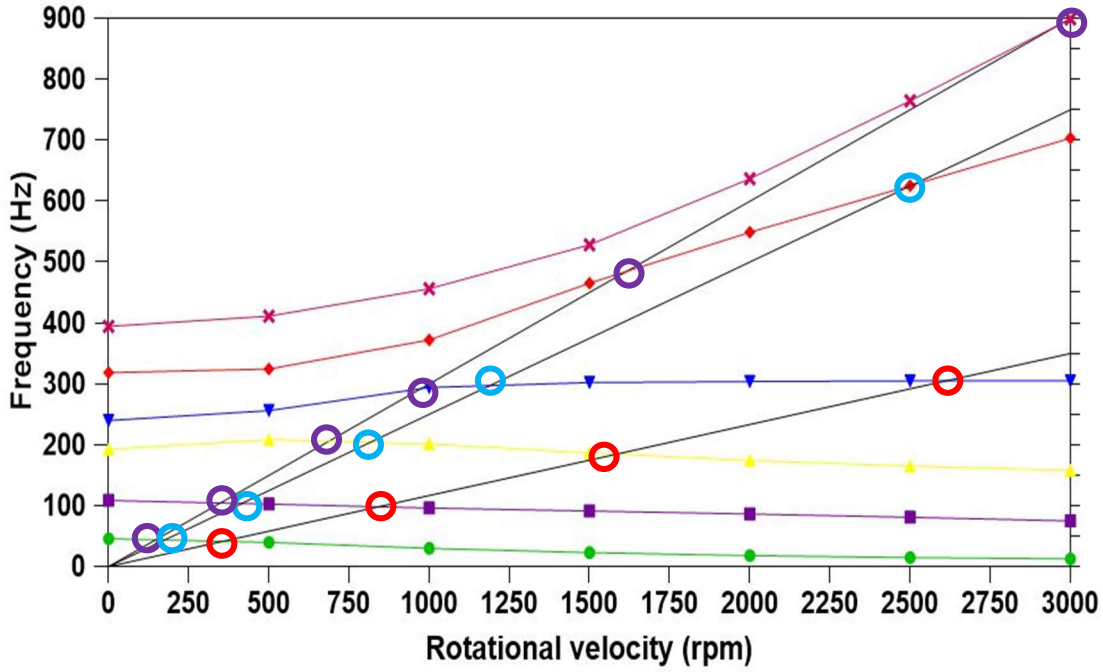

Figure 5.16: Campbell Diagram of LP steam turbine blade

Table 5.5: Critical Speed at 7th, 15th, 18th harmonic lines

7th harmonic line	**15th harmonic line**	**18th harmonic line**
356.3 rpm	175.25 rpm	147.2 rpm
842.94 rpm	414.65 rpm	348.19 rpm
1584.4 rpm	815.82 rpm	686.12 rpm
2613.1 rpm	1188.3 rpm	973.49 rpm
	2504.6 rpm	1617.2 rpm
		2967.1 rpm

5.5 Results and Discussion

This research analyzes a real case LP steam turbine blade made of material X10CrNiMoV12-2-2 alloy to identify the critical areas and failure regions or zones

during operation. When a load of 778 kN/blade was applied to the blade, then maximum deformation of 47 mm was observed near the tip of the blade. This shows that the tip of the blade is critical for failure. Other stresses such as Von-Mises stress, maximum principal stress, maximum principal strain, and shear stress of the LP steam turbine blade are also evaluated computationally to identify the blade areas prone to failure.

Dynamic analysis is also performed to evaluate the natural frequencies of the blade so that resonance conditions can be avoided during operation. Further, the first six natural frequencies at 0 rpm, 500 rpm, 1000 rpm, 1500 rpm, 2000 rpm, 2500 rpm, and 3000 rpm have been evaluated. The low-pressure steam turbine runs at 3000 rpm and 50 Hz, and when the turbine starts from zero rpm to reach 3000 rpm, it has to pass through many critical speeds. The critical speeds are obtained by the intersection of the harmonics line with the natural frequencies line, as shown in the Campbell diagram in Fig. 5.16. The operator needs to prevent a long run on these critical speeds and should move in the safe zone as soon as possible to avoid resonance. So, it has been necessary to provide safe zones to the operator for machines such as steam turbine blades with different natural frequencies. Campbell diagram helps the operator find the regions of safe limits where resonance can be avoided. The intersection of the harmonics line with the frequency line obtains the critical speeds. Critical speeds at the 7^{th}, 15^{th} and 18^{th} harmonic lines are tabulated in Table 5.5.

5.6 Conclusion

Computational analysis of the LP steam turbine blade was carried out to detect the areas on the blade that are critical and prone to failure. The following conclusions were

drawn:

i) L-0 low-pressure steam turbine blade has been analyzed computationally to determine the most critical areas that are prone to failure during the running of the turbine. The failed blade was scanned that effectively captured the geometry of the blade and a high-fidelity three-dimensional CAD model was created. Static structural analysis of the blade was done using ANSYS,*19* software to predict its deformation, von Mises stress, principal stresses and strains, and distribution of shear stresses throughout the blade. The findings showed that the concave root region around the trailing edge was the area that most susceptible to stress concentration which was about 678 MPa as a combination of centrifugal and steam loading forces hence showing it as a possible location of crack initiation and propagation. The level of stress is not too much to cause the material to blow out due to the applied loading conditions, but the results pointed at the high stresses in the real working conditions where dynamic changes take place.

ii) Dynamic analysis of the blade provides first six natural frequencies and the mode shapes which is very crucial to understand the vibrational behavior of the blade. The difference in natural frequencies was observed, which highlighted the necessity of resonance avoidance that was further discussed using the Campbell diagram. The identification of intersections between harmonic excitation lines and higher vibration frequencies at particular rotational speeds indicates the presence critical rotational speeds which may compromise the structural integrity of the turbine blade.

iii) The significant contribution of this chapter is that it combines the geometric precision (3D CAD model) with the detailed finite element analysis and, as a result, it is possible to conduct the systematic examination of the vulnerable areas, the structural stability, and the dynamic nature of the blade when subjected to realistic service loads. The next chapter will observe the fatigue crack growth behavior of a cracked L-0 steam turbines blade. To simulate the crack propagation and measure its stability, a 3D hybrid simulation model that combines ANSYS with FRANC3D is utilized to give a better understanding of the mechanisms of failure and to make predictions of the life of the turbine blades reliably.

turnitin Page 130 of 178 - Integrity Submission Submission ID trn:oid:::29034:134939416

CHAPTER 6

Computational Approach for Crack Growth Simulation and Fatigue Life Prediction in Low-Pressure Steam Turbine Blades

In the previous chapter Static structural and dynamic analysis of a low-pressure steam turbine is carried out using finite element-based software ANSYS. Static structural analysis measures the stress distribution to locate the critical regions where the blade could fail during operation, Dynamic analysis is performed to determine the vibration characteristics of the blade including modal frequencies and mode shapes. In the present chapter a coupled simulation framework integrating finite element analysis using ANSYS and crack growth modeling with FRANC 3D was developed to investigate the fatigue crack propagation behavior and fatigue life assessment. The results highlight the significance of stress intensity factor K_I, wherein crack propagation becomes unstable when K_I exceed the fracture toughness K_C, ultimately resulting in catastrophic failure.

6.1 Introduction

Fatigue failure is one of the major reasons of failure of Low-pressure steam turbine blade, which can result in unintended turbine shutdowns, thus influencing the reliability and efficiency of power generation systems *(Rani & Agrawal, 2024; W. Z. Wang et al., 2007*). Fatigue failures in engineering components can occur in various forms depending on the type of loading and environmental conditions. (*Mazur et al., 2009; Perkins & Bache, 2005*). The simplest form is mechanical fatigue, which is caused by cyclic variations in the stresses or strains applied to the component in an essentially isothermal environment (*Singh et al., 2020*). When combined with the effects of elevated temperatures, in which the time-dependent inelastic deformation process of creep interacts with cyclically induced plastic strain, a phenomenon known as creep-fatigue interaction emerges (*L. Chen et al., 2007*). On the other hand, thermomechanical fatigue is experienced in conditions when both temperature and mechanical loading changes simultaneously and lead to complicated interactions between thermal expansion and mechanical stresses (*Yin et al., 2022*).

3 Corrosion fatigue is a type of fatigue failure, which takes place when a material is subjected to cyclic loading in a chemically aggressive or embrittling environment. In these circumstances, the combined effect of mechanical fatigue damage and electrochemical 87 degradation significantly reduced the fatigue life of the material. In the low-pressure (LP) stages, the presence of wet-steam environment, makes the turbine blades susceptible to these types of damages. The synergistic interaction of moisture, dissolved impurities along with cyclic stresses, promotes rapid initiation and propagation of cracks (*Adnyana, 2018;*

Salzman & Gandy, 2011). Further, fretting fatigue presents a major concern at the interface of blades and turbine discs, where the cyclic stresses acting on the parent material are accompanied by low-amplitude oscillatory micro-slip and associated frictional sliding at the contact interfaces, facilitate crack initiation and accelerate damage evolution under fatigue conditions (*Xue et al., 2014*) the implication of these processes extends well beyond turbomachinery, since majority of fatigue failures in structural and mechanical components during service can be attributed to one or more of these governing mechanisms. It is therefore critical to understand the operative fatigue mechanisms to predict the service life of cyclically stressed components and to understand the rate at which damage nucleates and propagates. Fatigue life is typically divided into two stages - crack initiation and crack propagation - which are interrelated and progressive. In the crack initiation period, repeated plastic straining occurs at micro-structural non-homogeneities (such as inclusions, grain boundaries, surface flaws, or stress concentrators) and gives rise to the formation of persistent slip bands (PSBs) and the nucleation of small cracks. During the crack propagation phase, the major crack grows step-by-step with each cycle of loading, resulting in the formation of fatigue striations on the fracture surface (*Kuželka et al., 2019*).

Fatigue analysis is critical in predicting service life and ensuring the structural integrity of LPST blades. Conventional fatigue analysis approaches are primarily based on experimental derived methodologies, including the stress life (S-N) approach for high cycle fatigue and the strain-life (ϵ-N) approach for low-cycle fatigue conditions (*Bhamu et al., 2021; Tulsidas et al., 2014*). Despite their effectiveness, these approaches are associated with high experimental cost, as well as dependencies on material availability and the need for standardized test specimens. This led to the

development of computational simulation methods, particularly Finite Element Modeling (FEM) and Extended Finite Element Modeling (XFEM) being invaluable tool in exploring the complex behavior of turbo-machinery components (*Bayesteh & Mohammadi, 2011; Z. Chen et al., 2022*). The advanced commercial simulation software programs like ANSYS and ABAQUS are widely used to obtain the detailed stress distributions, deformation behavior and thermal gradient of the turbine blades under the practical operating conditions *(Kocharla et al., 2022)*. These numerical techniques would help to understand the mechanisms of crack initiation and growth mechanisms, which play a critical role in governing fatigue failure in turbine components (*Salehnasab & Poursaeidi, 2020)*.

FRANC3D, a specialized fracture mechanics analysis tool, is widely used to simulate complex three-dimensional crack propagation problems. It can capture the complex geometries, localized loading conditions, and evolving crack fronts which makes it particularly useful in investigating fracture mechanics behavior in engineering structures and turbo-machinery components (*Fernandes et al., 2016)*. Furthermore, the software has been designed to be used together with general-purpose finite element solvers like ANSYS and ABAQUS, thus, extending its capability to allow detailed and comprehensive analyses of fracture mechanics (*Bhachu et al., 2017; Zhang et al., 2023*). (*Poursaeidiet al., 2014*) conducted a study on rotary compressor blades, demonstrating that single cracks can originate from the coalescence or merging of two semi-elliptical cracks. Using FRANC3D, both single and double-crack conditions were simulated and observed that the stress intensity factors were similar in the crack tip in both scenarios. The study further indicated that crack length increased significantly in the course of crack coalescence and this substantially increased the risk of blade failure.

Li et al., (2023) introduced a novel way of studying crack propagation in turbine blades under varying preloads by using tabular and sinusoidal loading. This study found that, looking at it in the top view, both the convex and concave blade surfaces would develop cracks facing the trailing end and the cracks propagate very little on the leading end. The cracks had a slight deviation along a straight path e when the cracks were loaded under the sinusoidal conditions. *(W. Wang et al., 2023)* studied fatigue crack formation in airfoil blades under aerodynamic and centrifugal loads. Their finding showed that aerodynamic loads promoted crack growth towards the trailing edge, while centrifugal loads directed crack towards the leading edge. Under combined loading, cracks propagated primarily along a single plane, with centrifugal loads exerting a dominant influence on the longest crack paths. This highlights the significance of considering centrifugal loads in airfoil blade design and durability assessments.

This research investigates fatigue crack growth behavior in LPST blade composed of X10CrNiMoV12-2-2 martensitic stainless steel alloy using a new coupled simulation approach. By integrating ANSYS (finite element software) and FRANC3D (crack growth simulation tool to compute the stress intensity factor and understand fatigue crack propagation under operating conditions. The stress intensity factor, K_I was determined to be a primary governing parameter in crack propagation and crack growth instability, potentially leading to rapid propagation and catastrophic turbine blade failure when the stress intensity factor K_I exceeds the material's critical stress intensity factor K_C.

6.2 Fractography of LPST blade

A failed L-0 LPST blade composed of X10CrNiMoV12-2-2 alloy was collected from a 210 MW thermal electric power station. Upon Visual inspection, a transverse crack was observed 350 mm from the blade tip as depicted in the Fig.6.1. The blade was examined using fractographic techniques i.e, Energy-dispersive X-ray spectroscopy (EDS) in conjunction with scanning electron microscopy (SEM). The repeated impact of Sio_2 particles on the blade material leads to the accumulation of deposits, causing surface damage characterized by pitting and groove formation. The process, combined with corrosive influences, ultimately results in fatigue that contributed to the failure of the LPST blade *(Sehra & Rani, 2023)*.

Figure 6.1: (a) Location of crack (b) Transverse crack on the leading edge of L-0 LPST blade

6.3 Computational modeling and analysis of LPST blade

A 3D (three-dimensional) CAD model of the blade was created by employing a 3D laser scanning technique, which captured the exact dimensions and contours of the blade. Using ANSYS finite element software, the 3D CAD model of the scanned blade was converted into solid model, as illustrated in Fig 6.2.

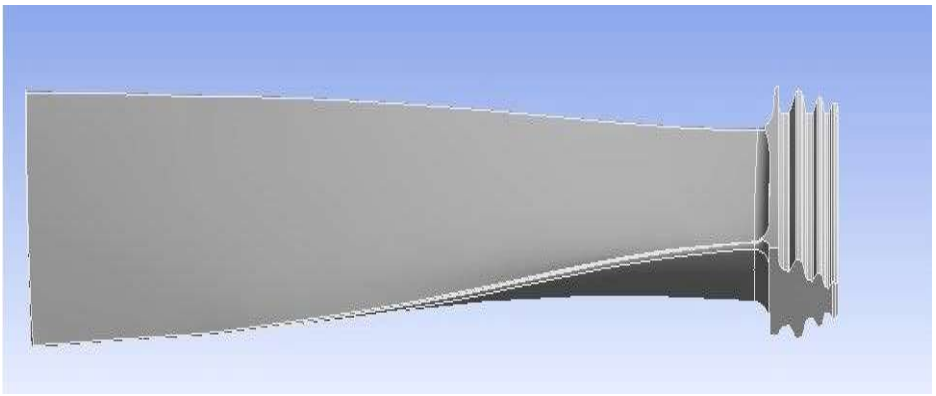

Figure 6.2: Three-dimensional CAD model of LPST blade

To simplify the stress analysis process, a 3D model of a rotor sector corresponding to a single blade was developed, instead of modeling the entire rotor assembly. Fig. 6.3(a) illustrates the sectional view of the LPST blade along with the rotor sector. To further optimize the computational approach, cyclic symmetry was employed as a boundary condition. This methodology significantly simplifies the meshing process, thereby reducing computational complexity and processing time. Additionally, it enables a more detailed and accurate evaluation of the blade's structural responses and modal characteristics. The complete assembly of the LP steam turbine blade and rotor is depicted in Fig. 6.3(b).

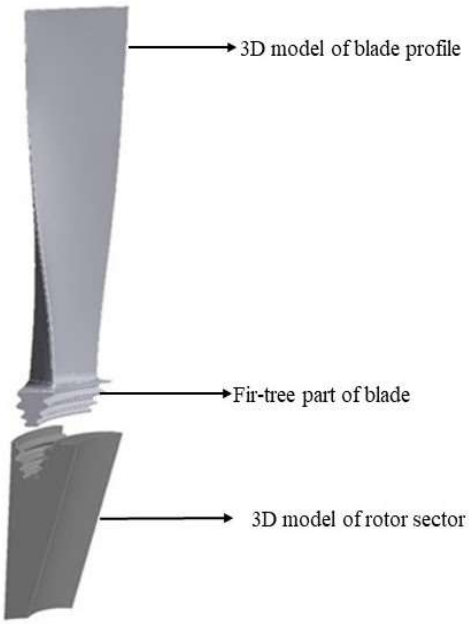

Figure 6.3(a): Sectional view of LPST blade and rotor sector

Figure 6.3(b): Assembled view of LPST blade and rotor sector

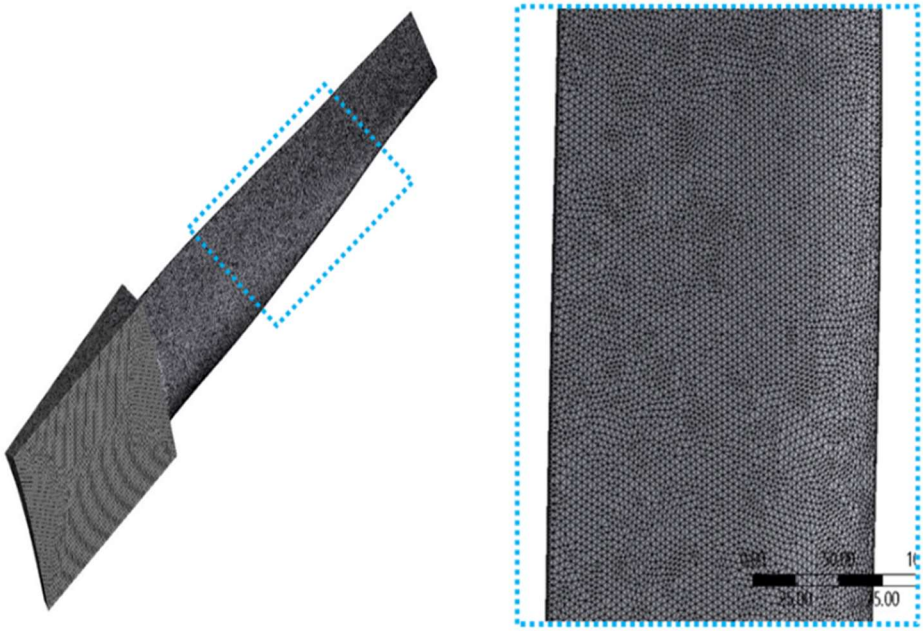

Figure 6.4 Mesh Model of turbine blade-rotor with magnified view of section of blade assembly

Fig. 6.4 shows a 3-D mesh model of the LPST blade and rotor assembly, generated using the auto meshing capabilities and a ten-nodded tetrahedral approach of ANSYS software, employing SOLID 187 elements. A body-size meshing of 5 mm and a face-size meshing of 3 mm are used for meshing the turbine blade-rotor assembly. The mesh model of turbine blade-rotor assembly comprises of 746778 nodes and 468662 elements as demonstrated in magnified mesh model of blade section in Fig. 6.4.

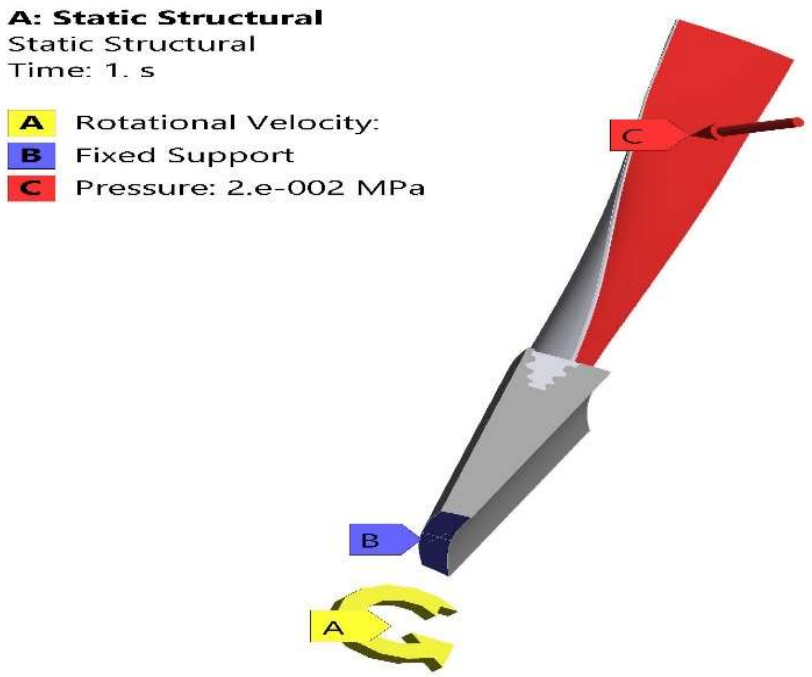

Figure 6.5: Boundary conditions of turbine blade-rotor assembly

In the analysis of the LPST blade-rotor assembly, specific boundary conditions are applied to simulate operational conditions accurately. The fir-tree region of the LPST blade is constrained using fixed supports, thereby imposing fixed boundary conditions along its outer surfaces as illustrated in Fig. 6.5. The blade operates at a rotational speed of 3000 rpm. Additionally, the steam impinging on the turbine blade is

characterized by a pressure of 2 MPa and a temperature of 120^0C, which are critical parameters influencing the blade's performance under these conditions.

6.3.1 Static Structural Analysis of LPST blade

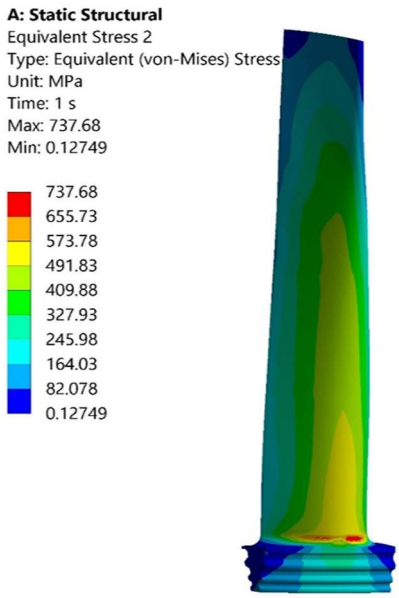

Figure 6.6: Equivalent stress of LPST blade

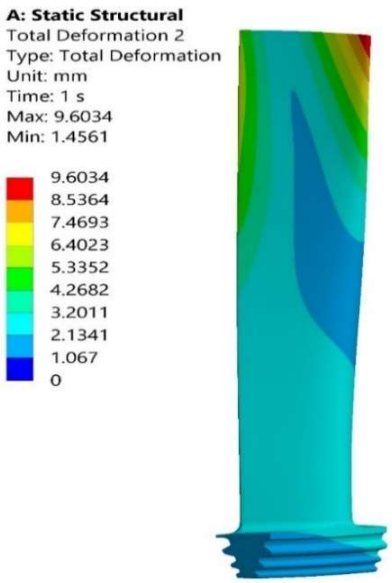

Figure 6.7: Total Deformation of LPST blade

A numerical static structural assessment was carried out to determine the deformation and stress distribution in a LPST blade. This approach enabled the identification of critical zones, potential failure points, and regions at elevated risk during operation. The simulations were carried out using ANSYS software. The results presented in Fig 6.6 and Fig 6.7 shows the equivalent stress and total deformation of the blade, respectively. The maximum equivalent stress was found to be 737.68 MPa at the root of the blade, while the maximum deformation of 9.6 mm was obtained at the blade's tip.

It is observed that the location where the crack was initiated, as shown in Fig. 1, differed from the location of the equivalent stresses, as shown in Fig. 6. This discrepancy can be attributed to factors such as material defects or fluctuations in operational conditions. Hence, there is a need to understand crack growth behavior i.e. the mode of crack initiation and its propagation. FRANC3D code is used to understand in-depth crack growth behavior. The results of equivalent stress of turbine blade are imported into the Franc 3D Code to analyze crack growth behavior.

6.3.2 Grid Independence Test

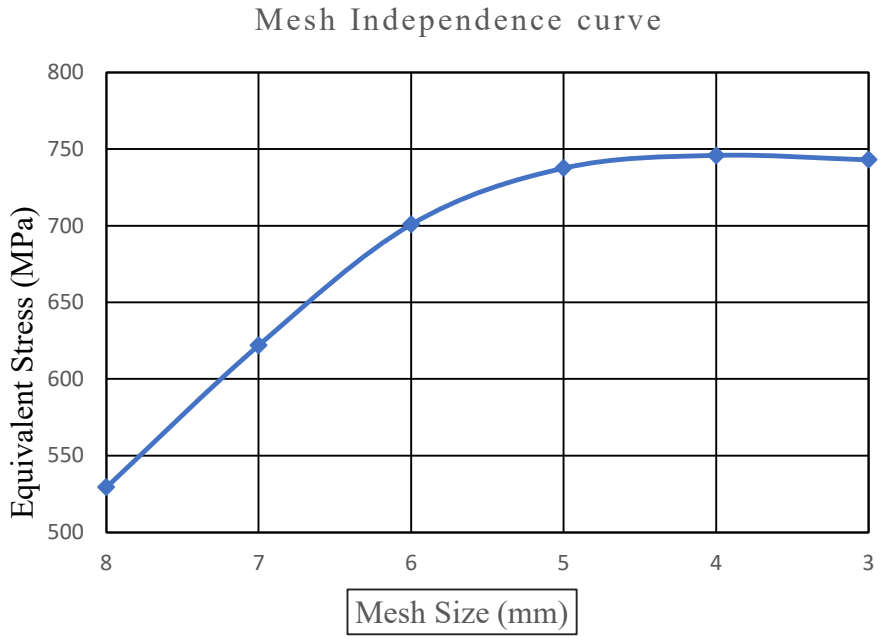

Figure 6.8: Grid Independence test

A mesh convergence study was performed to verify that the finite element analysis results were not influenced by mesh density. The analysis involved testing various mesh sizes ranging from 8 mm to 3 mm while examining the equivalent stress at the critical location. Fig 6.8 shows that the equivalent stress or von-misses stress values

initially changed significantly with mesh refinement but gradually stabilized around 737.68 MPa, indicating convergence. The mesh independence curve confirmed that refining the mesh beyond 5 mm led to less than 1.5 % stress variations. Therefore, a 5 mm mesh was chosen for further simulations, effectively compromising computational cost and result accuracy.

6.3.3 Fatigue crack growth theory

Fatigue crack theories are introduced by the researchers to understand the crack propagation behavior as crack propagation leads to catastrophic failure of structures. Researchers have used advanced fracture mechanics software like FRANC3D to understand the behavior of fatigue crack growth rates *(Chowdhury et al., 2019)*. In this research two fatigue crack growth models namely the Paris-Erdogan equation and the NASGRO model are used to understand the behavior of crack developed in LPST blade.

6.3.3.1 Paris-Erdogan equation

The Paris-Erdogan equation (Eq. 6.1) correlates the stress intensity factor range (ΔK) to the crack growth rate *(Ishikawa et al., 1993)*.

$$da/_{dN} = C(\Delta K)^m = C(K_{max} - K_{min})^m \quad (6.1)$$

In Eq. (6.1), C and m are the material constants having values of $1.3* 10^{-13}$ and 3.45 respectively *(Poursaeidi & Bakhtiari, 2014b)*. The crack-growth rate (da/dN) depends on the stress intensity factor range ΔK and the R ratio. The values of stress intensity

factor range (ΔK) and stress ration (R) are calculated by using equations from Eq. (6.2) to Eq. (6.4).

$$\Delta K = \Delta\sigma \sqrt{\pi a}\, Y \tag{6.2}$$

In Eq. (6.2), $\Delta\sigma$ is the stress range, a is the crack length, Y is dimensionless geometric factor, depending upon the loading conditions and specific geometry of the crack.

Also, ΔK is defined as the difference of the maximum and minimum stress intensity factor (SIF)

$$\Delta K = K_{max} - K_{min} \tag{6.3}$$

The stress intensity factor ratio, R is evaluated as

$$R = \frac{K_{min}}{K_{max}} \tag{6.4}$$

Further, the value of the fatigue crack-growth threshold (ΔK_{th}) is calculated from Eq. (6.5).

$$\Delta K_{th} = K_{OP} - K_{min} \tag{6.5}$$

Where Kop is the stress intensity factor for crack opening and its value is equal to K_{max}

As the stress intensity factor range (ΔK) exceeds the fatigue crack-growth threshold (ΔK_{th}), the crack propagates. The crack propagation is divided into three modes/stages. The stress intensity factors K_I, K_{II} and K_{III} are Mode I SIF, Mode II SIF and Mode III SIF respectively. K_I represents opening mode; K_{II} signifies sliding and K_{III} indicates tearing of the crack.

The equivalent stress intensity factor (K_{equiv}) is calculated from Eq. (6.6)

$$K_{\text{equiv}} = \frac{K_I}{2} + \frac{1}{2}\sqrt{K_I + 4(1.55K_{II})^2 + 4K_{III}^2} \tag{6.6}$$

The critical stress intensity factor also known as material's fracture toughness (K_c) and the equivalent stress intensity factor (K_{equiv}) are crucial in formulating a fracture criterion for determining rapid and unstable fatigue crack growth (FCG) in linear elastic materials. Various conditions relate to crack propagation and its stability depending upon K_{equiv} and K_c are

Condition 1: When the equivalent stress intensity factor (K_{equiv}) is equal to or exceeds the critical stress intensity factor (K_c), resulting in rapid and unstable crack growth. While simulation, when $\Delta K \geq \Delta K_{th}$and $K_{equiv} < K_c$, fatigue crack growth (FCG) analysis advances to ascertain the direction angle (θ_c) and the length of growth extent to Δa.

Condition 2: When $\Delta K < \Delta K_{th}$ and $K_{equiv} \geq K_c$, resulting in no further propagation of crack. It may be noted that when both K_{II} and K_{III} tend to zero and $K_{equiv} = K_I$.

Cracks are naturally curved, which can be approximated by a series of short, straight segments for simplification in mathematical modeling. By dividing the curved crack into numerous short lines, an approximate representation of the crack's shape can be achieved. Furthermore, this methodology assists in ascertaining the direction of crack propagation, which is a crucial factor in addressing catastrophic failure in engineering components. This approach establishes the crack growth direction using the circumferential hoop stress criterion. This criterion suggests that cracks propagate

at a right angle to the direction of the maximum principal stress applied. The angle representing the crack growth direction is represented as θ_c (*Hu et al., 2013)*, which is shown in Fig. 6.9. The process of crack growth is illustrated in three steps as

Step 1: The maximum circumferential stress or hoop stress and kink angle is calculated for every node (direction) by using Eq. (6.7) - (6.8). The crack kinks in a direction perpendicular to the hoop stress (Fig 6.9).

$$\sigma_\theta = \frac{1}{\sqrt{2\pi}}\left[K_I cos^3\left(\frac{\theta}{2}\right) - 3K_{II} sin\left(\frac{\theta}{2}\right) cos^2\left(\frac{\theta}{2}\right)\right] \quad (6.7)$$

Where,

σ_θ = circumferential (hoop) stress

r = radial distance from crack tip

θ = angle measured from crack plane

K_I = Mode I stress intensity factor (opening mode)

K_{II} = Mode II stress intensity factor (sliding mode)

$$\theta_c = 2\arctan\left(\frac{K_I - \sqrt{K_I^2 + 8K_{II}^2}}{4K_{II}}\right) \quad (6.8)$$

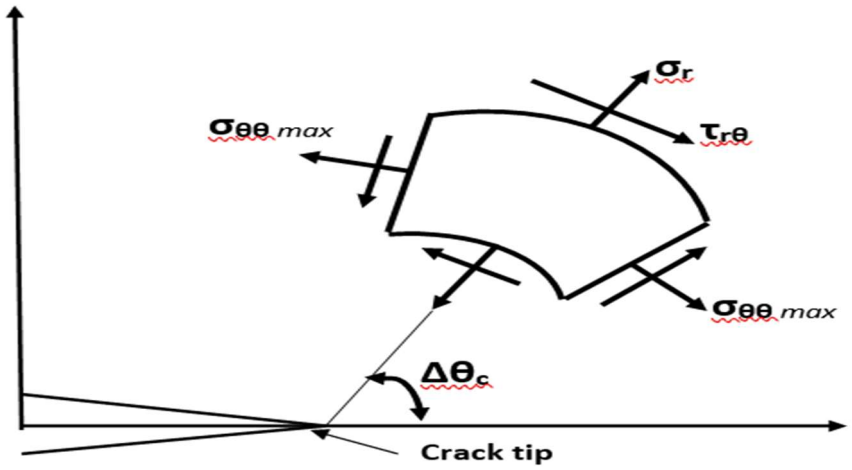

Figure 6.9: Crack propagation Kink angle

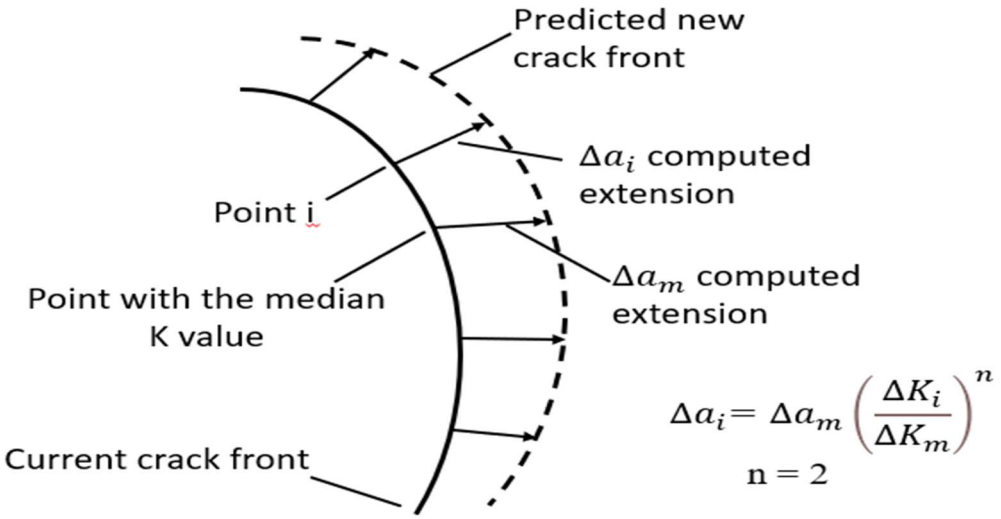

Figure 6.10: Crack Extension rule in Franc 3D

Step 2: Relative amount of local crack extension for each FE node is computed by using Paris model. The extension of the crack along its front is dictated by the ratio of ΔK_i to the median ΔK_m along the crack front and the maximum extension of the crack as shown in Fig. 6.10

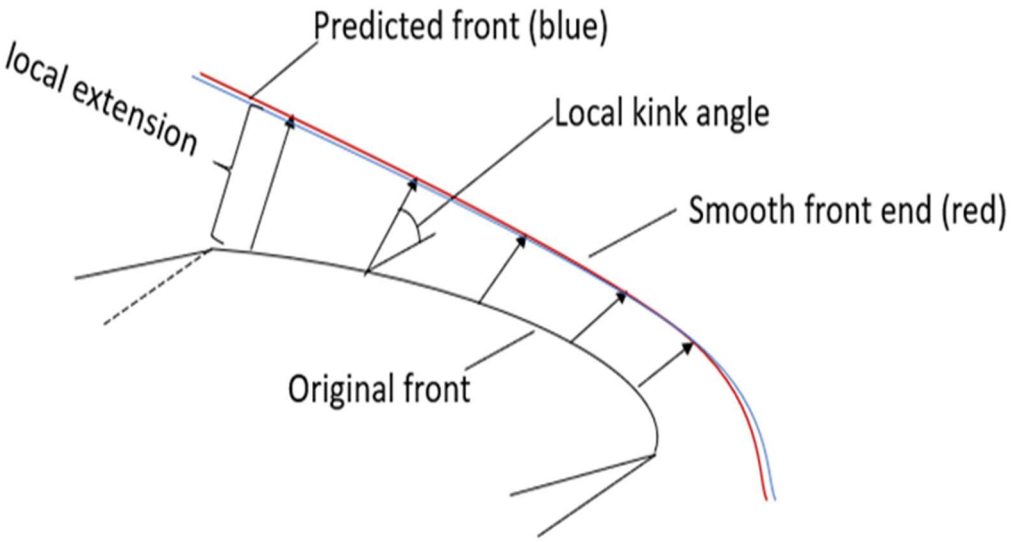

Figure 6.11: Crack growth Prediction

.

Step 3: The polynomial curve is used to smoothen and extrapolate the crack front, as shown in Fig. 6.11.

6.3.3.2 NASGRO model

To address the nonlinear nature of crack advancement during initial and final stages of crack growth, the NASGRO model estimates the crack's progression (Skorupa et al., 2007). The equation of the NASGRO model, which represents the correlation between the crack progression rate and the stress intensity factor (SIF) range (ΔK) is shown as Eq. (6.9).

$$\frac{da}{dN} = C\left[\left(\frac{1-f}{1-R}\right)\Delta K\right]^m \frac{\left(1-\frac{\Delta K_{th}}{\Delta K}\right)^p}{\left(1-\frac{K_{max}}{K_C}\right)^q} \tag{6.9}$$

The parameters used in this equation, i.e., C, m, p, q, and Kc are chosen from the NASGRO database and integrated into FRANC3D. The values of parameters for the material AISI 410 are C = 2.02* 10^{-11}, m = 2.66, K_c = 3605 MPa$\sqrt{mm}$, p = 0.25, q = 0.25.

In Eq. (6.9), 'f' is the Newman closure function, which is used to modify the stress intensity range (ΔK), based on the stress ratio (R), and the crack closure behavior of the material. The Newman defined the value of 'f' as Eq. 6.10.

$$f = \frac{K_{op}}{K_{max}} = \begin{cases} \max(R, A_0 + A_2R + A_2R^2 + A_3R^s) & R \geq 0 \\ A_0 + A_1R & -2 \leq R < 0 \\ A_0 - 2A_1 & R < -2 \end{cases} \tag{6.10}$$

The coefficients A_0, A_1, A_2 *and* A_3 are define as:

$$A_0 = (0.825 - 0.34\alpha + 0.05\alpha^2)\left[\cos\left(\frac{\pi}{2}S_{\max}/\sigma_0\right)\right]^{\frac{1}{\alpha}}$$
$$A_1 = (0.415 - 0.071\alpha)S_{\max}/\sigma_0 \quad (6.11)$$
$$A_2 = 1 - A_0 - A_1 - A_7$$
$$A_3 = 2A_0 + A_1 - 1$$

Where α is the plane stress/strain constraint factor, and S_{max}/σ_0 is the ratio of the maximum applied stress to the flow stress. The values of α and S_{max}/σ_0 are provided by the NASGRO material database. The values of α and S_{max}/σ_0 For AISI 410, the martensitic steels are 2.5 and 0.3, respectively.

Further, the threshold stress intensity factor is calculated by using Eq. (6.12)

$$\Delta K_{th} = \Delta K_0 \left(\frac{a}{a+a_0}\right)^{\frac{1}{2}} / \left(\frac{1-f}{(1-A_0)(1-R)}\right)^{(1+C_{th}R)} \quad (6.12)$$

Where,

R is the stress ratio,

A_0 is a constant as used in Eq. (6.10)

ΔK_0 is the threshold SIF range,

a is the crack length

a_0 is the intrinsic crack length

C_{th} is threshold coefficient

The values of ΔK_0&C_{th} can be taken from the NASGRO material database. The values of ΔK_0 & C_{th} for AISI 410 martensitic steels are taken as 71.5 MPa $\sqrt{mm}$ and 0.65, respectively.

The NASGRO model considers thickness effects by incorporating the critical stress intensity factor. (K_{crit}) as shown in Eq. (6.13).

$$\frac{K_{crit}}{K_{Ic}} = 1 + B_k e^{-\left(A_k \frac{t}{t_0}\right)^2} \quad (6.13)$$

$$t_0 = 2.5\left(K_{Ic}/\sigma_{ys}\right)^2 \quad (6.14$$

Where,

K_{Ic} is Plane strain fracture toughness (Mode I),

A_k - 0.7 (Fit Parameter)

B_k - 0.2 (Fit Parameter)

a_0= 0.381mm

t - thickness

t_0 = Reference thickness at plane strain condition

σ_{ys} = 843 MPa (yield stress of the material)

During simulation, crack instability is presumed to take place when K_{max} surpasses the material's fracture toughness (K_C), which is chosen as the *failure criterion*. Further, if the yield strength of the material is lower than the net section strength, then it is considered a checkpoint *(Poursaeidi & Bakhtiari, 2014b)*

6.3.4. Fatigue crack growth simulation

The current research utilized a combined approach, integrating the finite element capabilities of ANSYS with the crack propagation simulation capabilities of FRANC 3D, to investigate fatigue crack growth in LPST blade fabricated from material (X10 CrNiMoV12-2-2) martensitic stainless steel alloy. The process began with the creation of a CAD-based finite element model in ANSYS, which was used to determine the distribution of von Mises equivalent stresses across the blade. The stress results were

then imported in FRANC3D, where they were utilized to simulate crack growth by applying linear elastic fracture mechanics principles. This combined approach allowed for a detailed analysis of how cracks propagate under fatigue conditions. The procedure for fatigue crack growth simulation is shown in the Fig.6.12.

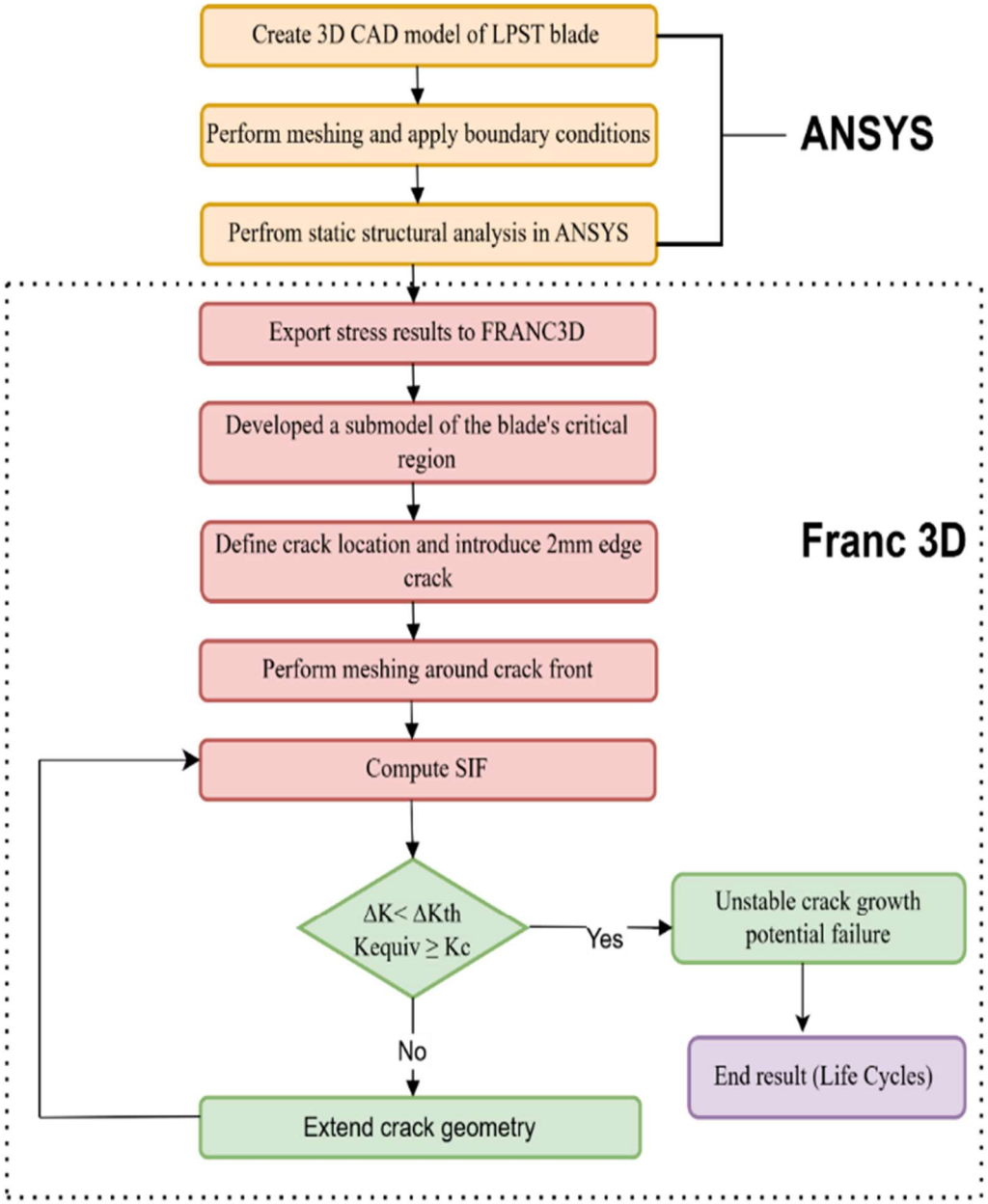

Figure 6.12: Flow chart for fatigue crack growth simulation

A sub-model focusing on the blade's critical region was developed to optimize computational efficiency. This sub-model employed a flexible contour, often referred to as a "rubber-band box," to encompass the front section of the blade, as shown in Fig. 6.13 (a). Within this isolated region, an initial edge crack measuring 2 mm in length with a template radius of 0.5 mm was introduced to represent a pre-existing crack, as depicted in Fig. 6.13 (b).

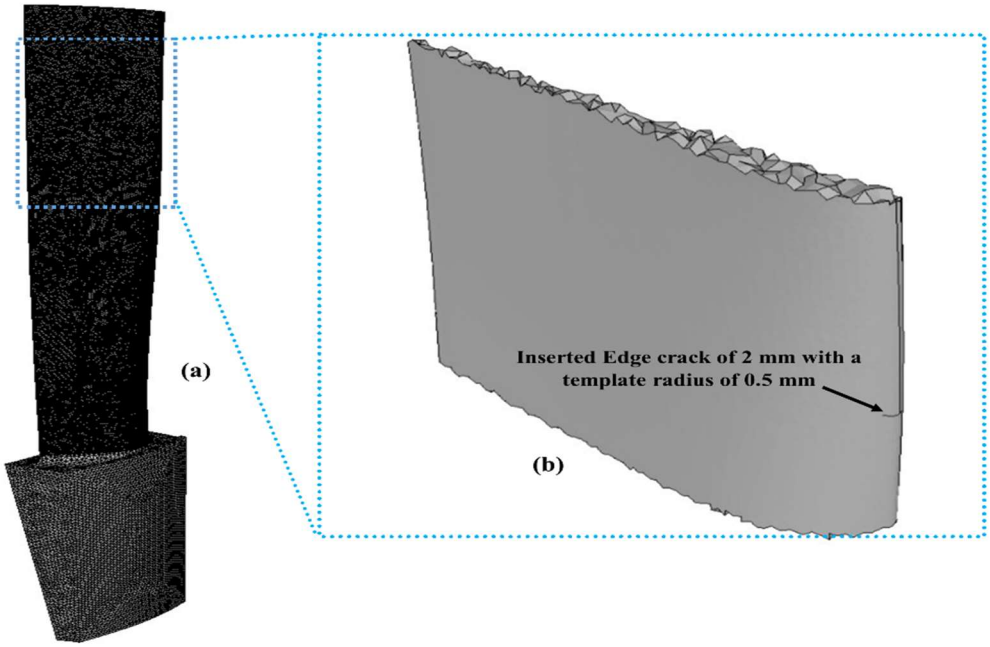

Figure 6.13 (a)Rubber-band box on the front part of the blade (b) an edge crack of 2 mm inserted into the submodel of the blade.

The sub-model of the LPST blade was meshed with 150,464 nodes and 91,080 triangular elements around the crack, as illustrated in Fig. 6.14(a), with magnified view of the initial 2 mm crack provided in Fig. 6.14(b)-(c). During the simulation in FRANC3D, Initially the crack length was incrementally extended from 2 mm to 6.5 mm as shown in Fig. 6.15(a) and the stress intensity factors (SIFs) at the crack front were calculated iteratively to determine the crack growth direction.

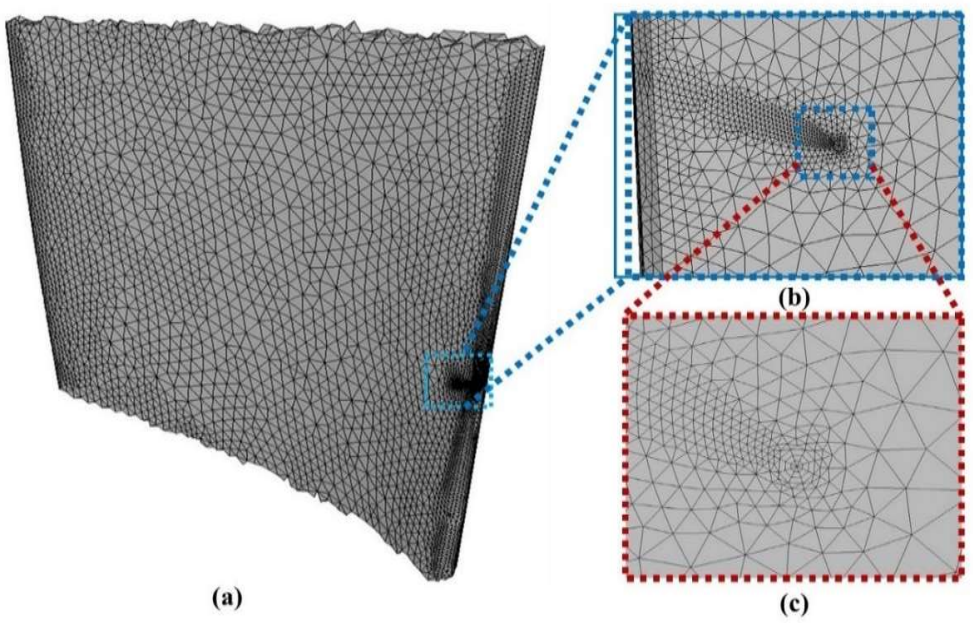

Figure 6.14 (a) Mesh model of front part of the blade (b) & (c) Magnified view of 2 mm crack

Crack growth was governed by two key conditions: $\Delta K \geq \Delta K_{th}$ and $K_{equiv} < K_C$ Here, ΔK represents the range of the stress intensity factor, ΔK_{th} is the threshold below which crack growth terminates, and K_C is the material's critical stress intensity factor, beyond which catastrophic failure occurs. The simulation continued as long as the stress intensity factor range exceeded the threshold (ΔK_{th}) and the equivalent stress intensity factor remained below the critical value (K_C). It automatically terminated when ΔK dropped below ΔK_{th} or K_{equiv} reached or exceeded K_C, this iterative approach provided a detailed analysis of crack growth behavior and its propagation path under operational loading conditions. The fully meshed model with the 6.5 mm crack and its magnified views are presented in Fig.6.15 (b)-(d).

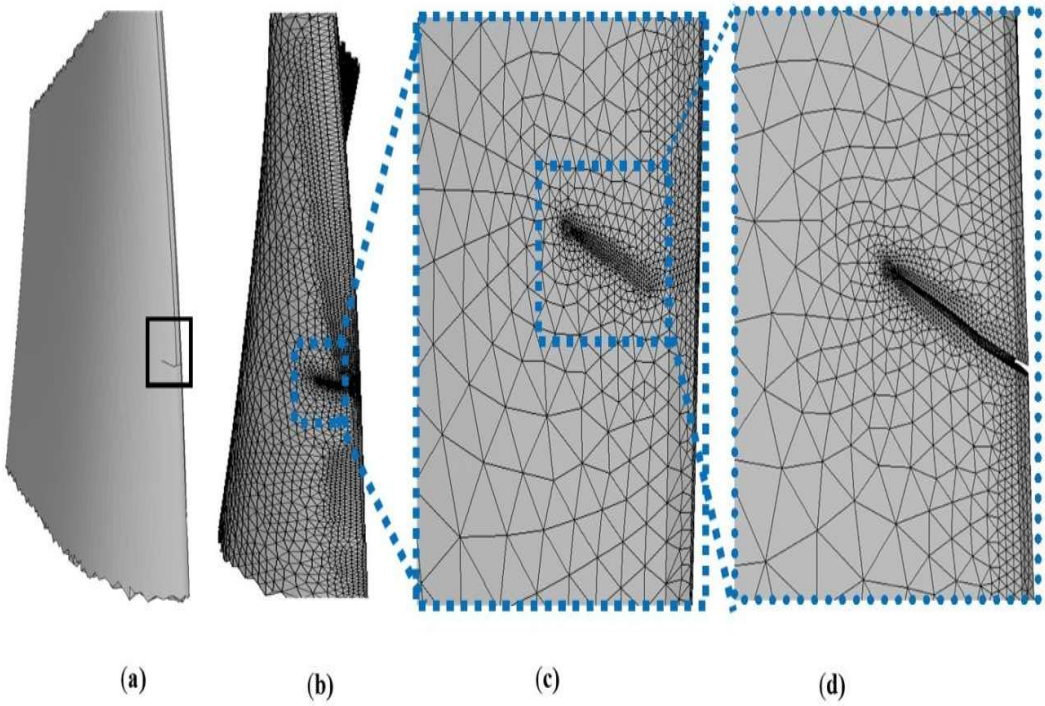

Figure 6.15 (a) Crack growth direction from 2 mm to mm (b) Meshing at the crack front for 6.5 mm crack (c) magnified view of meshed crack front (d) Magnified view of 6.5mm crack

6.4 Results and discussion

The three-dimensional crack front forms an irregular curve, varying in length. The normalization process is used to standardize the crack front length, in which normalized distance along the crack front is computed as a ratio of the arc length from a point on the crack front to the starting point by the total arc length (*Bhamu* et al., 2021). For fatigue crack analysis, the Paris's law and NASGRO model is used, and the value of various parameters to evaluate stress intensity factors (SIFs), K_I, K_{II}, and K_{III} for the material AISI 410 are

C = 2.02* 10^{-11}, m = 2.66 and K_C = 3605 MPa $\sqrt{mm}$.

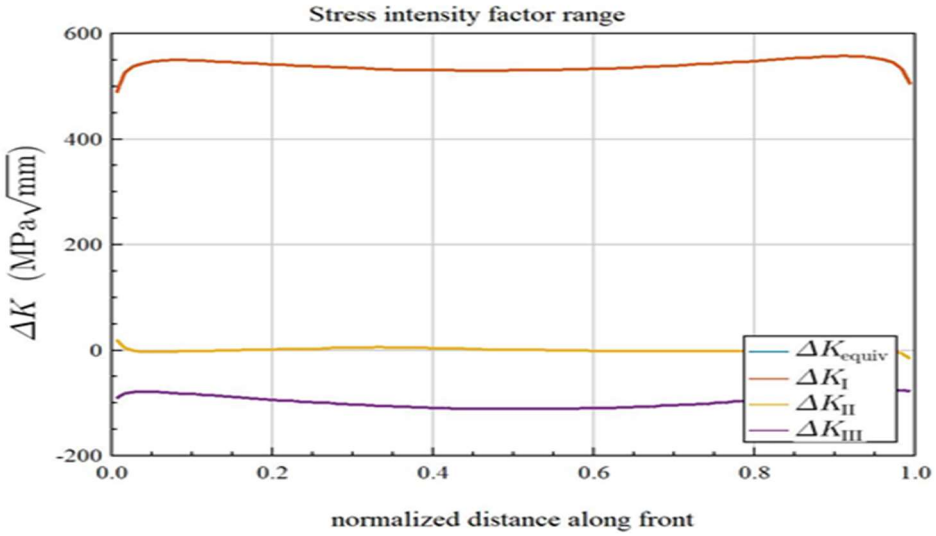

Figure 6.16: Average Stress Intensity Factors (SIFs) K_I, K_{II} and K_{III}

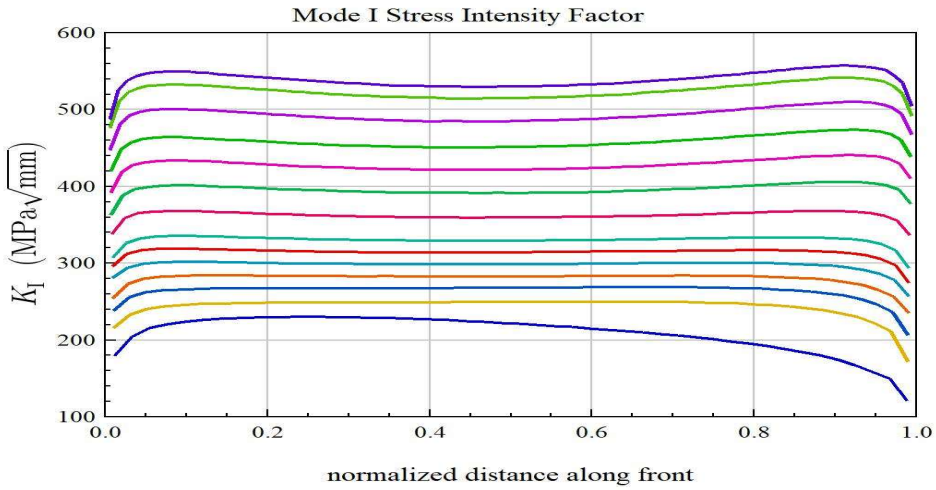

Figure 6.17: Stress intensity factor (K_I) at the crack front 2 mm to 6.5 mm

Fig 6.16 represents the average stress intensity factors (SIFs) values K_I, K_{II} and K_{III} at the crack front 2 mm to 6.5 mm. On comparing K_I, K_{II} and K_{III}, it is observed that stress intensity factors (SIFs) K_{II} and K_{III} are at low level near the crack tip than stress intensity factor K_I. As demonstrated in Fig 6.17, the stress intensity factor K_I exhibits a high value, indicating that crack behavior near the crack tip is predominantly governed by Mode I deformation, which is the primary mode driving crack

82

propagation. K_I serves as a measure of the driving force behind crack growth and is compared to the critical stress intensity factor K_C to assess the potential for unstable crack propagation within the blade sub-model.

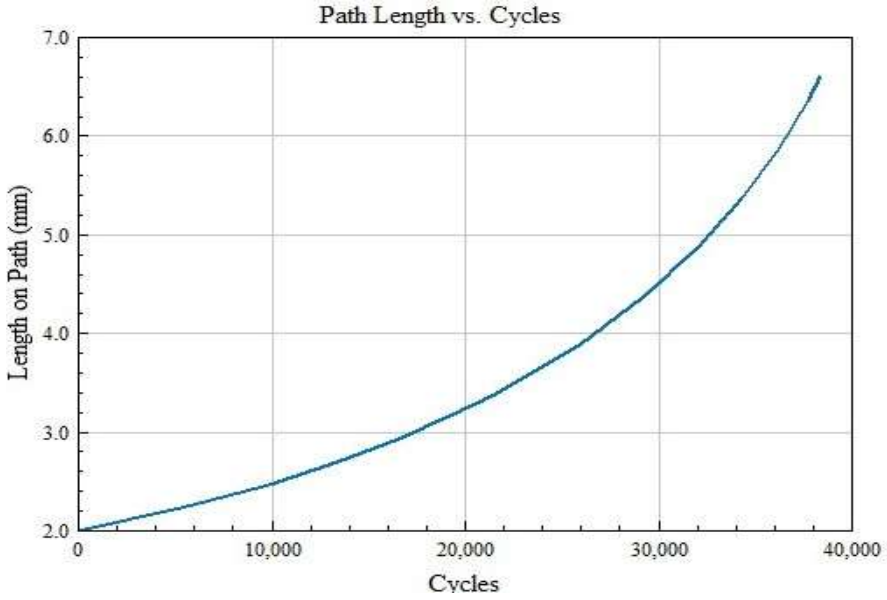

Figure 6.18: Crack Propagation Path Length vs. Cycles

Under cyclic loading, as the crack length increases from 2 mm to 6.5 mm in the sub model of the LPST blade, the stress intensity factor K_I exhibits a variation from 180 MPa$\sqrt{\text{mm}}$ to 550 MPa $\sqrt{\text{mm}}$ at the 13th step of crack propagation, as depicted in Fig. 6.17. The corresponding fatigue life is approximately 38,414 cycles, indicating stable fatigue crack growth conditions, as illustrated in Fig. 6.18.

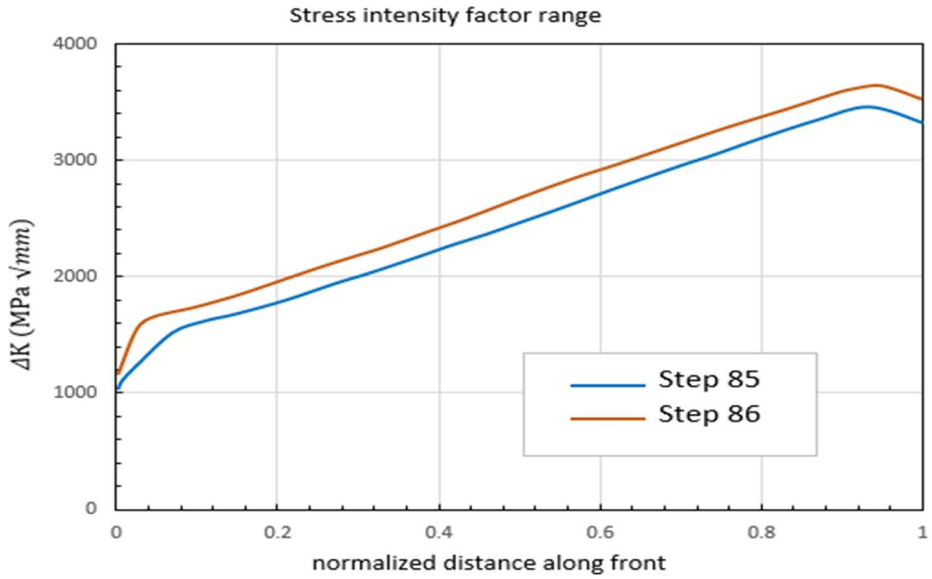

Figure 6.19: Mode I SIF *(K_I)* for 85th and 86th steps of crack propagation

The values of stress intensity factor K_I for steps 85th and 86th of crack advancement are shown in Fig.6.19. At the 85th step of crack propagation, the maximum value of stress intensity factor K_I at the crack front node is approximately 3598 MPa$\sqrt{mm}$, which is almost close to the material's critical stress intensity factor K_C, which is equal to 3605 MPa$\sqrt{mm}$ for AISI 410 martensitic steel. On reaching the 86th step of crack propagation, the maximum value of stress intensity factor K_I is 3640 MPa$\sqrt{mm}$, which surpasses to the material's critical stress intensity factor K_C, indicating that the crack growth becomes unstable and lead to rapid crack propagation, which results in catastrophic fatigue failure of the turbine blade. The corresponding load cycles for the 85th step and 86th step are 251168 cycles and 254123 cycles.

6.5 Conclusion

In this chapter, the crack initiation and its propagation in a Low-Pressure Steam Turbine blade made up of X10CrNiMoV12-2-2 alloy is analyzed using PARIS and NASGRO model of fatigue crack growth with FRANC3D code. The findings of the research work are as follows:

i) Initially, a CAD-based finite element model was created in ANSYS to calculate the von Mises stress equivalent stress distribution. These stress results were imported into FRANC3D for crack propagation analysis. The rubber-band box method was employed to create a sub-model of the blade's front part, where an edge crack of 2 mm was introduced with a template radius of 0.5 mm. The crack was allowed to propagate up to 6.5 mm.

ii) The average stress intensity factors (SIFs) K_I, K_{II} and K_{III} at the crack front were evaluated using the PARIS and NASGRO models. It was observed that SIF K_{II} and K_{III} were significantly lower than K_I, indicating that K_I is the primary driving force behind the crack propagation. The value of K_I varies from 180 MPa$\sqrt{mm}$ to 550 MPa$\sqrt{mm}$ during the initial stages of crack growth. The corresponding cyclic load for crack propagation from 2 mm to 6.5 mm is 38414 cycles.

iii) On further loading as the crack propagates and it reaches the 86th step, the maximum value of stress intensity factor K_I is 3640 MPa$\sqrt{mm}$ which surpasses the material's critical stress intensity factor K_C of to 3605 MPa$\sqrt{mm}$. Exceeding the critical stress intensity factor marks the shift from stable to unstable crack propagation, leading to failure of the blade. The narrow margin of 2,995 cycles (1.18% of total fatigue life) between the 85th and 86th steps highlight this transition.

Consequently, the operational fatigue life limitation for this turbine blade configuration is determined to be 251,168 cycles, beyond which the risk of catastrophic failure rapidly escalates.

iv) The detailed assessment of fatigue life yields essential parameters for developing condition-based maintenance strategies and ensuring operational safety margins in similar power generation systems.

The next will present the conclusion, future scope and social impact of the research.

CHAPTER 7

CONCLUSION, FUTURE SCOPE AND SOCIAL IMPACT

7.1 Conclusions

The main objective of this thesis is to investigate the root causes of failure and fatigue life assessment of a failed L-0 low-pressure steam turbine blade of a 210 MW thermal power plant. The collected failed blade is from the 29th stage and made up of material X10CrNiMoV12-2-2 martensitic stainless steel.

This research integrates experimental investigations, computational analysis and advanced simulation techniques to identify failure mechanism of low-pressure steam turbine blade; effect of residual stresses on the failure of turbine blade; static structural analysis to extract Von-Mises stress, maximum principal stress, maximum principal strain, and shear stress of the low pressure steam turbine blade; dynamic analysis to find dynamic characteristics of the low pressure steam turbine blade

including modal frequencies, mode shapes & critical frequencies; fatigue crack growth behavior and fatigue life assessment of the low pressure steam turbine blade.

The primary objective of the thesis is to identify the root causes of failure of a failed L-0 low-pressure steam turbine blade. The collected failed steam turbine blade was inspected through visual inspection, optical microscopy for microstructural characterization, fractographic analysis includes scanning electron microscopy (SEM) with energy dispersive spectroscopy (EDS) and mechanical testing by performing Vickers hardness test and tensile test. The findings of these investigations are as follows:

i. Microstructure of turbine blade observed by an optical microscope revealed that hardened and tempered martensite is uniformly distributed and shows no signs of micro structural deterioration. From the findings it is determined that there is no material flaw that causes the turbine blade to fail.

ii. Water droplets produce erosion pits on the leading edge of the blade, but they are not near the transverse crack and cannot be considered the cause of the blade's failure.

iii. The results of hardness and tensile test revealed that the blade material's mechanical properties were deteriorated, material become brittle due to an increase in hardness and decrease in ultimate tensile stress and yield stress.

iv. The presence of foreign particles and impurities in the steam such as chlorine, silicon, oxygen, and other corrosion promoting products triggers the failure mechanism.

v. SiO_2 particles repeatedly strike on the blade and form deposits that create grooves/pits on the blade surface that distort the steam passage. These pits act as stress concentrators and provide the sites for crack initiation.

vi. Once cracks initiated, these cracks propagated through the blade on further loading often towards the trailing edge of the turbine blade, which leads to fatigue striations and intergranular fracture, confirming the dominance of a corrosion fatigue mechanism.

vii. These cracks propagate through high cycle fatigue (HCF) mechanisms, especially where operating stresses are repetitive and below the yield strength.

Based on the above findings, it is concluded that, "*the synergistic interaction of continuous cyclic loading and corrosive environment has a detrimental effect on the fatigue endurance limit of the material which results in the premature failure of low-pressure steam turbine blade due to high cycle corrosion fatigue".*

Further, the effect of residual stresses on the failed L-0 low-pressure steam turbine blade was evaluated. The residual stresses of failed turbine were calculated by using X-ray diffraction (XRD) technique combined with the cosα method. The result predicted the internal stress distributions and their effect on crack initiation and fatigue life. It is demonstrated that the residual stresses play a detrimental effect on blade performance and structural integrity.

i. The X-ray diffraction (XRD) technique based on Cos α method has been established as a precise and reliable technique for accurately measuring residual

stresses in steam turbine blades, offering a non-destructive means of assessing the residual stress state in these critical components.

ii. Residual stress analysis revealed the presence of randomly oriented crystal grains on the turbine blade surface, contributes to uneven diffraction intensity across the Debye ring.

iii. The FWHM (Full Width at Half Maximum) distribution indicates that the tensile residual stresses are predominantly concentrated at the blade surface, potentially facilitating the crack initiation under fatigue and corrosion fatigue conditions.

iv. Incorporating residual stress analysis into regular inspections procedures, can improve the structural integrity and longevity of critical components.

Based on the above findings, it is concluded that, "*the analysis of full width at half maximum (FWHM) showed that tensile residual stresses were found mainly on the cracked blade surface. These tensile stresses are important as they can increase the rate of crack initiation and propagation due to cyclic loading and corrosive conditions, therefore act as a contributing factor to corrosion fatigue failure*".

Further, the low-pressure steam turbine blade is analyzed through both static structural and dynamic analysis using finite element approach. The investigation focuses on identifying the stress distributions and critical areas on which the blade is likely to fail during operation. Dynamic analysis of the LP steam turbine blade is done to find the natural frequencies in order to prevent resonance conditions during the operation.

29

i. Computational analysis has been carried out on a real case failed low-pressure steam turbine blade. The three-dimensional CAD model of the blade is generated through a 3D scanning process so that dimensions, contour and blade profiles are accurately and efficiently captured.

ii. Static structural analysis of the blade was done using *ANSYS,19* software to predict its deformation, von Mises stress, principal stresses and strains, and distribution of shear stresses throughout the blade.

iii. Due to centrifugal force and steam flow forces, the stress distribution pattern clearly shows that the concave root side of the blade's trailing edge carrying maximum stress of 678 MPa and hence it will be the vulnerable zone for crack initiation and propagation during severe dynamic conditions. However, the maximum stresses are lower than the yield strength of the blade, so the blade is safe at this load but owing to other dynamic running conditions and steam force; these may be elevated.

iv. A turbine blade allowed to run several times at different speeds for dynamic analysis of the blade at variable speed. The first six natural frequencies of the blade are obtained as 45.984 Hz, 108.62 Hz, 192.75 Hz, 240.2 Hz, 318.54 Hz and 394.54 Hz, and their respective mode shapes have been drawn so that resonance condition could be avoided during operation.

v. As there is significant variation in natural frequencies of the blade and this variation may affect the critical speed of components which may fail within the operational range. Hence, the Campbell diagram analysis is done to evaluate the critical speed of the blade in that condition.

vi. The Campbell diagram shows three harmonic lines, i.e., 7th, 15th and 18th, intersecting with the 4th, 5th and 6th modes of the blade at 2613 rpm, 2504 rpm, and 2967 rpm, respectively. These speeds are critical for the blade; resonance can occur at these speeds.

From the above findings following conclusions were drawn *"the zones which are vulnerable for crack initiation and propagation are identified using static structural analysis and the dynamic analysis has been performed to evaluate the natural frequencies so that resonance conditions could be avoided during operation. Campbell diagram is drawn to find critical speed at the intersecting fundamental frequency with the harmonic's lines to avoid resonance conditions during operation to prevent catastrophic failure of turbine blade".*

A hybrid simulation approach integrating ANSYS and FRANC 3D software is introduced and applied to investigate the fatigue crack growth behavior of a crack in low-pressure steam turbine blade. The stress intensity factors K_I, K_{II}, K_{III} are evaluated and stress intensity factor (K_I) is considered as the parameter for checking the stability of the crack.

i. For crack growth analysis in LPST blade made of X10CrNiMoV12-2-2 martensitic stainless steel alloy, FRANC3D code is used in which the equivalent stress (von-misses stress) CAD model of blade is imported for analysis of crack propagation.

ii. The rubber box method is used at the blade's front part to get the LPST blade sub-model. An edge crack of 2 mm with a template radius of 0.5 mm is inserted

into the sub-model of the blade. The crack is allowed to propagate up to 6.5 mm of crack length.

iii. The average stress intensity factors (SIFs) value K_I, K_{II}, and K_{III} at the crack front from 2 mm to 6.5 mm propagation are evaluated using PARIS and NASGRO model. It is observed that stress intensity factors (SIFs) K_{II} and K_{III} are at low level than stress intensity factor K_I. It is concluded that the stress intensity factor K_I quantifies the driving force behind crack propagation.

iv. The value of stress intensity factor K_I varies from 180 MPa$\sqrt{mm}$to 550 MPa$\sqrt{mm}$at the 13th step of crack propagation. As the crack length varies from 2 mm to 6.5 mm, the corresponding cyclic load for crack propagation from 2 mm to 6.5 mm is 38414 cycles.

v. On reaching the 86th step of crack propagation, the maximum value of stress intensity factor K_I is 3640 MPa$\sqrt{mm}$, which surpasses the material's critical stress intensity factor K_C, that is equal to 3605 MPa$\sqrt{mm}$ for AISI 410 martensitic steel, indicating that the crack growth becomes unstable and lead to rapid crack propagation resulting into catastrophic fatigue failure of the turbine blade. The corresponding load cycles for the 85th step and 86th step are 251168 cycles and 254123 cycles.

Based on the above findings it is concluded that "*the stress intensity factor K_I quantifies the driving force behind crack propagation and at the 85th step and 86th step of crack propagation has the maximum value of stress intensity factor K_I that surpasses the material's critical stress intensity factor K_C and crack growth becomes unstable which leads to rapid crack propagation resulting into*

catastrophic fatigue failure of the turbine blade, the corresponding load cycles at these steps are 251168 cycles and 254123 cycles".

7.2 Future Scope

- The chance of pitting is increased by steam contamination which contains dissolved salts, chlorides, or other impurities and could raise the corrosion potential. Regular monitoring of steam quality can help to detect contamination earlier. This can include the measurement of parameters such as conductivity, pH, and dissolved oxygen levels.

- The establishment of the corrosion fatigue as the predominant failure mechanisms emphasize the significance of advanced blade materials to enhance the performance of the blade materials through advanced alloys, protective coatings, or metal matrix composite (MMC) coatings can be applied by thermal spray processes such as plasma spray and high velocity oxy-fuel (HVOF).

- The existence of residual stresses and surface defects contribute largely to the development of the crack, and hence future studies should aim at methods such as shot peening, laser shock peeling and thermal treatment to generate favourable compressive residual stress and consequently increase the fatigue life.

- The integration of sensor based monitoring systems into turbine blades allows the constant evaluation of vibration, stress and crack propagation. These

systems can be used to support predictive maintenance plans when used in conjunction with the data analytics and machine learning so that the unexpected failures of the blades can be reduced.

- Future computational simulation can be improved with fluid-structure interaction (FSI), thermal analysis, and corrosion kinetics, and can enable a more realistic simulation of operating conditions, such as interaction of the steam flow with the particles, impingement, and response of the blades.

- Probability-based and uncertainty-based models of fatigue life prediction under variable loading and environmental conditions. Reliability analysis was incorporated by merging with stochastic modeling of material behavior and crack growth, improved accuracy in life prediction can be realized. The method allows a sophisticated evaluation of the probability of failure and helps to develop strong and dependable design safety margins of turbine blades.

- Uncertainty-based modeling and probabilistic approaches can be used for fatigue life prediction under variable loading and environmental conditions. By integrating reliability analysis with stochastic modelling of material behavior and crack growth, improved accuracy in life prediction can be realized. This approach enables refined assessment of failure probability and supports the establishment of robust and reliable design safety margins of turbine blade systems.

- Optimization of blade geometry can be done through computational simulations by incorporating parametric modelling with CFD and FEA. The advanced optimization method can be applied to the repeated alteration of the geometric variables in the goal of reducing the stress concentrations and improving the aerodynamic efficiency. This would allow the creation of blade designs that have a higher structural integrity and efficiency.

- Future studies can be focused on the development of data-driven and AI-based models to predict turbine failures based on the comparison of the operational parameters and the failure patterns. These models can be used to enable early fault detection and proactive maintenance strategies by using real-time and historical data. This would improve the reliability of the systems, minimize unplanned downtimes and increase the overall efficiency of turbine systems.

7.3 Social Impact of the Research

7.3.1. Improved reliability of power plant operations

- Reduced unexpected shutdowns
- Stable electricity generation
- Enhanced efficiency of thermal and nuclear power generation systems.

7.3.2 Accurate prediction of crack initiation and propagation prevents catastrophic blade failures and improves operational safety

- Ensuring the safety of plant personnel
- Avoiding high-risk accidents
- Providing safer workplaces.

7.3.3 Economic benefits

- Reduction in maintenance and replacement cost
- Prolonged operational life of turbine components
- Minimized down-time losses in power generation systems'

This research has directly benefited for both industry and national economy.

7.3.4 Contribution to the advancement of existing engineering knowledge

The synergistic combination of experimental characterization (SEM/EDS, XRD) with numerical Simulation techniques such as (ANSYS, FRANC 3D)

- Advanced Interdisciplinary research
- Promotes research and development in academia, industry
- Aligns theoretical models with practical engineering applications

1

The present research gives a detailed of root causes of failure and fatigue failure analysis of low-pressure steam turbine blades through experimental characterization and numerical simulation. The future work should focus on multi-physics models, AI-assisted predictive maintenance, and material development, and its impacts on society were in the form of more reliable energy, safety, cost-effectiveness, and sustainable power generation.

References

1	Aayog, N. (2023) *India's power generation capacity mix*, *2023 or 2024*..
2	Adnyana, D.N. (2018) "Corrosion Fatigue of a Low-Pressure Steam Turbine Blade," *Journal of Failure Analysis and Prevention*, 18(1), pp. 162–173.
3	Aghajani Derazkola, H. *et al.* (2025) "Room temperature tribological properties of molybdenum-titanium-zirconium (TZM) in metal forming processes," *Results in Engineering*, 25, p. 104465.
4	Agripa, H. and Botef, I. (2019) "Titanium Alloys: A Review," *Titanium Alloys: Novel Aspects of Their Manufacturing and Processing*, p. 9.
5	Ahmad, M., Schatz, M. and Casey, M. V. (2018) "An empirical approach to predict droplet impact erosion in low-pressure stages of steam turbines," *Wear*, 402–403, pp. 57–63.
6	Ahmed, S. and Narayan Biswas, A. (2022) "René 41 & waspaloy based comparative study for high pressure turbine blades used in turboshaft engines," *Materials Today: Proceedings*, 56, pp. 1234–1241.
7	Ao, S. *et al.* (2020) "Determination of residual stress in resistance spot-welded joint by a novel X-ray diffraction," *Measurement: Journal of the International Measurement Confederation*, 161.
8	Aruna Prabha, K. *et al.* (2023) "Structural and thermal analysis on high-pressure steam turbine blade to determine the optimum material for its manufacturing," *Materials Today: Proceedings*, 92, pp. 1193–1199..
9	Azevedo, C.R.F. and Sinátora, A. (2009) "Erosion-fatigue of steam turbine blades," *Engineering Failure Analysis*, 16(7), pp. 2290–2303.
10	Banaszkiewicz, M. (2018) "The low-cycle fatigue life assessment method for online monitoring of steam turbine rotors," *International Journal of Fatigue*, 113, pp. 311–323.
11	Bayesteh, H. and Mohammadi, S. (2011) "XFEM fracture analysis of shells: The effect of crack tip enrichments," *Computational Materials Science*, 50(10), pp. 2793–2813.
12	Bendeich, P. *et al.* (2006) "Residual stress measurements in laser clad repaired low pressure turbine blades for the power industry," *Materials Science and Engineering: A*, 437(1), pp. 70–74.
13	Bhagi, Loveleen Kumar *et al.* (2018) "Dynamic Stress Analysis of L-1 Low Pressure Steam Turbine Blade: Mathematical Modelling and Finite Element Method," *Materials Today: Proceedings*, 5(14), pp. 28117–28126.
14	Bhagi, L K *et al.* (2018) *Dynamic stress analysis of L-1 low pressure steam turbine blade: mathematical modelling and finite element method. Materials Today: Proceedings, 5(14), 28117-28126*

15	Bhagi, L.K., Rastogi, V. and Gupta, P. (2017) "Study of corrosive fatigue and life enhancement of low pressure steam turbine blade using friction dampers," *Journal of Mechanical Science and Technology*, 31(1), pp. 17–27.
16	Bhamu, R.K., Shukla, Akash, *et al.* (2021) "Low-Cycle Fatigue Life Prediction of LP Steam Turbine Blade for Various Blade–Rotor Fixity Conditions," *Journal of Failure Analysis and Prevention*, 21(6), pp. 2256–2277.
17	Bhattacharjee, A., Saha, B. and Williams, J.C. (2017) "Titanium Alloys: Part 2---Alloy Development, Properties and Applications," in N.E. Prasad and R.J.H. Wanhill (eds.) *Aerospace Materials and Material Technologies : Volume 1: Aerospace Materials*. Singapore: Springer Singapore, pp. 117–148.
18	Binner, M. and Seume, J.R. (2013) "Flow Patterns in High Pressure Steam Turbines During Low-Load Operation," *Journal of Turbomachinery*, 136(6), p. 61010.
19	Cano, S. *et al.* (2019) "Detection of damage in steam turbine blades caused by low cycle and strain cycling fatigue," *Engineering Failure Analysis*, 97(January), pp. 579–588.
20	Chaplin, R.A. (2009) *Thermal power plants*. Encyclopedia of Life Support Systems.
21	Chen, Z. *et al.* (2009) "Fatigue life prediction of regulating valves on the intermediate-pressure section of a 400 MW steam turbine," *Engineering Failure Analysis*, 16(5), pp. 1483–1492.
22	Chen, Z. *et al.* (2022) "Numerical prediction based on XFEM for mixed-mode crack growth path and fatigue life under cyclic overload," *International Journal of Fatigue*, 162.
23	Citarella, R. *et al.* (2016) "FEM-DBEM approach for crack propagation in a low pressure aeroengine turbine vane segment," *Theoretical and Applied Fracture Mechanics*, 86, pp. 143–152.
24	Cziesla, F. *et al.* (2009) "Advanced 800+ MW steam power plants and future CCS options," *Siemens Ind Turbomach*, pp. 1–21.
25	Darwish, M.A., Al Awadhi, F.M. and Bin Amer, A.O. (2010) "Combining the nuclear power plant steam cycle with gas turbines," *Energy*, 35(12), pp. 4562–4571.
26	Das, G. *et al.* (2003) "Turbine blade failure in a thermal power plant," *Engineering Failure Analysis*, 10(1), pp. 85–91.
27	Ding, T. *et al.* (2019) "CNC Planing Process for Turbine Twisted Blade Profile," *IOP Conference Series: Materials Science and Engineering*, 686, p. 12022.
28	Dudova, N. (2022) "9--12\% Cr heat-resistant martensitic steels with increased boron and decreased nitrogen contents," *Metals*, 12(7), p. 1119.

29	Escalero, M. *et al.* (2018) "Study of alternatives and experimental validation for predictions of hole-edge fatigue crack growth in 42CrMo4 steel," *Engineering Structures*, 176, pp. 621–631.
30	Farhat, H. (2021) "Typical service-induced damages," *Operation, Maintenance, and Repair of Land-Based Gas Turbines*, pp. 107–130..
31	Fedorova, I. (2018) *Alloy development for high Cr martensitic steel*.
32	Gao, J. *et al.* (2024) "Study of cracks in the last-stage rotor blade of a steam turbine and the corrosion fatigue properties of its materials," *Heliyon*, 10(17).
33	Gelfi, M. *et al.* (2004) "X-ray diffraction Debye Ring Analysis for STress measurement (DRAST): A new method to evaluate residual stresses," *Acta Materialia*, 52(3), pp. 583–589.
34	Gialanella, S. and Malandruccolo, A. (2020) "Titanium and Titanium Alloys," *Aerospace Alloys*. Cham: Springer International Publishing, pp. 129–189.
35	Graciano, D.M. *et al.* (2023) "Damage evaluation and life assessment of steam turbine blades," *Theoretical and Applied Fracture Mechanics*, 124.
36	Gülen, S.C. (2021) "Steam Turbine—Quo Vadis?," *Frontiers in Energy Research*, Volume 8.
37	Gupta, A. (2019) "Determination of residual stresses for helical compression spring through Debye-Scherrer ring method," *Materials Today: Proceedings*. Elsevier Ltd, pp. 654–658.
38	Gupta, A. *et al.* (2020) "Experimental investigation of fatigue failure in an ASTM A401 compression spring of a passenger car". *Materials Testing, 62(6), 626-632.*
39	Guy, h.l. and parsons, s.i.r.c. (1939) "some researches on steam-turbine nozzle-efficiency. The sir charles parsons memorial lecture, 1939. ," Journal of the Institution of Civil Engineers, 13(2), pp. 91–124.
40	Hafshejani, H.N., Hajidavalloo, E. and Moradi, S. (2025) "Modeling and simulation of 5-stage low-pressure steam turbine to analyze L-2 stage blade failure," *Applied Thermal Engineering*, 277, p. 126998.
41	Hassen, M. Ben, Fakhari, S.M. and Mrad, H. (2023) "Assessment of Crack Growth and Fatigue Life of an Axial Fan Blade Based on a Co-Simulation Approach," *Advances in Materials Science*, 23(3), pp. 61–79.
42	He, H. *et al.* (2020) "Failure analysis of steam turbine blade roots," *Engineering Failure Analysis*, 115(May), pp. 1–11.
43	Hu, X.F. and Yao, W.A. (2013) "A new enriched finite element for fatigue crack growth," *International Journal of Fatigue*, 48, pp. 247–256.
44	Huang, X., Liu, Z. and Xie, H. (2013) "Recent progress in residual stress measurement techniques," *Acta Mechanica Solida Sinica*, 26(6), pp. 570–583.
45	Hurd, P. *et al.* (2005) "Modern Reaction HP/IP Turbine Technology Advances and Experiences." (ASME Power Conference), pp. 425–435.

46	James, M.N. *et al.* (2010) "Shot-peening of steam turbine blades: Residual stresses and their modification by fatigue cycling," *Procedia Engineering*, pp. 441–451.
47	Jonas, O. (1985) "Steam Turbine Corrosion.," *Materials Performance*, pp. 9–18.
48	Jones, R.H. (2003) "Stress-corrosion cracking," *Corrosion: fundamentals, testing, and protection*. ASM international, pp. 346–366.
49	Kaneko, Y. (2022) "Mechanical design and vibration analysis of steam turbine blades," *Advances in Steam Turbines for Modern Power Plants*, pp. 139–162.
50	Katinić, M. *et al.* (2019) "Corrosion fatigue failure of steam turbine moving blades: A case study," *Engineering Failure Analysis*, 106.
51	Katinić, M. and Kozak, D. (2018) "Steam turbine moving blade failure caused by corrosion fatigue - Case history," *Procedia Structural Integrity*. Elsevier B.V., pp. 2040–2047.
52	Kim, H. (2011) "Crack evaluation of the fourth stage blade in a low-pressure steam turbine," *Engineering Failure Analysis*, 18(3), pp. 907–913.
53	Kocharla, R.P.B. *et al.* (2022) "Finite element modeling aspects in the fracture assessment of a low pressure steam turbine blade," *International Journal on Interactive Design and Manufacturing* [Preprint].
54	Kovacs, S., Beck, T. and Singheiser, L. (2013) "Influence of mean stresses on fatigue life and damage of a turbine blade steel in the VHCF-regime," *International Journal of Fatigue*, 49, pp. 90–99.
55	Kubiak Sz., J. *et al.* (2007) "Failure analysis of steam turbine last stage blade tenon and shroud," *Engineering Failure Analysis*, 14(8 SPEC. ISS.), pp. 1476–1487.
56	Kubiak Sz, J. *et al.* (2009) "Failure analysis of the 350 MW steam turbine blade root," *Engineering Failure Analysis*, 16(4), pp. 1270–1281.
57	Kuželka, J. *et al.* (2019) "Numerical simulations of fatigue crack growth in a steam turbine rotor blade groove," *Procedia Structural Integrity*. Elsevier B.V., pp. 780–787.
58	LaRue, J.E. and Daniewicz, S.R. (2007) "Predicting the effect of residual stress on fatigue crack growth," *International Journal of Fatigue*, 29(3), pp. 508–515.
59	Lesiuk, J.F. (2020) "توربین بخاری(Steam Turbine)," p. 2020. Available at: http://steamturbine.blogfa.com/.
60	Leyzerovich, A.S. (2021) *Steam turbines for modern fossil-fuel power plants*. River Publishers.
61	Liu, Y. *et al.* (2022) "Experimental Study on the Aerodynamic Characteristics of Blades at the Last Stage of a Steam Turbine at Off-Design Conditions," *International Journal of Aerospace Engineering*, 2022(1), p. 8785963.

62	Liu, Y.G. *et al.* (1995) "The effect of initial microstructure on heat-affected zone microfissuring in Incoloy 903," *Materials Science and Engineering: A*, 202(1), pp. 179–187.
63	Lucacci, G. (2017) "Steels and alloys for turbine blades in ultra-supercritical power plants," *Materials for Ultra-Supercritical and Advanced Ultra-Supercritical Power Plants*, pp. 175–196.
64	Luthman Jr, N.G. (2017) *Evaluation of Impulse Turbine Performance Under Wet Steam Conditions*.
65	Lynch, S. (2019) "A review of underlying reasons for intergranular cracking for a variety of failure modes and materials and examples of case histories," *Engineering Failure Analysis*. Elsevier Ltd, pp. 329–350.
66	MACHINES, E.P. (2024)"https://ems-powermachines.com/steam-turbine-types-and-applications"
67	Mazur, Z. *et al.* (2008) "Steam turbine blade failure analysis," *Engineering Failure Analysis*, 15(1–2), pp. 129–141.
68	Mazur, Z., Garci\' a-Illescas, R. and Herna\' ndez-Rossette, A. (2009) "Steam turbine low pressure blades fatigue failures caused by operational and external conditions," *Turbo Expo: Power for Land, Sea, and Air*, pp. 93–106.
69	Mazur, Z., García-Illescas, R. and Hernández-Rossette, A. (2009) "Steam turbine low pressure blades fatigue failures caused by operational and external conditions".
70	McCloskey, T.H. (2003) "Steam turbines," *Handbook of Turbomachinery*. CRC Press, pp. 386–513.
71	Miyazaki, T. *et al.* (2015) "Improvement of X-ray stress measurement from a Debye-Scherrer ring by oscillation of the X-ray incident angle," *Powder Diffraction*, 30(3), pp. 250–255.
72	Mohan, R.S., Sarkar, A. and Sekhar, A.S. (2014) "Vibration analysis of a steam turbine blade," *INTERNOISE 2014 - 43rd International Congress on Noise Control Engineering: Improving the World Through Noise Control*, pp. 1–10.
73	MUKHOPADHYAY, N.K. *et al.* (2001) "An investigation of the failure of low pressure steam turbine blades," *Failure Analysis Case Studies II*. Elsevier, pp. 211–223.
74	Navinesh, B.C. *et al.* (2020) "Better wear resistance of HVOF coating CrC-NiCrFeSiBCoC(35%-65%) and CrC-NiCrFeSiBCoC(80%-20%)on SS316 steels," *Materials Today: Proceedings*. Elsevier Ltd, pp. 155–160.
75	Neilson, R.M. (1908) *The steam turbine*. Longmans, Green, and Company.
76	Newby, M., James, M.N. and Hattingh, D.G. (2014) "Finite element modelling of residual stresses in shot-peened steam turbine blades," *Fatigue*

	and Fracture of Engineering Materials and Structures. Blackwell Publishing Ltd, pp. 707–716.
77	Niu, L. Bin *et al.* (2018) "Effect of chloride and sulfate ions on crevice corrosion behavior of low-pressure steam turbine materials," *Corrosion Science*, 132(November), pp. 284–292.
78	Peng, W.W. (2007) *Fundamentals of turbomachinery*. John Wiley \& Sons.
79	Perkins, K.M. and Bache, M.R. (2005) "The influence of inclusions on the fatigue performance of a low pressure turbine blade steel," *International Journal of Fatigue*, 27(6), pp. 610–616.
80	Plesiutschnig, E. *et al.* (2016) "Fracture analysis of a low pressure steam turbine blade," *Case Studies in Engineering Failure Analysis*, 5–6, pp. 39–50.
81	Raj, B. *et al.* (2009) "X-ray diffraction based residual stress measurements for assessment of fatigue damage and rejuvenation process for undercarriages of aircrafts," *Journal of Nondestructive Evaluation*, 28(3–4), pp. 157–162.
82	Ramakokovhu, U. *et al.* (2021) "Significance of residual stresses in fatigue life prediction of micro gas turbine blades," *Engineering Failure Analysis*, 120.
83	Rani, P. and Agrawal, A.K. (2022) "Failure analysis of a low-pressure stage steam turbine blade," *Nondestructive Testing and Evaluation* [Preprint].
84	Rani, S., Agrawal, A.K. and Rastogi, V. (2019) "Vibration analysis for detecting failure mode and crack location in first stage gas turbine blade," *Journal of Mechanical Science and Technology*, 33(1), pp. 1–10.
85	Ritz, F., Beck, T. and Kovacs, S. (2018) "Fatigue behavior of X10CrNiMoV12-2-2 under the influence of mean loads and stress concentration factors in the very high cycle fatigue regime," *Fatigue of Materials at Very High Numbers of Loading Cycles*. Springer Fachmedien Wiesbaden, pp. 253–272.
86	Rivaz, A., Mousavi Anijdan, S.H. and Moazami-Goudarzi, M. (2020) "Failure analysis and damage causes of a steam turbine blade of 410 martensitic stainless steel after 165,000 h of working," *Engineering Failure Analysis*, 113..
87	Rodríguez, J.A. *et al.* (2019) "Fatigue of steam turbine blades at resonance conditions," *Engineering Failure Analysis*, 104, pp. 39–46.
88	Rossini, N.S. *et al.* (2012) "Methods of measuring residual stresses in components," *Materials and Design*, pp. 572–588.
89	Ruchert, C.O.F.T. and Carvalho, M. (2024) "Failure analysis of a martensitic stainless steel steam turbine blade," *Journal of the Brazilian Society of Mechanical Sciences and Engineering*, 46(7), p. 406.

90	Ruchert, C.O.F.T., de Carvalho, M.C. and Montezuma, M.F.V. (2021) "Fretting fatigue in-service failure of X20CrMo13 stainless steel turbine blade," *Materials Research*, 24(5).
91	Salehnasab, B. and Poursaeidi, E. (2020) "Mechanism and modeling of fatigue crack initiation and propagation in the directionally solidified CM186 LC blade of a gas turbine engine," *Engineering Fracture Mechanics*, 225.
92	Sanvito, M. *et al.* (2012) *Analysis of LP steam turbine blade vibrations: Experimental results and numerical simulations*, *Institution of Mechanical Engineers - 10th International Conference on Vibrations in Rotating Machinery*. Woodhead Publishing Limited.
93	Sarim Khan, M. and Sasikumar, C. (2022) "Failure analysis of AISI 420 steel turbine blade operating at low-pressure," *Materials Today: Proceedings*, 66, pp. 3804–3808.
94	Saxena, S. *et al.* (2015) "Coupled mechanical, metallurgical and FEM based failure investigation of steam turbine blade," *Engineering Failure Analysis*, 52, pp. 35–44.
95	Schönbauer, B.M., Salzman, R.N. and Zhou, S. (2011) Crack initiation and propagation in 12% Cr steam turbine blade steel Symposium on Risk analysis and Safety of Technical Systems (ECF22 conference, Serbia) *View project Christian Doppler Laboratory for Fundamentals of Wood Machining View project.*
96	Shajari, Y. *et al.* (2023) "Nondestructive Method to Measure Residual Stress and Structural Properties of 1.4923 (X22CrMoV12-1) Martensitic Stainless Steel," *Journal of Materials Engineering and Performance* [Preprint].
97	Shankar, M., Kumar, K. and Ajit Prasad, S.L. (2010) "T-root blades in a steam turbine rotor: A case study," *Engineering Failure Analysis*, 17(5), pp. 1205–1212.
98	Shetkar, K.A.D.R. and Srinivas, J. (2021) "Analytical Modeling and Vibration Analysis of the Last-Stage LP Steam Turbine Blade Made of Functionally Graded Material," *Arabian Journal for Science and Engineering*, 46(8), pp. 7363–7377.
99	Shlyannikov, V.N., Yarullin, R.R. and Zakharov, A.P. (2014) "Fatigue of Steam Turbine Blades With Damage on the Leading Edge," *Procedia Materials Science*, 3, pp. 1792–1797.
100	Shukla, A. and Harsha, S.P. (2016) "Vibration Response Analysis of Last Stage LP Turbine Blades for Variable Size of Crack in Root," *Procedia Technology*, 23, pp. 232–239.
101	Sieradzki, K. and Newman, R.C. (1987) "Stress-corrosion cracking," *Journal of Physics and Chemistry of Solids*, 48(11), pp. 1101–1113..

102	Singh, S. *et al.* (2020) "Brief survey on mechanical failure and preventive mechanism of turbine blades," *Materials Today: Proceedings*. Elsevier Ltd, pp. 2515–2524.
103	Subramanian, C. *et al.* (2026) "Fatigue fracture of last stage X20Cr13 low pressure turbine (LPT) blade from 600 MW thermal power station," *International Journal of Pressure Vessels and Piping*, 221, p. 105751.
104	Tanaka, K. (2017) *X-ray Stress Measurement by The Cos a Method Using Two-Dimensional Detector Part 1: Fundamentals of Measurements 総 説*, *Journal of the Society of Materials Science*.
105	Tanuma, T. (2017) "Design and analysis for aerodynamic efficiency enhancement of steam turbines," *Advances in Steam Turbines for Modern Power Plants*, pp. 109–126.
106	Tanuma, T. (2022) "Development of last-stage long blades for steam turbines," *Advances in Steam Turbines for Modern Power Plants*, pp. 329–357.
107	Tulsidas, D., Shantharaja, M. and Bharath, V.G. (2014) "Life Estimation of a Steam Turbine Blade Using Low Cycle Fatigue Analysis," *Procedia Materials Science*, 5, pp. 2392–2401.
108	Wang, W.Z. *et al.* (2007) "Failure analysis of the final stage blade in steam turbine," *Engineering Failure Analysis*, 14(4), pp. 632–641.
109	Wei, Y. *et al.* (2020) "Analysis on corrosion fatigue cracking mechanism of 17-4PH blade of low pressure rotor of steam turbine," *Engineering Failure Analysis*, 118.
110	Xue, F. *et al.* (2014) "Fretting fatigue crack analysis of the turbine blade from nuclear power plant," *Engineering Failure Analysis*, 44, pp. 299–305.
111	Yang, T. *et al.* (2021) "Crack investigation of martensitic stainless steel turbine blade in thermal power plant," *Engineering Failure Analysis*, 127.
112	Yang, Y. and Vormwald, M. (2017) "Fatigue crack growth simulation under cyclic non-proportional mixed mode loading," *International Journal of Fatigue*, 102, pp. 37–47.
113	You, C. *et al.* (2017) "Numerical modelling of the fatigue crack shape evolution in a shot-peened steam turbine material," *International Journal of Fatigue*, 104, pp. 120–135.
114	Yuan, W. *et al.* (2026) "Crack Failure Analysis of Low-Pressure Rotor Steam Turbine Blades in Thermal Power Plant," *Journal of Failure Analysis and Prevention* [Preprint].
115	Zhang, X. *et al.* (2017) "Experimental and numerical investigation of fatigue crack growth in the cracked gear tooth," *Fatigue and Fracture of Engineering Materials and Structures*, 40(7), pp. 1037–1047.

116	Zhang, Z. *et al.* (2021) "Water droplet erosion life prediction method for steam turbine blade materials based on image recognition and machine learning," *Journal of Engineering for Gas Turbines and Power*, 143(3).
117	Zhao, W. *et al.* (2018a) "Vibration analysis for failure detection in low pressure steam turbine blades in nuclear power plant," *Engineering Failure Analysis*, 84(July 2016), pp. 11–24.
118	Zhao, W. *et al.* (2018b) "Vibration analysis for failure detection in low pressure steam turbine blades in nuclear power plant," *Engineering Failure Analysis*, 84, pp. 11–24.
119	Zhu, P. *et al.* (2019) "Study of residual stresses in A7N01 aluminum alloy with X-ray diffraction Debye ring analysis," *International Journal of Modern Physics B*.